Elsevier Editorial System(tm) for Journal of Colloid and Interface Science

Manuscript Draft

Manuscript Number: JCIS-20-377R2

Title: Microstructure and Antibacterial Efficacy of Graphene Oxide Nanocomposite Fibres

Article Type: Full length article

Section/Category: E. Biomaterials and Nanomedicine

Keywords: Antibacterial; graphene oxide; nanocomposite; fibers; Raman scattering

Corresponding Author: Professor Mohan Edirisinghe, DSc

Corresponding Author's Institution: UCL

First Author: Rupy K Matharu

Order of Authors: Rupy K Matharu; Tanveer A Tabish; Thithawat Trakoolwilaiwan; Jessica Mansfield; Julian Moger; Tongfei Wu; Cláudio Lourenço; Biqiong Chen; Lena Ciric; Ivan P Parkin; Mohan Edirisinghe, DSc

Abstract: Antibacterial polymer nanocomposite fibre meshes containing graphene oxide (GO) nanosheets were successfully prepared by pressurised gyration. The morphological and chemical composition of the resulting fibre meshes were determined using Scanning Electron Microscopy (SEM), Raman spectroscopy, Raman mapping and Fourier-Transform Infrared Spectroscopy (FT-IR). SEM showed the fibres to have an average diameter increasing from ~ 1 - 4 μm as the GO loading increased. FT-IR and Raman spectroscopy confirmed the inclusion of GO nanosheets on the fibre surface. The antibacterial potential of GO nanocomposite fibres were investigated using Escherichia coli K12. Average bacterial reduction ranged from 46 - 85 % with results favouring the strongest bioactivities of the nanocomposite containing 8 wt% of GO. Finally, bacterial toxicity of the nanocomposites was evaluated by reactive oxygen species (ROS) formation. A mechanism for the antibacterial behaviour of the nanocomposite fibres is presented. Stimulated Raman scattering imaging and spectra of the fibres post antibacterial studies showed flakes of GO distributed across the surface of the poly(methyl 2-methylpropenoate) (PMMA) fibres, which contribute to the high killing efficacy of the composites towards E. coli. GO nanosheets embedded in a polymer matrix have demonstrated the ability to retain their antibacterial properties, thus offering themselves as a promising antibacterial agent.

*3: Graphical Abstract
Click here to download high resolution image

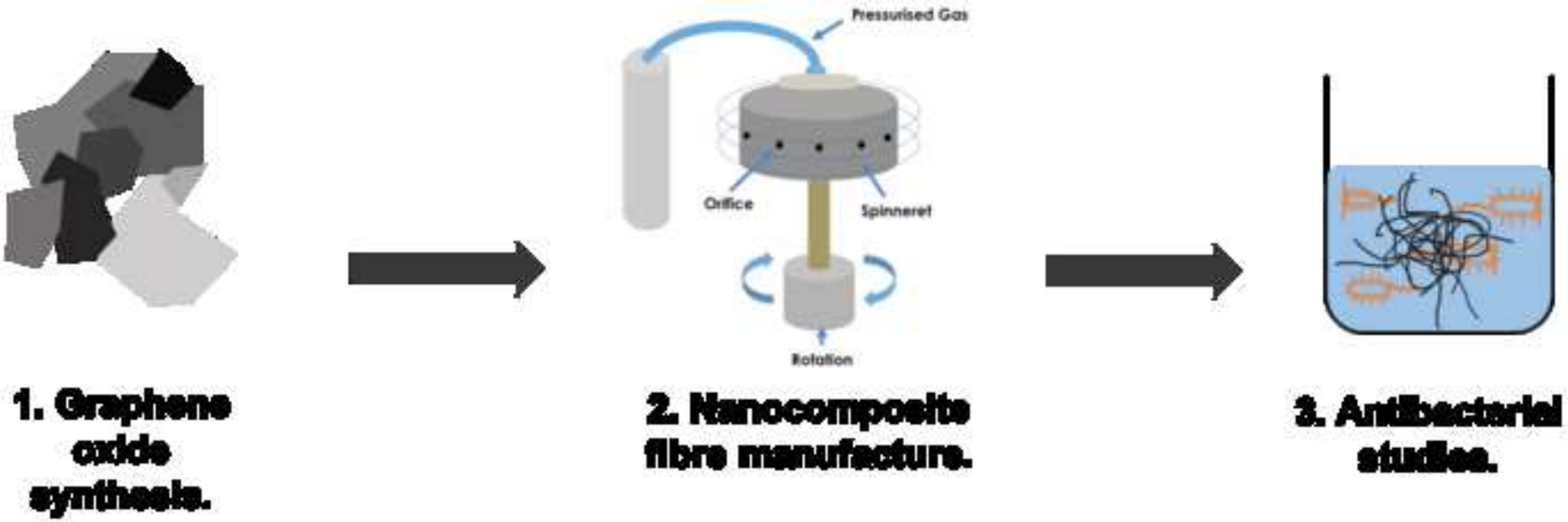

Microstructure and Antibacterial Efficacy of Graphene Oxide Nanocomposite Fibres

Rupy Kaur Matharu[a,b], Tanveer A. Tabish[c], Thithawat Trakoolwilaiwan[a], Jessica Mansfield[c], Julian Moger[c], Tongfei Wu[d], Cláudio Lourenço[e], Biqiong Chen[f], Lena Ciric[b], Ivan P. Parkin[e], Mohan Edirisinghe[a*]

[a] Department of Mechanical Engineering, University College London, Torrington Place, London, WC1E 7JE, UK.

[b] Department of Civil, Environmental and Geomatic Engineering, University College London, London, WC1E 7JE, UK.

[c] School of Physics and Astronomy, University of Exeter, North Park Road, Exeter, EX4 4QL, UK.

[d] Department of Materials Science and Engineering, University of Sheffield, Mappin Street, Sheffield, S1 3JD, UK.

[e] Department of Chemistry, University College London, Gordon Street, London, WC1H 0AJ, UK.

[f] School of Mechanical and Aerospace Engineering, Queen's University Belfast, Stranmillis Road, Belfast, BT9 5AH, UK.

* Corresponding author email: m.edirisinghe@ucl.ac.uk

Abstract

Antibacterial polymer nanocomposite fibre meshes containing graphene oxide (GO) nanosheets were successfully prepared by pressurised gyration. The morphological and chemical composition of the resulting fibre meshes were determined using Scanning Electron Microscopy (SEM), Raman spectroscopy, Raman mapping and Fourier-Transform Infrared Spectroscopy (FT-IR). SEM showed the fibres to have an average diameter increasing from ~ 1 – 4 μm as the GO loading increased. FT-IR and Raman spectroscopy confirmed the inclusion of GO nanosheets on the fibre surface. The antibacterial potential of GO nanocomposite fibres were investigated using *Escherichia coli* K12. Average bacterial reduction ranged from 46 – 85 % with results favouring the strongest bioactivities of the nanocomposite containing 8 wt% of GO. Finally, bacterial toxicity of the nanocomposites was evaluated by reactive oxygen species (ROS) formation. A mechanism for the antibacterial behaviour of the nanocomposite fibres is presented. Stimulated Raman scattering imaging and spectra of the fibres post antibacterial studies showed flakes of GO distributed across the surface of the poly(methyl 2-methylpropenoate) (PMMA) fibres, which contribute to the high killing efficacy of the composites towards *E. coli*. GO nanosheets embedded in a polymer matrix have demonstrated the ability to retain their antibacterial properties, thus offering themselves as a promising antibacterial agent.

Graphical Abstract

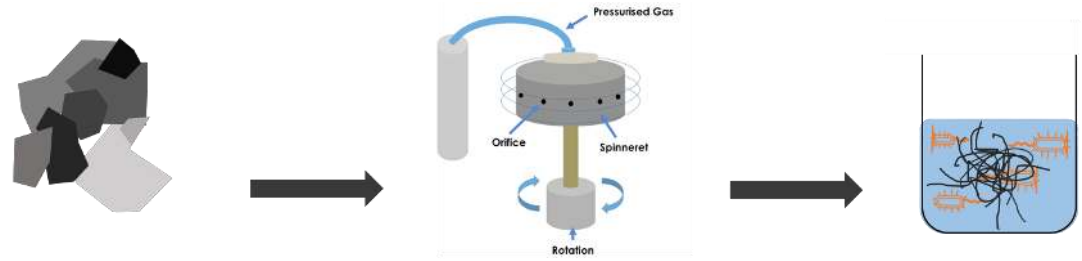

Keywords:

Antibacterial; Graphene Oxide; Nanocomposite; Fibers; Reactive Oxygen Species; Raman Scattering; Nanosheets.

1. Introduction

Airborne and waterborne pathogens are responsible for causing numerous diseases, infections, allergies and toxic reactions[1-5]. These microorganisms are easily spread in a non-uniform manner with air and water currents[1-5]. The concentration of these biological threats in the environment and water supplies greatly fluctuate depending on numerous factors including human activity and environmental exposure [6-10]. Their existence in high concentrations serves as an indication of contamination, thus the implementation of regulators in the industrial, commercial and consumer markets, to reduce, or ideally prevent microbial colonisation and proliferation has become increasingly vital to human health[11]. Sterilisation methods utilising ultraviolet radiation, ions and high pressure and temperature treatments have been used as a means of reducing the number of pathogenic microorganisms[12-16]. However, these techniques have been deemed inefficient and potentially toxic to human health.

Mechanical filtration technologies have emerged as a viable means of controlling aerosols and hydrosols. In particular, micro- and nano- fibres provide chemical-free, cost-effective and environmentally friendly approach for enhancing filtration efficiency and performance[17-22]. Fibrous filtration systems consist of a layer of randomly aligned fibres oriented across the direction of flow[23]. These membranes have an interconnected pores and/or

finer pore structure that allows an effective permeability resulting a higher throughput in comparison to conventional filters[24]. The individual fibres in the mesh typically have a circular or rectangular cross-section, with a small fibre diameter distribution and are ideally porous[23]. The exploitation of fibrous filtration systems has increased over the last 20 years due to their ability to capture particles and microorganisms proficiently via factors including direct interception by fibres, inertial impaction, Brownian movement, convection, gravitational settling and electrostatic effects. One of the challenges in currently used fibre-based filtration systems is that the microorganisms trapped within the fibre meshes are able to survive and proliferate, consequently leading to contamination of air-handling systems, ventilation and air conditioning units and water supply systems [1, 25-32]. This ultimately diminishes filter efficiency and consequently leads to the release of pathogenic microorganisms both dormant and germinating, into the environment and water supplies[1]. Therefore, various antimicrobial treatments, such as antibiotics and antivirals, have been incorporated into filter media to bestow antimicrobial activities[33-37]. However, microorganisms have the ability to resist such treatments from working against it (antimicrobial resistance) and rendering them ineffective. For this reason, the use of alternative antimicrobial agents has been extensively explored.

Graphene-based 2D nanomaterials, such as graphene oxide (GO), porous graphene nanosheets and reduced GO, have demonstrated effective antibacterial properties[38-42]. These carbon-based materials having a higher surface area to volume ratio results in a stronger potency toward bacteria[43-45]. In particular, studies have shown GO to possess the highest antibacterial activity among its counterparts[38]. GO is one of the most extensively explored materials for a wide range of applications. GO is the product formed from the chemical exfoliation of graphite oxide into mono-sheets and is composed of a single atomic plane of carbon molecules arranged in a honeycomb structure with carboxylic groups at its edges and hydroxyl groups in its basal plane[46, 47]. As a result, GO is hydrophilic making it ideal for filtration applications. Recent studies have revealed that a multitude of microorganisms can be inactivated by GO, such as *Escherichia coli*, *Staphylococcus aureus*, Xanthomonas oryzae pv. Oryzae, *Pseudomonas aeruginosa*, *Streptococcus faecalis* and *Candida albicans*[38, 48-54].

The purpose of this study is to fabricate novel antibacterial fibre meshes loaded with GO nanosheets were fabricated using pressurised gyration. In this work, GO nanosheets were synthesised, characterised and the minimum concentration required to inhibit bacterial growth was investigated. The as-prepared nanosheets were incorporated into polymeric fibres using pressurised gyration.

The physical and chemical structure of the nanocomposite fibres were analysed in detail. The antibacterial performance of the fibrous meshes were measured against *E. coli*. The resulting meshes demonstrate a promising scope to inhibit microbial colonisation and proliferation.

2. Experimental Procedures

2.1 Materials

Graphite powder (<20 μm), poly(methyl 2-methylpropenoate) (PMMA) (M_w ~ 120,000 g/mol), chloroform, concentrated sulfuric acid (98%), sodium nitrate, potassium permanganate, hydrogen peroxide (30 wt% in water), ethanol, hydrochloric acid (37%), Luria Bertani (LB) broth, phosphate buffered saline (PBS), glutaraldehyde, 1% osmium tetroxide and hexamethyldisilazane were purchased from Sigma-Aldrich (Gillingham, UK). LB agar was purchased from Invitrogen (Paisley, UK). LIVE/DEAD BacLight Bacterial Viability and Counting Kit was purchased from ThermoFisher Scientific (Paisley, UK). 2-(3,6-diacetyloxy-2,7-dichloro-9H-xanthen-9-yl)benzoic acid (DCFH) was purchased from Cayman Chemicals (Michigan, US). All solvents and chemicals were of analytical grade and used as received or as instructed by the supplier.

2.2 Synthesis of Graphene Oxide Nanosheets

GO nanosheets were prepared by following a modified Hummers' method[55]. Concentrated sulfuric acid (69 mL) was added to graphite flakes (3.0 g) and sodium nitrate (1.5 g), followed by slowly adding potassium permanganate (9.0 g). The reaction temperature was maintained below 20 °C. The initial reactants were heated to 35 °C and stirred for 12 hours. Potassium permanganate (9.0 g) was again added, and was stirred for 8 hours which was maintained at a temperature of 35 °C. The reaction was then cooled to room temperature (25°C) and put into an ice bath (~400 mL) with 30% hydrogen peroxide (3 mL).

The mixture was filtered through filter paper with a particle retention of 12-15 µm. The extracts were washed in succession with distilled water (200 mL), 30% hydrochloric acid (200 mL), and distilled water (200 mL). The remaining solid material was then washed twice with ethanol (200 mL) by centrifugation (9000 rpm for 4 hours, Eppendorf Centrifuge 5804). The purified product was dispersed in distilled water and sifted through a metal U.S. Standard testing sieve (161 µm) after sonication for 1 hour. The GO aqueous suspension was freeze-dried to obtain GO powder.

2.3 Fabrication of Graphene Oxide/ Poly(methyl 2-methylpropenoate) Fibres

Polymer solutions containing varying concentrations of GO nanosheets (0, 2, 4 and 8 wt%) were prepared in a three-step process for fibre forming using

pressurised gyration. (i) GO was added to chloroform as described in Table 1 and sonicated (Branson Ultrasonics Sonifier S-250A) for 24 hours in an ice bath to homogenously disperse GO nanosheets. Then, PMMA was dissolved in chloroform and mixed with the GO dispersion under magnetic stirring for 1 hour. 8 wt% was easily processed by pressurised gyration[56].

The as-prepared GO/PMMA suspensions were processed using pressurized gyration. The experimental setup was made up of a rotating aluminium cylindrical pot (6 cm diameter, 3.5 cm height) with 24 circular orifices (0.5 mm in diameter) along its central horizontal axis. The bottom of the pot was attached to a high-speed rotary motor, whilst the top was connected to a nitrogen gas supply. 5 mL aliquots of the GO/PMMA suspension were loaded into the pot. The system was immediately switched on and allowed to reach the apparent maximum speed of 36000 rpm before applying 0.1 MPa of pressure (nitrogen gas) to the rotating pot. The system was spun until all the suspension had been ejected from the pot. Pressurised gyration experiments were performed at controlled temperature (21±2 °C) and relative humidity (55 ± 3.5%). All fibre samples were prepared in triplicate.

2.4 Characterisation

GO was flushed onto fresh-cleaved mica discs and analysed using Atomic Force Microscopy (AFM) (Veeco) imaging in a tapping mode with a scan rate of 0.5 Hz. Image analysis was carried out using XEI software. Surface tension of the GO/PMMA suspensions were measured using the Du Nouy (Ring) Tensiometry Method and a KRUSS K9 Tensiometer. The surface tension of water was also calculated against a reference value of 73 mN/m. Four measurements were repeated for each suspension to calculate an average. Solvent evaporation during the spinning process induces changes in the viscosity of the plyometric suspensions. Viscosity was calculated using a Brookfield digital rheometer (model DV – III). Morphology of the resulting GO/PMMA hybrid fibres were analysed using a Scanning Electron Microscope (SEM) (JEOLJSM-6301F). The accelerating voltage was kept at 5 kV. Nanocomposites were gold-coated for 90 seconds using a Quoram Q150R ES sputter coater. The average size of fibres was calculated the diameter of 100 fibres using SEM micrographs at low magnifications and ImageJ software (National Institutes of Health, Bethesda, MD, USA). SEM imaging was also performed on fixed fibres post incubation with bacterial cells. Fibres were fixed using glutaraldehyde and 1% osmium tetroxide. The samples were then dried using a series of ethanol and hexamethyldisilazane solutions.

Raman mapping was performed using an inVia Raman microscope. The spectra of samples excited at the wavelength of 514.5 nm with the power of less than 1 mW, spot size of ~1 μm (with a ×50 objective lens (numerical aperture = 0.55)), pixel size of 1 μm (for both x and y directions) and spectral resolution of 2.5 cm^{-1}. The low power was used to avoid heating. The final spectrum of each sample was the average result of three acquisitions. The intensity of the peak was determined from the value of D and G peaks. FT-IR spectra of GO, PMMA and the 8 wt% GO/PMMA fibre samples were determined using a Bruker Optics Tensor-27 FT-IR spectrometer. The spectra were recorded in the wavenumber range of 4,000–500 cm^{-1}. The samples were pressed into pellets by mixing with KBr. Detailed Raman spectra of the 8 wt% GO/PMMA fibres were measured using laser excited 532 nm and at the power of 6 mW.

2.5 Antibacterial Activity of Graphene Oxide Nanosheets and Graphene Oxide in Polymeric Fibres

Escherichia coli K12 was chosen as the model microorganism to assess the antibacterial properties of the synthesised GO and the GO loaded polymeric fibres.

For GO, a single colony of *E. coli* was suspended in 30 mL of sterile LB broth and incubated at 37°C and 150 rpm for approximately 4 hours. 3 mL of this

suspension was then added to GO suspensions, containing 0.5, 1.0 and 2.0 w/v% of GO in 27 mL of sterile LB broth. The suspensions were incubated for 24 hours at 37^{o}C and 150 rpm (Orbital Shaker S150, Stuart).

Flow cytometry (Guava easyCyte®, Merck, UK) was used to determine the viable cell counts with a LIVE/DEAD BacLight bacterial viability kit and InCyte software (Merck, UK). A stock solution containing both dyes (propidium iodide and SYTO®9) was prepared according to manufacturers' recommended protocol. The staining solution was added to the suspensions and incubated in the absence of light at room temperature (22^{o}C) for 15 minutes[57]. Cells were then acquired using a calibrated Guava easyCyte® flow cytometer (Merck, UK) and InCyte software (Merck, UK)[57]. Acquisition gates/regions were outlined using positive (*E. coli* only), negative (media and GO only), fluorescence minus one and compensation controls. *E. coli* populations were identified and gated using forward and side scatter channels. The gated *E. coli* population was then analysed using green and red fluorescent channels (live populations - SYTO®9, and dead populations - propidium iodide). 50,000 events were collected overall. FlowJo (V10, TreeStar, USA) was used to enumerate the number of cells in both live and dead populations.

For GO/PMMA fibres, 0.02 g of each GO/PMMA sample and LB agar plates were sterilised using UV light for 1 hour. A single colony of *E. coli* was harvested using a sterile plastic inoculating loop and suspended in sterile LB broth. The suspension was incubated at 37^{o}C and 150 rpm until the culture reached its mid-exponential phase (at approximately 4 hours, and OD_{600} of 0.035). The culture was then centrifuged at 4600 rpm for 15 minutes (accuSpin 3R, Fisher Scientific). The supernatant was removed. The cells were then pelleted by centrifuging (4600 rpm for 15 minutes) the suspensions. The cells were collected and washed with PBS, before being re-suspended in PBS. The number of live cells present in each suspension was counted using the colony counting method.

The GO/PMMA fibres were incubated with the *E. coli* suspensions for 24 hours at 37^{o}C and 150 rpm. Pure PMMA fibres with no GO nanosheets were used as the control group. The number of live cells remaining in the suspension was estimated using the colony counting method. The number of cells before and after incubation were compared and the bacteria cell reduction was calculated. Experiments were repeated on three separate occasions.

2.6 Reactive Oxygen Species Generation

Reactive oxygen species (ROS) production was measured using the peroxide dependent oxidation of DCFH to form the fluorescent compound 2',7'-dichloro-3',6'-dihydroxy-3H-spiro[2-benzofuran-1,9'-xanthen]-3-one (DCF)[58]. 0.01g of 8 wt% GO/PMMA fibres were incubated in 1.5 mL of PBS, alongside 1.5 mL of a 1:1 dilution of 30% hydrogen peroxide in PBS (positive control) and PBS only (negative control). Then 10 µM of DCFH were added to each well (in the 24 well plate) incubated at 37°C and 150 rpm using a fluorimeter with incubation capacity, the Fluoroskan Ascent - Labsystems. The fluorescent intensity of DCF was measured every 10 minutes for 12 hours using the aforementioned instrument with excitation at 485 nm and emission at 535 nm. The experiment was completed in triplicate and each sample was measured 37 times.

2.7 Imaging Using Stimulated Raman Scattering

Stimulated Raman scattering (SRS) imaging was performed using an InsightX3 fs laser (Newport SpectraPhysics), 1045 nm (as the Stokes beam) and 800 nm (as the pump and probe beam) output. The powers at the sample were 2 mW for the 1045 nm beam and 4 mW for the 800 nm beam. The beams were chipped to generate pulses (ps) and spatially covered in the spectral converging unit (Newport SpectraPhysics)[59]. The temporal overlay was scanned via the Spectral Focusing Timing and Recombination Unit (SF-TRU) to produce Coherent Raman Scattering (CRS) spectra of the samples. Imaging was achieved

on a modified confocal microscope (Olympus FV3000), using a 1.2 NA water immersion objective (Olumpus UPlanSApo 60x). SRS was recorded in the forward direction, with a 1.4NA oil immersion condenser (Nikon D CUO DIC). SRS signals were detected using a photodiode and LockIn amplifier (APE SRS detection set) and the 1045 nm stokes beam was blocked from the photodiode using the following filters (Chroma CARS 890-210 and 950 nm 4OD short pass filter Edmund Optics). The samples were mounted between 2 coverslips.

3.Results and Discussion

3.1 Morphologies of Graphene Oxide

The morphology of as-prepared GO aqueous suspension deposited on mica was examined using AFM (Figure 1). The thickness of single GO sheets was ~0.72 nm according to the literature [60]. The AFM height profile of GO prepared in this study illustrates a thickness of 0.85 ± 0.12 nm for most of the GO single sheets, confirming their monolayer nature. The AFM image shows irregular shapes of GO nanosheets with a typical lateral dimension in the range of 1 – 4 μm.

3.2 Antibacterial Effect of Graphene Oxide Suspensions

E. coli K12 was chosen as a model bacterium to assess the antibacterial properties of GO. The proportion of live and dead cells after seeding with GO was determined using flow cytometry. LB broth without GO particles was used

as a control. The fundamental principle of the use of flow cytometry to determine antibacterial activity relies on the use of fluorescent dyes, Propidium Iodide (PI) and SYTO®9, to allow a clear discrimination between dead and viable cells to be made. SYTO®9 is a green nucleic acid stain that stains both live and dead bacteria in a population, whilst PI is a red nuclear and chromosome counterstain that only penetrates bacteria with damaged membranes.

As shown in Figure 2, the 2 wt% GO dispersion suppressed the growth of *E. coli* the strongest, leading to a bacterial reduction of 96%. Exposure to 1 wt% GO resulted in the death of 91% of the bacterial population, whilst exposure to 0.5 wt% GO caused the death of 53% of the bacterial population (2% cell death detected in the control population).

A number of physical and chemical mechanisms have been proposed which may contribute to the antibacterial activity of GO. Akhavan *et al.* have suggested that antimicrobial actions of GO are typically induced by the physical interaction of the sharp edges of GO with the microbial membrane[61, 62]. During this interaction the GO particles pierce the cell membrane, thus disrupting plasma membrane integrity which outcomes in the release of intra- and sub-cellular contents. This phenomenon was further confirmed by other studies[63-66]. In

addition to membrane disruption, GO particles can wrap around and trap microbial cells in agglomerates, thus isolating them from their neighbouring environment[64, 67, 68]. This also indicate that the essential nutrients in starving cells is important for cell survival.

Researchers have also argued that GOs toxicity is indeed not attributed to its physical interaction with bacterial cells but instead a chemical reaction. Several studies have demonstrated that GO may inactivate bacterial cells without having any direct contact with the particles, therefore suggesting the physical interaction is not a major part of the toxicity mechanism[69, 70]. Few other research work has shown that the antibacterial activity of GO is mainly induced by oxidative stress. During this cascade GO triggers either the ROS-dependent or ROS-independent pathway. Activation of these pathways inhibits bacterial metabolism, disturbs important functions at cellular or sub-cellular, causes intra- and sub-cellular protein inactivation and induces lipid peroxidation, consequently leading to cellular inactivation, programmed cell death (necrosis or apoptosis)[38, 51].

It has evidently been explored that the antibacterial actions of GO are the result of physical-chemical interactions between microbiota and GO, and thus, all

three mechanisms suggested could be responsible for the results observed in this experiment.

3.3 Characterisation of Graphene Oxide/Polymer Suspensions

3.3.1 Surface Tension

GO/PMMA nanocomposite fibres were prepared by pressurised gyration of PMMA and GO chloroform suspensions. The surface tension of PMMA solutions containing various concentrations of GO are shown in Figure 3(a). As can be seen, the surface tension of the nanofluids decrease with increasing GO concentration. However, the range of decrease is not large, as only a 2.4% reduction was observed. The pure PMMA solution had an average surface tension of 28.5 ±1.2 mN/m, this dropped to 28.1 ±0.8 mN/m upon the addition of 2 wt% GO. In this instance GO behaves as a surfactant and increases the electrostatic forces between particles and consequently reduces surface energy and surface tension[71]. Both 4 and 8 wt% GO reduced the average surface tension to 27.8 ±1.1 mN/m.

3.3.2 Viscosity

Figure 3(b) demonstrates the effect GO concentration has on the viscosity of PMMA chloroform solution. It can be seen that the introduction of a small quantity of GO initially reduces the average viscosity from 49.3 ±0.2 mPa·s to

47.7 ±0.6 mPa·s. After which, the increase in GO concentration results in an increase in average viscosity, with 4 wt% GO leading to an average viscosity of 48.9 ±0.3 mPa·s and 8 wt% GO resulting in 48.6 ±0.6 mPa·s. The introduction of a small quantity of GO nanosheets was found to initially decrease viscosity as GO behaved as a surfactant[72, 73]. Thereafter, the viscosity of the solution was found to increase with the volumetric loading of GO nanosheets. When in chloroform suspension, GO nanosheets can easily form clusters and aggregates due to its poor compatibility with chloroform. Clustering and aggregation increase the hydrodynamic diameter of nanosheets leading to the increase in viscosity[74].

3.4 Graphene Oxide/Polymer Fibres

3.4.1 Characterisation of Nanocomposite Fibres

A PMMA-chloroform system was selected for this work as previous work has considered this combination highly suitable for composite fibre fabrication and filtration applications[75-77].

SEM micrographs of the GO/PMMA fibres prepared from the suspension systems showed the fibres formed were generally continuous, porous and had a circular cross section. The successful formation of fibres suggests that for all four GO/PMMA suspensions the intermolecular entanglement and chain overlap

was appropriate to stabilise the polymer jet emitting from the orifices on the pressurised gyration vessel, despite the increasing GO load. The formation of non-beaded fibres also indicates the homogenous dispersion of GO nanosheets in the polymer solution.

From Figure 4 it can be said that the concentration of GO greatly dictates fibre morphology. The introduction of a small quantity of GO drastically decreased the average fibre diameter from 3.9 ±2.0 μm to 1.4 ±0.9 μm. A positive correlation can then be observed between the concentration of GO and the average fibre diameter; as the GO concentration increases within the polymer matrix, the fibres become larger in diameter with a wider fibre diameter distribution. This observation can be related to the viscosity measurements recorded for the corresponding polymer solutions. Previous literature has proven that the solution parameters and processing conditions are responsible for changes in fibre morphology during pressurised gyration[78]. However, as the processing parameters were consistent in this work it can be theorised that the GO incorporation is the sole factor influencing fibre morphology.

The trend seen in the fibre diameters can be attributed to the rheological properties of the GO/PMMA suspension. In this instance GO acted as a surfactant at low concentrations (2 wt%), thus prevented the formation of a

strong polymer network and consequently lowered viscosity and surface tension. This gave rise to thin fibres. At higher GO concentrations (4 and 8 wt%), the solution viscosity of the suspensions slightly increased, and though the applied centrifugal force and pressure difference was sufficiently high to modify the surface tension in supporting the fibre preparation, it was not strong enough to give rise to thin fibres. In addition, the dispersion of GO in the PMMA had a significant impact on fibre morphology. At low GO content, the nanosheets were dispersed relatively well in the polymer, hence the fibre diameter and distribution rates are reduced when compared to the others. High concentration of GO content resulted in improved Van der Waals forces between the GO nanosheets and the PMMA, therefore resulting in the agglomeration of GO and non-uniform dispersion of GO thus leading to a broad fibre diameter distribution [79-82].

Fibre topography included spherical surface pore structures, and its formation has been illustrated using the breath figures model (Figure 4(g)[77, 83]. Such surface features are ideal for filtration applications, as not only do they increase the surface area for bacteria to interact with, but they also work to physically trap the bacteria within their pits.

Raman mapping was used to identify GO in GO-loaded PMMA fibres, as shown in Figure 5. The dark areas in Figure 5(a) is GO, confirmed by Raman spectroscopy in Figure 5(b). The D peak (at 1350 cm^{-1}) arises from the breathing mode of the sp^2 hybridized carbon and induces the disorders including edges, functional groups, and structural defects[84]. The intensity ratio of D and G peaks (I_D/I_G) for GO was 0.88. The sharp peak seen at ~2800 cm^{-1} is due to the single layer of GO in the fibre. It also indicates that the GO may have some defects as a result of fibre formation during pressurised gyration. This peak can also be attributed to the overtone of the D′ peak and is called a 2D′ peak. Figure 5(c, d) show individual Raman mapping images of D peak and G peak within the surface of the PMMA fibre.

The FT-IR spectra of GO, PMMA and GO/PMMA fibres (Figure 6) showed the specific functional groups of C−O−C (~1000 cm^{-1}), C−O (1230 cm^{-1}), C=C (~1620 cm^{-1}) and C=O (1740–1720 cm^{-1}) bonds. The band in the region of 3600–3300 cm^{-1} corresponds to O−H stretching vibrations of hydroxyl and carboxyl functional groups of GO[85, 86]. The spectrum of PMMA showed a peak around 3500 cm^{-1} and a very sharp signal at 1732 cm^{-1}, corresponding to the stretching of hydroxyl and ester groups present in PMMA, respectively[87]. Typical bands at 987 and 1453 cm^{-1} correspond to O–CH_3 bending and stretching deformation of PMMA, respectively, while bands at 1730 and 1250

cm^{-1} belong to stretching of C=O groups[87]. Bands at 1065 and 1197 cm^{-1} represent C–O stretching vibration and chain vibration, respectively. The other bands in the 3000–2800 cm^{-1}, 1490–1275 cm^{-1} and 900–750 cm^{-1} spectral regions belong to CH_3 and CH_2 vibrational modes[88, 89]. The typical characteristics of GO in the FT-IR spectrum (Figure 6) are peaks conforming to the C=O stretching vibrations from carbonyl and carboxylic groups at 1735 cm^{-1}, C-C in aromatic ring at 1639 cm^{-1} and C–O–C stretching from epoxy groups at 1072 cm^{-1}, which confirms the existence of oxygen-related functional groups. Furthermore, a peak at 1382 cm^{-1} and a wide-ranging band at 3400 cm^{-1} are attributed to the stretching vibration of O–H groups[86, 90].

After pressurised gyration, the FT-IR spectra of GO-covered PMMA reveal typical peaks corresponding to PMMA (3001 and 2954 cm^{-1} for C–H stretching, 1735 cm^{-1} for C=O stretching, 1200 and 1148 cm^{-1} for C–O stretching) as well as O–H stretching peak at 3500 cm^{-1}, which is due to oxygen functional groups of GO[91]. These spectra clearly represent the chemical interaction between GO and PMMA. Previously reported work on CNT-PMMA nanocomposites showed the unpaired electrons associated with CNT activates the p-bond of CNT, which binds CNT with polymer chain[92]. GO has comparable physio-chemical characteristics and high specific surface area (in comparison to CNTs). Both

compounds show similar bands in their FT-IR spectra, suggesting that the GO nanosheets are successfully grafted onto the surface of PMMA.

Detailed Raman spectroscopy of the GO/PMMA fibres was performed. The Raman spectrum was compared with those of 'free' GO to investigate the effect of GO on the surface of PMMA. The Raman spectrum of GO/PMMA fibres is presented in Figure 7. The typical Raman peak of GO was characterized by a G band (at ca. 1604 cm-1) and D (1354 cm^{-1}) bands which represent the sp^2 hybridisation of carbon atoms and the breathing mode of k-point phonons of A1g symmetry respectively[86, 90]. The six characteristic bands of GO-covered PMMA observed at 2953, 2848, 1739, 1605, 1453, 1348 cm^{-1}. Raman band 2953 represents the C-H stretching vibration[93]. The band at 1739 cm^{-1} is ascribed to the combination band arising out of ν(C=C) and ν(C–COO) modes[93].

PMMA triggers slight hardening and wide-ranging of the G and 2D peaks. Both G and D peaks are slightly shifted from 1604 and 1354 to 1605 and 1348 cm^{-1} respectively owing to the residual compression strain persuaded by the temperature involved in fibre preparation. The D band indicates defects including vacancies, grain boundaries, and amorphous carbon species[90, 94]. In the GO-covered PMMA fibres, a small change in the D peak is observed, resulting in a slight increase in the ID/IG, undoubtedly demonstrating that sp^3

grafting sites are being introduced onto the carbon lattice. The ID/IG ration can be used to calculate the interdefect distance and number density of grafted sites per unit area[95, 96]. The spectra for graphene related materials show D, G and 2D peaks, allowing the classification of these materials in different hybridisation profiles[97], where the defect density does not exceed the Tunstra-Koenig limit[95]. It has been evidently proved that this peak arises from double resonance in addition to phonon confinement[98]. The decrease in intensities of both peaks (D and G) also indicates improved graphitization. For monolayer graphene, there is a sharp peak at ca. 2848 cm^{-1} which typically represent of the number of layers of graphene. In the current work, the band is observed to be sharp, indicating that as-prepared GO comprises single layer with defects. These defects are also an indication of processing of fibre preparation[99].

Both FT-IR and Raman spectroscopy of the GO/PMMA nanocomposite fibres confirmed the presence of GO on the fibre surface. This fibre characteristic plays a vital role in the antimicrobial mechanism of action of the fibres.

3.4.2 Antibacterial Activity of Graphene Oxide in Polymeric Fibres

The antibacterial activity of GO in PMMA fibres was investigated using *E. coli* K12. As discussed above, antibacterial activity of pure GO nanosheets was

observed at a concentration of 2 wt%, therefore the fibres investigated had GO concentrations of 0, 2, 4 and 8 wt%. In comparison to pure PMMA fibres, the results confirmed that GO-covered PMMA fibres proficiently reduced the number of *E. coli* K-12 cells. The percentage bacterial reductions are shown in Figure 8. The PMMA fibres (negative control) exhibited no antimicrobial activity, as a bacterial increase of 25 ±7.9% was observed. In contrast, all the GO/PMMA fibre meshes displayed antibacterial behaviour. At the lowest GO-covered PMMA concentration, 45 ±2.2% of the total *E. coli* K-12 viability was significantly reduced, while 70 ±2.4% of the total bacteria was reduced after incubation with PMMA with 4 wt% GO. The maximum antibacterial activity was noticed in the case of 8 wt% GO loaded-PMMA, with an 85 ±1.4% reduction in cell numbers being observed. The results showed that the antibacterial activity of the GO/PMMA fibre meshes are a function of GO concentration. The bacterial reduction observed with 8 wt% GO loaded-PMMA is comparable to 8 wt% graphene nanoplatelet loaded-PMMA fibres, where a reduction of 85 ±5% was noted[100]. GO loaded-PMMA fibres present themselves as a favourable alternative, as GO is more easily accessible when compared to pure graphene. The antimicrobial properties of GO loaded-PMMA fibres were less potent than free GO, however incorporating GO into fibres broadens the number of applications GO can be used in. Also, increasing the quantity of GO in PMMA provide evidences for bacteria to interact with GO, therefore causing the

decreased levels of *E. coli*. Our results are consistent with other previously reported work revealing the concentration-dependent GO toxicity[38, 100, 101].

Pure PMMA fibres proved to have little interference with normal bacterial growth and proliferation as a percentage increase in bacterial numbers was observed, despite previous studies showing the contrary[100]. This suggests that the PMMA had no antibacterial properties, and the antibacterial activities seen with the GO/PMMA fibre meshes are solely due to the presence of GO.

The antibacterial activity of PMMA fibres containing 2 wt% of GO were initially tested. These fibres exhibited antibacterial properties with an average bacterial reduction of 45 ±2.2%. This percentage reduction is significantly lower than the observed reduction of pure GO nanosheets. This is due to the GO nanosheets being embedded within the PMMA fibres and not just on the surface. Increasing the GO concentration to 4 wt% increased the antibacterial action of the fibres, showing bacterial reduction at 70%. This indicates a higher concentration of GO nanosheets on the fibre surface, therefore there is more GO for the bacteria to interact with. Increasing the GO concentration further to 8 wt% significantly enhanced the antibacterial action of the fibre, as these fibres showed the strongest antibacterial activity with a cell inactivation percentage of 85 ±1.4% being achieved. Previous literature has reported different minimum inhibition

concentrations (MICs) for GO. Nanda *et al.*, have reported the MIC to be 1 µg/mL[102]. Liu *et al.*, reported the MIC to be 80 µg/mL, with a 91.6% inhibition[38]. Whilst Shubha et al., have reported a MIC of 50000 µg/mL[103]. In this research, when 8 wt% fibres were used, the GO concentration was 530 µg/mL.

A multitude of GO-based antibacterial mechanisms has been explained in literature. However, as the GO nanosheets are not floating free in the bacterial suspension, but instead they are trapped within PMMA fibres and not protruding from the fibre surface, it can be presumed that in this instance the antibacterial mechanism of action involves a chemical reaction, such as oxidative stress.

3.4.3 Reactive Oxygen Species Generation

The oxidative stress caused by GO has been reported as a main toxicity mechanism[104]. In this work, the prepared GO/PMMA nanocomposite fibres were studied to see if they produce ROS. From Figure 9 it is evident that ROS production began at approximately 70 minutes and steadily increased over the 400-minute incubation period. DCFH can react with different ROS such as hydrogen peroxide, HO and other free radicals therefore the delay in the signal may be explained by the participation of other ROS than the hydrogen peroxide

used in the control. Also while the hydrogen peroxide present in the control is readily available to reduce the probe while the GO fibres ROS generation may depend on the generation of an intermediary[105]. Overproduction of ROS is a principal representative of oxidative stress, hence the measurement of ROS indicates ROS-mediated oxidative stress is the likely antibacterial mode of action[104, 106]. It is thought that the GO present on the surface of the fibre produces ROS via the singlet oxygen-superoxide anion radical pathway, which plays a significant role in release of cytochrome c and other pro-apoptotic proteins, which in turn mediate caspase activation and apoptosis through the generation of protein radicals, activation of lipid peroxidation, DNA-strand breakage, modification to nucleic acids, gene expression through activation of redox-sensitive transcription factors and modulation of inflammatory responses through signal transduction[107-114].

3.4.4 Post Treatment Characterisation

3.4.4.1 Imaging Using Stimulated Raman Spectroscopy

GO revealed a strong signal within the SRS channel, this signal has a broad spectral profile which can be attributed to pump-probe interactions within the GO, rather than more chemically specific Raman vibrations[115]. PMMA is also visualised in the SRS channel, the signal from the PMMA shows a strong peak at 2940cm^{-1} which can be attributed to the CH_3 Raman vibrations. Figure 10 a)

compares the spectra of the PMMA and GO-PMMA-bacteria. The intensity of the SRS signal in GO-PMMA is much higher than PMMA alone. Figure 10 b shows the results of Multi Curve Regression (MCR) analysis[116] performed on a hyperspectral data stack of the sample containing PMMA, GO and bacteria. The analysis enabled the signal from the PMMA shown in red from the GO shown in green to be separated based on their spectral properties. The images show flakes of GO distributed across the surface of the PMMA fibres, which contribute to the high killing efficacy of composites towards *E. coli* (which is also demonstrated from antibacterial activities of composites towards programmed cell death of bacteria).

3.4.4.2 Scanning Electron Microscopy

SEM analysis was used to examine the interaction between the microbes and the 8 wt% GO/PMMA fibres and to assess any changes in cell morphology. **Figure 11** shows the bacterial cells, *E. coli*, on the 8 wt% GO/PMMA fibres.

In the presence of 8 wt% GO/PMMA fibres the bacteria showed changes in cell morphology. Healthy prokaryotic cells form a capsule, a protective layer rich in sugars, proteins and alcohol, and/or lipids that help stick bacteria to each other as well as onto the substrate [117, 118]. In addition to this layer, Gram-negative bacteria (*E. coli*) also contain an asymmetric outer membrane whose inner

leaflet is composed largely of glycerophospholipids and an outer leaflet composed of lipopolysaccharides. These capsules cover the entire bacteria as well as the whole space between bacteria. As shown in **Figure 11**, exposure of the bacterial cells to 8 wt% GO/PMMA fibres caused capsule degradation, as the capsule is removed from the exposed parts of bacteria. In addition, visible damage on the *E. coli* cell surface can be seen as the cells have a distorted structure. This characteristic is symptomatic of ROS degradation[119, 120].

The toxic effect of the 8 wt% GO/PMMA on bacterial cells is evident from this research, however their effect on human cells needs to be further investigated. Existing literature gives conflicting opinions, some articles state that GO is cytotoxic, whilst others state that composited GO is not cytotoxic to mammalian cells and can be used in various biomedical constructs [121-124].

4.0 Conclusions

This research showcases the antibacterial activity of prepared GO nanosheets and GO/PMMA nanocomposite fibres for filtration applications. The results collected in this study support the hypothesis that as-prepared GO nanosheets are able to retain their antibacterial properties when processed into composite fibres, therefore demonstrating their effectiveness in the real world.

GO/PMMA nanocomposite fibre meshes were successfully prepared using pressurised gyration and characterised by SEM, FT-IR, Raman mapping, Raman spectroscopy and stimulated Raman mapping. Average fibre diameters ranged between 1.4 μm and 3.9 μm. FT-IR and Raman analysis confirmed the presence of GO nanosheets on the surface of the polymeric fibres. The interaction between bacterial cells and GO/PMMA fibres, demonstrated the fibres antibacterial properties. Colony counting method results showed 8 wt% GO/PMMA fibre meshes to have the strongest antibacterial activity, as a bacterial reduction of 85 ±1.4% was observed, which is stronger to what was observed with GO/poly (vinyl alcohol) fibres when considering poly (vinyl alcohol) is water soluble[125]. These studies showed the biocidal activities of GO to be retained when processed using pressurised gyration. The antibacterial properties of the nanocomposite fibres were dose-dependent, as average bacterial reductions steadily rose from 45 ±2.2% to 85 ±1.4%. The cytotoxicity properties of the nanocomposite fibres are attributed to the production of oxidative stress. Increasing the concentration of GO in the fibres, the bacteria have a higher chance to interact with the toxic GO nanoparticles on the surface of the fibres (as confirmed by post-treatment SEM and stimulated Raman spectroscopy). Compared with previous reports of antimicrobial GO, this work demonstrates the translation of lab-based science to real life application. With the knowledge obtained in this study it can be concluded that GO nanosheets

retain their antibacterial properties when composited in non-water-soluble polymeric fibres, thus providing insight of their potential in a number of applications including filtration.

Acknowledgements

This work was supported by EPSRC grant EP/N034228/1. The authors would like to thank Dr Melisa Canales for her assistance in the Healthy Infrastructure Research Group Laboratory, Department of Civil, Environmental and Geomatic Engineering, University College London, London, WC1E 7JE, UK. Sincerest gratitude to Dr Elaine Allan for use of her equipment in the ROS studies is also acknowledged. The SRS imaging was carried out using the CONTRAST facility which is funded by the EPSRC grant number EP/5009957/1.

CRediT Authorship Contribution:

Rupy Kaur Matharu: conceptualisation, methodology, validation, formal analysis, investigation, writing – original draft, writing – review and editing, visualisation, project administration. **Tanveer A Tabish**: validation, formal analysis, investigation, resources, writing – review and editing, visualisation. **Thithawat Trakoolwilaiwan**: methodology, validation, formal analysis, investigation, writing – review and editing, visualisation. **Jessica Mansfield**: methodology, formal analysis, investigation, resources, writing – review and editing, funding

acquisition. **Julian Moger**: methodology, formal analysis, investigation, resources, writing – review and editing, funding acquisition. **Tongfei Wu**: methodology, formal analysis, investigation, resources, writing – review and editing. **Cláudio Lourenço**: methodology, formal analysis, investigation, resources, writing – review and editing. **Biqiong Chen**: formal analysis, resources, writing – review and editing, supervision, project administration. **Lena Ciric**: writing – review and editing, funding acquisition. **Ivan P Parkin**: project resources, writing – review and editing. **Mohan Edirisinghe**: conceptualisation, methodology, resources, writing – review and editing, supervision, project administration, funding acquisition.

References:

[1] M.C. Verdenelli, C. Cecchini, C. Orpianesi, G.M. Dadea, A. Cresci, Efficacy of antimicrobial filter treatments on microbial colonization of air panel filters, J Appl Microbiol 94(1) (2003) 9-15.

[2] E.S. Chong, G.B. Hwang, C.W. Nho, B.M. Kwon, J.E. Lee, S. Seo, G.N. Bae, J.H. Jung, Antimicrobial durability of air filters coated with airborne Sophora flavescens nanoparticles, Sci Total Environ 444 (2013) 110-114.

[3] H. Burge, Bioaerosols - Prevalence and Health-Effects in the Indoor Environment, J Allergy Clin Immun 86(5) (1990) 687-701.

[4] S. Clark, R. Rylander, L. Larsson, Airborne Bacteria, Endotoxin and Fungi in Dust in Poultry and Swine Confinement Buildings, Am Ind Hyg Assoc J 44(7) (1983) 537-541.

[5] R.E. Dales, S. Cakmak, R.T. Burnett, S. Judek, F. Coates, J.R. Brook, Influence of ambient fungal spores on emergency visits for asthma to a regional children's hospital, Am J Resp Crit Care 162(6) (2000) 2087-2090.

[6] J.M. Daisey, W.J. Angell, M.G. Apte, Indoor air quality, ventilation and healthy symptoms in schools: an analysis of existing information., Indoor Air 13 (2003).

[7] L. Bonadonna, A. Marconi, Aerosol biologici e microclima abitativo. Effetti sanitari e problemi di determinazione., Ambiente. Risorse. Salute 104 (1990) 6.

[8] M. Pitzurra, A. Savino, C. Pasquarella, Microbiological environment monitoring., Annali di Igiene 9 (1997) 6.
[9] A.P. Jones, Indoor air quality and health, Atmos Environ 33(28) (1999) 4535-4564.
[10] J.D. Spengler, K. Sexton, Indoor Air-Pollution - a Public-Health Perspective, Science 221(4605) (1983) 9-17.
[11] P. Jain, T. Pradeep, Potential of silver nanoparticle-coated polyurethane foam as an antibacterial water filter, Biotechnol Bioeng 90(1) (2005) 59-63.
[12] G.B. Hwang, J.H. Jung, T.G. Jeong, B.U. Lee, Effect of hybrid UV-thermal energy stimuli on inactivation of S. epidermidis and B. subtilis bacterial bioaerosols, Sci Total Environ 408(23) (2010) 5903-5909.
[13] J.H. Jung, J.E. Lee, S.S. Kim, Thermal effects on bacterial bioaerosols in continuous air flow, Sci Total Environ 407(16) (2009) 4723-4730.
[14] B.U. Lee, S.H. Yun, J.H. Ji, G.N. Bae, Inactivation of S. epidermidis, B. subtilis, and E. coli bacteria bioaerosols deposited on a filter utilizing airborne silver nanoparticles, J Microbiol Biotechnol 18(1) (2008) 176-82.
[15] C.Y. Lin, C.S. Li, Control effectiveness of ultraviolet germicidal irradiation on bioaerosols, Aerosol Sci Tech 36(4) (2002) 474-478.
[16] J. Peccia, M. Hernandez, UV-induced inactivation rates for airborne Mycobacterium bovis BCG, J Occup Environ Hyg 1(7) (2004) 430-435.
[17] A. Podgórski, A. Bałazy, L. Gradoń, Application of nanofibers to improve the filtration efficiency of the most penetrating aerosol particles in fibrous filters, Chemical Engineering Science 61(20) (2006).
[18] R.S. Barhate, S. Ramakrishna, Nanofibrous filtering media: Filtration problems and solutions from tiny materials, J Membrane Sci 296(1-2) (2007) 1-8.
[19] R. Przekop, L. Gradon, Deposition and filtration of nanoparticles in the composites of nano- and microsized fibers, Aerosol Sci Tech 42(6) (2008) 483-493.
[20] J. Li, H.A. Chase, Applications of membrane techniques for purification of natural products, Biotechnol Lett 32(5) (2010) 601-608.
[21] N. Porcelli, S. Judd, Chemical cleaning of potable water membranes: A review, Sep Purif Technol 71(2) (2010) 137-143.
[22] A. Sato, R. Wang, H.Y. Ma, B.S. Hsiao, B. Chu, Novel nanofibrous scaffolds for water filtration with bacteria and virus removal capability, J Electron Microsc 60(3) (2011) 201-209.
[23] C.S. Wang, Electrostatic forces in fibrous filters - a review, Powder Technol 118(1-2) (2001) 166-170.
[24] A. Cooper, R. Oldinski, H.Y. Ma, J.D. Bryers, M.Q. Zhang, Chitosan-based nanofibrous membranes for antibacterial filter applications, Carbohyd Polym 92(1) (2013) 254-259.
[25] G.A. Mcfeters, D.G. Stuart, Survival of Coliform Bacteria in Natural Waters - Field and Laboratory Studies with Membrane-Filter Chambers, Appl Microbiol 24(5) (1972) 805-811.
[26] R.B. Simmons, S.A. Crow, Fungal Colonization of Air Filters for Use in Heating, Ventilating, and Air-Conditioning (Hvac) Systems, J Ind Microbiol 14(1) (1995) 41-45.
[27] D.G. Ahearn, S.A. Crow, R.B. Simmons, D.L. Price, S.K. Mishra, D.L. Pierson, Fungal colonization of air filters and insulation in a multi-story office building: Production of volatile organics, Curr Microbiol 35(5) (1997) 305-308.
[28] R.B. Simmons, D.L. Price, J.A. Noble, S.A. Crow, D.G. Ahearn, Fungal colonization of air filters from hospitals, Am Ind Hyg Assoc J 58(12) (1997) 900-904.
[29] D.L. Price, R.B. Simmons, I.M. Ezeonu, S.A. Crow, D.G. Ahearn, Colonization of Fiberglass Insulation Used in Heating, Ventilation and Air-Conditioning Systems, J Ind Microbiol 13(3) (1994) 154-158.

[30] T.H. Keuhn, D.Y.H. Pui, D. Vesley, C.D. Berg, M. Peloquin, Matching filtration with health requirements, ASHRAE Trans 97 (1991) 164-169.
[31] S.J. Kemp, T.H. Kuehn, D.Y.H. Pui, D. Vesley, A.J. Streifel, Growth of microorganisms on HVAC filters under controlled temperature and humidity conditions, Ashrae Tran 101 (1995) 305-316.
[32] T.H. Keuhn, D.Y.H. Pui, D. Vesley, C.D. Berg, M. Peloquin, Matching filtration with health requirements, ASHRAE Transactions 97 (1991) 164-169.
[33] G.H. Wagman, J.V. Bailey, M.J. Weinstein, Binding of Aminoglycoside Antibiotics to Filtration Materials, Antimicrob Agents Ch 7(3) (1975) 316-319.
[34] T. Ren, T.V. Dormitorio, M.Y. Qiao, T.S. Huang, J. Weese, N-halamine incorporated antimicrobial nonwoven fabrics for use against avian influenza virus, Vet Microbiol 218 (2018) 78-83.
[35] J.V. Cento, S. Barbaliscia, C.F. Perno, Biotech innovations in the prevention of respiratory infectious diseases, New Microbiol 40(3) (2017) 155-160.
[36] G. Borkow, J. Gabbay, Putting copper into action: copper-impregnated products with potent biocidal activities, Faseb J 18(12) (2004) 1728-+.
[37] B. De Gusseme, L. Sintubin, L. Baert, E. Thibo, T. Hennebel, G. Vermeulen, M. Uyttendaele, W. Verstraete, N. Boon, Biogenic silver for disinfection of water contaminated with viruses, Appl Environ Microbiol 76(4) (2010) 1082-7.
[38] S.B. Liu, T.H. Zeng, M. Hofmann, E. Burcombe, J. Wei, R.R. Jiang, J. Kong, Y. Chen, Antibacterial Activity of Graphite, Graphite Oxide, Graphene Oxide, and Reduced Graphene Oxide: Membrane and Oxidative Stress, Acs Nano 5(9) (2011) 6971-6980.
[39] C. Bora, P. Bharali, S. Baglari, S.K. Dolui, B.K. Konwar, Strong and conductive reduced graphene oxide/polyester resin composite films with improved mechanical strength, thermal stability and its antibacterial activity, Composites Science and Technology 87 (2013) 1-7.
[40] R.K. Matharu, L. Ciric, M. Edirisinghe, Nanocomposites: suitable alternatives as antimicrobial agents, Nanotechnology 29(28) (2018) 282001.
[41] Z.M. Marković, D.M. Matijašević, V.B. Pavlović, S.P. Jovanović, I.D. Holclajtner-Antunović, Z. Špitalský, M. Mičušik, M.D. Dramićanin, D.D. Milivojević, M.P. Nikšić, B.M. Todorović Marković, Antibacterial potential of electrochemically exfoliated graphene sheets, Journal of Colloid and Interface Science 500 (2017) 30-43.
[42] L.Q. Xu, Y.B. Liao, N.N. Li, Y.J. Li, J.Y. Zhang, Y.B. Wang, X.F. Hu, C.M. Li, Vancomycin-assisted green synthesis of reduced graphene oxide for antimicrobial applications, Journal of Colloid and Interface Science 514 (2018) 733-739.
[43] S.M. Dizaj, A. Mennati, S. Jafari, K. Khezri, K. Adibkia, Antimicrobial Activity of Carbon-Based Nanoparticles, Adv Pharm Bull 5(1) (2015) 19-23.
[44] S. Kang, M. Herzberg, D.F. Rodrigues, M. Elimelech, Antibacterial effects of carbon nanotubes: Size does matter, Langmuir 24(13) (2008) 6409-6413.
[45] C. Buzea, I.I. Pacheco, K. Robbie, Nanomaterials and nanoparticles: Sources and toxicity, Biointerphases 2(4) (2007) Mr17-Mr71.
[46] S. Park, R.S. Ruoff, Chemical methods for the production of graphenes, Nat Nanotechnol 4(4) (2009) 217-224.
[47] O.C. Compton, S.T. Nguyen, Graphene Oxide, Highly Reduced Graphene Oxide, and Graphene: Versatile Building Blocks for Carbon-Based Materials, Small 6(6) (2010) 711-723.
[48] S.R.V. Castrillon, F. Perreault, A.F. de Faria, M. Elimelech, Interaction of Graphene Oxide with Bacterial Cell Membranes: Insights from Force Spectroscopy, Environ Sci Tech Let 2(4) (2015) 112-117.
[49] J.H. Li, G. Wang, H.Q. Zhu, M. Zhang, X.H. Zheng, Z.F. Di, X.Y. Liu, X. Wang, Antibacterial activity of large-area monolayer graphene film manipulated by charge transfer, Sci Rep-Uk 4 (2014).

[50] J.N. Chen, X.P. Wang, H.Y. Han, A new function of graphene oxide emerges: inactivating phytopathogenic bacterium Xanthomonas oryzae pv. Oryzae, J Nanopart Res 15(5) (2013).
[51] S. Gurunathan, J.W. Han, A.A. Dayem, V. Eppakayala, J.H. Kim, Oxidative stress-mediated antibacterial activity of graphene oxide and reduced graphene oxide in Pseudomonas aeruginosa, Int J Nanomed 7 (2012) 5901-5914.
[52] S.S. Nanda, D.K. Yi, K. Kim, Study of antibacterial mechanism of graphene oxide using Raman spectroscopy, Sci Rep-Uk 6 (2016).
[53] R.F. Al-Thani, N.K. Patan, M.A. Al-Maadeed, Graphene oxide as antimicrobial against two gram-positive and two gram-negative bacteria in addition to one fungus., OnLine Journal of Biological Sciences 14 (2014) 230-239.
[54] M. Hu, Z. Cui, J. Li, L. Zhang, Y. Mo, D.S. Dlamini, H. Wang, B. He, J. Li, H. Matsuyama, Ultra-low graphene oxide loading for water permeability, antifouling and antibacterial improvement of polyethersulfone/sulfonated polysulfone ultrafiltration membranes, Journal of Colloid and Interface Science 552 (2019) 319-331.
[55] D.C. Marcano, D.V. Kosynkin, J.M. Berlin, A. Sinitskii, Z.Z. Sun, A. Slesarev, L.B. Alemany, W. Lu, J.M. Tour, Improved Synthesis of Graphene Oxide, Acs Nano 4(8) (2010) 4806-4814.
[56] A. Amir, S. Mahalingam, X. Wu, H. Porwal, P. Colombo, M.J. Reece, M. Edirisinghe, Graphene nanoplatelets loaded polyurethane and phenolic resin fibres by combination of pressure and gyration, Composites Science and Technology 129 (2016) 173-182.
[57] C. Bankier, R.K. Matharu, Y.K. Cheong, G.G. Ren, E. Cloutman-Green, L. Ciric, Synergistic Antibacterial Effects of Metallic Nanoparticle Combinations, Sci Rep-Uk 9(1) (2019) 16074.
[58] B. Kalyanaraman, V. Darley-Usmar, K.J. Davies, P.A. Dennery, H.J. Forman, M.B. Grisham, G.E. Mann, K. Moore, L.J. Roberts, 2nd, H. Ischiropoulos, Measuring reactive oxygen and nitrogen species with fluorescent probes: challenges and limitations, Free Radic Biol Med 52(1) (2012) 1-6.
[59] A. Zeytunyan, T. Baldacchini, R. Zadoyan, Module for multiphoton high-resolution hyperspectral imaging and spectroscopy, SPIE2018.
[60] J.W. Suk, R.D. Piner, J. An, R.S. Ruoff, Mechanical properties of monolayer graphene oxide, Acs Nano 4(11) (2010) 6557-64.
[61] O. Akhavan, E. Ghaderi, Escherichia coli bacteria reduce graphene oxide to bactericidal graphene in a self-limiting manner, Carbon 50(5) (2012) 1853-1860.
[62] O. Akhavan, E. Ghaderi, Toxicity of Graphene and Graphene Oxide Nanowalls Against Bacteria, Acs Nano 4(10) (2010) 5731-5736.
[63] I.Y. Kim, S. Park, H. Kim, S. Park, R.S. Ruoff, S.J. Hwang, Strongly-Coupled Freestanding Hybrid Films of Graphene and Layered Titanate Nanosheets: An Effective Way to Tailor the Physicochemical and Antibacterial Properties of Graphene Film, Adv Funct Mater 24(16) (2014) 2288-2294.
[64] J.N. Chen, H. Peng, X.P. Wang, F. Shao, Z.D. Yuan, H.Y. Han, Graphene oxide exhibits broad-spectrum antimicrobial activity against bacterial phytopathogens and fungal conidia by intertwining and membrane perturbation, Nanoscale 6(3) (2014) 1879-1889.
[65] J.L. He, X.D. Zhu, Z.N. Qi, C. Wang, X.J. Mao, C.L. Zhu, Z.Y. He, M.Y. Lo, Z.S. Tang, Killing Dental Pathogens Using Antibacterial Graphene Oxide, Acs Appl Mater Inter 7(9) (2015) 5605-5611.
[66] X.P. Wang, X.Q. Liu, H.Y. Han, Evaluation of antibacterial effects of carbon nanomaterials against copper-resistant Ralstonia solanacearum, Colloid Surface B 103 (2013) 136-142.
[67] A.R. Murray, E.R. Kisin, A.V. Tkach, N. Yanamala, R. Mercer, S.H. Young, B. Fadeel, V.E. Kagan, A.A. Shvedova, Factoring-in agglomeration of carbon nanotubes and nanofibers for better prediction of their toxicity versus asbestos, Part Fibre Toxicol 9 (2012).

[68] I.E.M. Carpio, C.M. Santos, X. Wei, D.F. Rodrigues, Toxicity of a polymer-graphene oxide composite against bacterial planktonic cells, biofilms, and mammalian cells, Nanoscale 4(15) (2012) 4746-4756.
[69] L. Hui, J.G. Piao, J. Auletta, K. Hu, Y. Zhu, T. Meyer, H. Liu, L. Yang, Availability of the basal planes of graphene oxide determines whether it is antibacterial, ACS Appl Mater Interfaces 6(15) (2014) 13183-90.
[70] J.D. Mangadlao, C.M. Santos, M.J.L. Felipe, A.C.C. de Leon, D.F. Rodrigues, R.C. Advincula, On the antibacterial mechanism of graphene oxide (GO) Langmuir-Blodgett films, Chem Commun 51(14) (2015) 2886-2889.
[71] S. Tanvir, L. Qiao, Surface tension of Nanofluid-type fuels containing suspended nanomaterials, Nanoscale Res Lett 7(1) (2012) 226.
[72] J. Cote Laura, J. Kim, C. Tung Vincent, J. Luo, F. Kim, J. Huang, Graphene oxide as surfactant sheets, Pure and Applied Chemistry, 2010, p. 95.
[73] T.M. McCoy, G. Turpin, B.M. Teo, R.F. Tabor, Graphene oxide: a surfactant or particle?, Current Opinion in Colloid & Interface Science 39 (2019) 98-109.
[74] S.M.S. Murshed, K.C. Leong, C. Yang, Investigations of thermal conductivity and viscosity of nanofluids, Int J Therm Sci 47(5) (2008) 560-568.
[75] U.E. Illangakoon, S. Mahalingam, P. Colombo, M. Edirisinghe, Tailoring the surface of polymeric nanofibres generated by pressurised gyration, Surf Innov 4(3) (2016) 167-178.
[76] U.E. Illangakoon, S. Mahalingam, K. Wang, Y.K. Cheong, E. Canales, G.G. Ren, E. Cloutman-Green, M. Edirisinghe, L. Ciric, Gyrospun antimicrobial nanoparticle loaded fibrous polymeric filters, Mat Sci Eng C-Mater 74 (2017) 315-324.
[77] U.E. Illangakoon, S. Mahalingam, R.K. Matharu, M. Edirisinghe, Evolution of Surface Nanopores in Pressurised Gyrospun Polymeric Microfibers, Polymers-Basel 9(10) (2017).
[78] S. Mahalingam, M. Edirisinghe, Forming of polymer nanofibers by a pressurised gyration process, Macromol Rapid Commun 34(14) (2013) 1134-9.
[79] M.P. Weir, D.W. Johnson, S.C. Boothroyd, R.C. Savage, R.L. Thompson, S.M. King, S.E. Rogers, K.S. Coleman, N. Clarke, Distortion of Chain Conformation and Reduced Entanglement in Polymer-Graphene Oxide Nanocomposites, Acs Macro Lett 5(4) (2016) 430-434.
[80] X.W. Wu, S. Mahalingam, A. Amir, H. Porwal, M.J. Reece, V. Naglieri, P. Colombo, M. Edirisinghe, Novel Preparation, Microstructure, and Properties of Polyacrylonitrile-Based Carbon Nanofiber-Graphene Nanoplatelet Materials, Acs Omega 1(2) (2016) 202-211.
[81] Y. Xu, B.K. Zhu, Y.Y. Xu, A study on formation of regular honeycomb pattern in polysulfone film, Polymer 46(3) (2005) 713-717.
[82] M. Weir, D. Johnson, S. Boothroyd, R. Savage, R. Thompson, S. King, S. Rogers, K. Coleman, N. Clarke, Distortion of chain conformation and reduced entanglement in polymer–graphene oxide nanocomposites, Acs Macro Lett 5(4) (2016) 430-434.
[83] A.J. Zhang, H. Bai, L. Li, Breath Figure: A Nature-Inspired Preparation Method for Ordered Porous Films, Chem Rev 115(18) (2015) 9801-9868.
[84] S. Stankovich, D.A. Dikin, R.D. Piner, K.A. Kohlhaas, A. Kleinhammes, Y. Jia, Y. Wu, S.T. Nguyen, R.S. Ruoff, Synthesis of graphene-based nanosheets via chemical reduction of exfoliated graphite oxide, Carbon 45(7) (2007) 1558-1565.
[85] T.A. Tabish, M.Z.I. Pranjol, D.W. Horsell, A.A.M. Rahat, J.L. Whatmore, P.G. Winyard, S. Zhang, Graphene Oxide-Based Targeting of Extracellular Cathepsin D and Cathepsin L As A Novel Anti-Metastatic Enzyme Cancer Therapy, Cancers 11(3) (2019).
[86] T.A. Tabish, M.Z.I. Pranjol, H. Hayat, A.A.M. Rahat, T.M. Abdullah, J.L. Whatmore, S. Zhang, In vitro toxic effects of reduced graphene oxide nanosheets on lung cancer cells, Nanotechnology 28(50) (2017) 504001.

[87] F.J. Tommasini, L.d.C. Ferreira, L.G.P. Tienne, V.d.O. Aguiar, M.H.P.d. Silva, L.F.d.M. Rocha, M.d.F.V. Marques, Poly (Methyl Methacrylate)-SiC Nanocomposites Prepared Through in Situ Polymerization, Materials Research 21 (2018).
[88] I.S. Elashmawi, N.A. Hakeem, Effect of PMMA addition on characterization and morphology of PVDF, Polymer Engineering & Science 48(5) (2008) 895-901.
[89] S. Ramesh, K.H. Leen, K. Kumutha, A.K. Arof, FTIR studies of PVC/PMMA blend based polymer electrolytes, Spectrochimica Acta Part A: Molecular and Biomolecular Spectroscopy 66(4) (2007) 1237-1242.
[90] T.A. Tabish, F.A. Memon, D.E. Gomez, D.W. Horsell, S. Zhang, A facile synthesis of porous graphene for efficient water and wastewater treatment, Sci Rep 8(1) (2018) 1817.
[91] S.N. Tripathi, P. Saini, D. Gupta, V. Choudhary, Electrical and mechanical properties of PMMA/reduced graphene oxide nanocomposites prepared via in situ polymerization., Journal of Materials Science 48(18) (2013) 6223-6232.
[92] S.H.R. Ali, M.K. Bedewy, M.A. Etman, H.A. Khalil, B.S. Azzam, Morphology and properties of polymer matrix nanocomposites, International Journal of Metrology and Quality Engineering 1(1) (2010) 33-39.
[93] K.J. Thomas, M. Sheeba, V.P.N. Nampoori, C.P.G. Vallabhan, P. Radhakrishnan, Raman spectra of polymethyl methacrylate optical fibres excited by a 532 nm diode pumped solid state laser., Journal of Optics A: Pure and Applied Optics 10(5) (2008) 055303.
[94] L.Z. Guan, Y.J. Wan, L.X. Gong, D. Yan, L.C. Tang, L.B. Wu, J.X. Jiang, G.Q. Lai, Toward effective and tunable interphases in graphene oxide/epoxy composites by grafting different chain lengths of polyetheramine onto graphene oxide. , Journal of Materials Chemistry A 2(36) (2014) 15058-15069.
[95] F. Tuinstra, J.L. Koenig, Raman Spectrum of Graphite, The Journal of Chemical Physics 53(3) (1970) 1126-1130.
[96] L.G. Cançado, A. Jorio, E.H.M. Ferreira, F. Stavale, C.A. Achete, R.B. Capaz, M.V.O. Moutinho, A. Lombardo, T.S. Kulmala, A.C. Ferrari, Quantifying Defects in Graphene via Raman Spectroscopy at Different Excitation Energies, Nano Letters 11(8) (2011) 3190-3196.
[97] A.C. Ferrari, Raman spectroscopy of graphene and graphite: Disorder, electron–phonon coupling, doping and nonadiabatic effects, Solid State Communications 143(1) (2007) 47-57.
[98] A.C. Ferrari, D.M. Basko, Raman spectroscopy as a versatile tool for studying the properties of graphene, Nat Nanotechnol 8 (2013) 235.
[99] M. Xia, Z. Su, S. Zhang, Raman spectra of bilayer graphene covered with Poly (methyl methacrylate) thin film., AIP Advances 2(3) (2012) 032122.
[100] R.K. Matharu, H. Porwal, L. Ciric, M. Edirisinghe, The effect of graphene-poly(methyl methacrylate) fibres on microbial growth, Interface Focus 8(3) (2018).
[101] J.N. Chen, L. Sun, Y. Cheng, Z.C. Lu, K. Shao, T.T. Li, C. Hu, H.Y. Han, Graphene Oxide-Silver Nanocomposite: Novel Agricultural Antifungal Agent against Fusarium graminearum for Crop Disease Prevention, Acs Appl Mater Inter 8(36) (2016) 24057-24070.
[102] S.S. Nanda, D.K. Yi, K. Kim, Study of antibacterial mechanism of graphene oxide using Raman spectroscopy, Sci Rep-Uk 6(1) (2016) 28443.
[103] P. Shubha, K. Namratha, K. Byrappa, Graphene oxide – a promising material for antimicrobial surface against nosocomial pathogens, Materials Research Innovations 22(2) (2018) 85-90.
[104] Y. Zhang, S.F. Ali, E. Dervishi, Y. Xu, Z. Li, D. Casciano, A.S. Biris, Cytotoxicity effects of graphene and single-wall carbon nanotubes in neural phaeochromocytoma-derived PC12 cells, Acs Nano 4(6) (2010) 3181-6.
[105] A. Gomes, E. Fernandes, J.L.F.C. Lima, Fluorescence probes used for detection of reactive oxygen species, J Biochem Bioph Meth 65(2-3) (2005) 45-80.

[106] S. Gurunathan, J.W. Han, V. Eppakayala, J.H. Kim, Green synthesis of graphene and its cytotoxic effects in human breast cancer cells, Int J Nanomedicine 8 (2013) 1015-27.
[107] E.R. Stadtman, B.S. Berlett, Reactive oxygen-mediated protein oxidation in aging and disease, Chem Res Toxicol 10(5) (1997) 485-94.
[108] G. Poli, G. Leonarduzzi, F. Biasi, E. Chiarpotto, Oxidative stress and cell signalling, Curr Med Chem 11(9) (2004) 1163-82.
[109] H.F. Poon, V. Calabrese, G. Scapagnini, D.A. Butterfield, Free radicals and brain aging, Clin Geriatr Med 20(2) (2004) 329-59.
[110] M.D. Evans, M. Dizdaroglu, M.S. Cooke, Oxidative DNA damage and disease: induction, repair and significance, Mutat Res 567(1) (2004) 1-61.
[111] P.P. Fu, Q. Xia, X. Sun, H. Yu, Phototoxicity and environmental transformation of polycyclic aromatic hydrocarbons (PAHs)-light-induced reactive oxygen species, lipid peroxidation, and DNA damage, J Environ Sci Health C Environ Carcinog Ecotoxicol Rev 30(1) (2012) 1-41.
[112] P.P. Fu, Q. Xia, H.M. Hwang, P.C. Ray, H. Yu, Mechanisms of nanotoxicity: generation of reactive oxygen species, J Food Drug Anal 22(1) (2014) 64-75.
[113] T.A. Tabish, C.J. Scotton, D.C.J. Ferguson, L. Lin, A.v.d. Veen, S. Lowry, M. Ali, F. Jabeen, M. Ali, P.G. Winyard, S. Zhang, Biocompatibility and toxicity of graphene quantum dots for potential application in photodynamic therapy, Nanomedicine 13(15) (2018) 1923-1937.
[114] T. Dutta, R. Sarkar, B. Pakhira, S. Ghosh, R. Sarkar, A. Barui, S. Sarkar, ROS generation by reduced graphene oxide (rGO) induced by visible light showing antibacterial activity: comparison with graphene oxide (GO), RSC Advances 5(98) (2015) 80192-80195.
[115] E. Hendry, P.J. Hale, J. Moger, A.K. Savchenko, S.A. Mikhailov, Coherent Nonlinear Optical Response of Graphene, Physical Review Letters 105(9) (2010) 097401.
[116] D. Zhang, P. Wang, M.N. Slipchenko, D. Ben-Amotz, A.M. Weiner, J.-X. Cheng, Quantitative Vibrational Imaging by Hyperspectral Stimulated Raman Scattering Microscopy and Multivariate Curve Resolution Analysis, Analytical Chemistry 85(1) (2013) 98-106.
[117] U. Cvelbar, M. Mozetic, N. Hauptman, M. Klanjšek-Gunde, Degradation of Staphylococcus aureus bacteria by neutral oxygen atoms, Journal of Applied Physics 106(10) (2009) 103303.
[118] T.-Y. Wang, M.D.J. Libardo, A.M. Angeles-Boza, J.-P. Pellois, Membrane oxidation in cell delivery and cell killing applications, ACS chemical biology 12(5) (2017) 1170-1182.
[119] S. Khan, M.R. P, A. Rizvi, M.M. Alam, M. Rizvi, I. Naseem, ROS mediated antibacterial activity of photoilluminated riboflavin: A photodynamic mechanism against nosocomial infections, Toxicol Rep 6 (2019) 136-142.
[120] A. Al-Sharqi, K. Apun, M. Vincent, D. Kanakaraju, L.M. Bilung, Enhancement of the antibacterial efficiency of silver nanoparticles against gram-positive and gram-negative bacteria using blue laser light, International Journal of Photoenergy 2019 (2019).
[121] F. Pahlevanzadeh, H. Bakhsheshi-Rad, E. Hamzah, In-vitro biocompatibility, bioactivity, and mechanical strength of PMMA-PCL polymer containing fluorapatite and graphene oxide bone cements, Journal of the mechanical behavior of biomedical materials 82 (2018) 257-267.
[122] G. Gonçalves, S.M. Cruz, A. Ramalho, J. Grácio, P.A. Marques, Graphene oxide versus functionalized carbon nanotubes as a reinforcing agent in a PMMA/HA bone cement, Nanoscale 4(9) (2012) 2937-2945.
[123] K.-H. Liao, Y.-S. Lin, C.W. Macosko, C.L. Haynes, Cytotoxicity of graphene oxide and graphene in human erythrocytes and skin fibroblasts, Acs Appl Mater Inter 3(7) (2011) 2607-2615.
[124] J. Liu, L. Cui, D. Losic, Graphene and graphene oxide as new nanocarriers for drug delivery applications, Acta biomaterialia 9(12) (2013) 9243-9257.

[125] X. Hu, N. Ren, Y. Chao, H. Lan, X. Yan, Y. Sha, X. Sha, Y. Bai, Highly aligned graphene oxide/poly(vinyl alcohol) nanocomposite fibers with high-strength, antiultraviolet and antibacterial properties, Composites Part A: Applied Science and Manufacturing 102 (2017) 297-304.

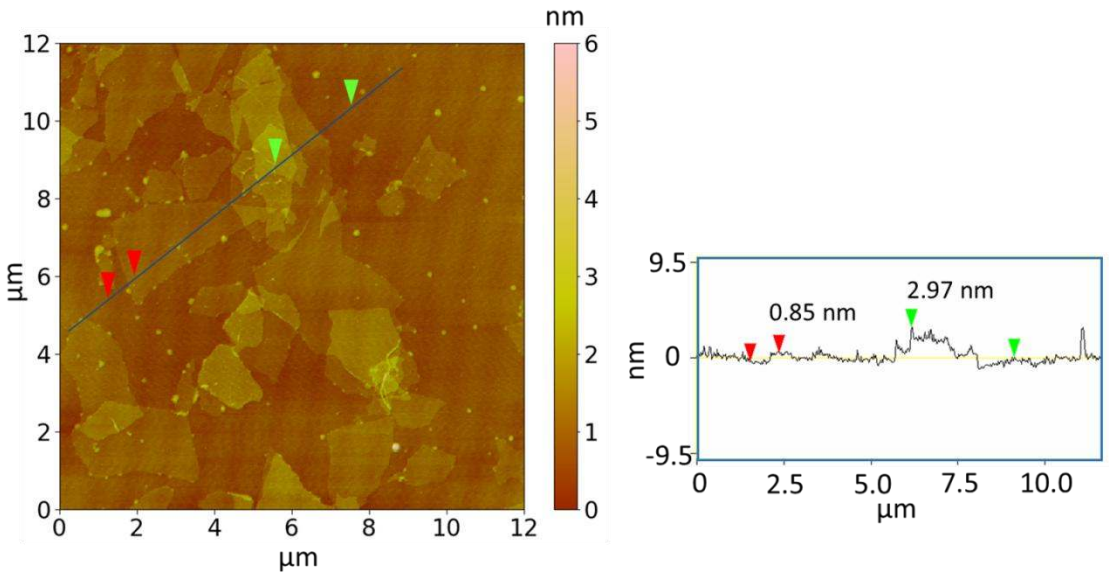

Figure 1: (A) AFM micrograph and (B) height profile of synthesised GO nanosheets showing its thickness.

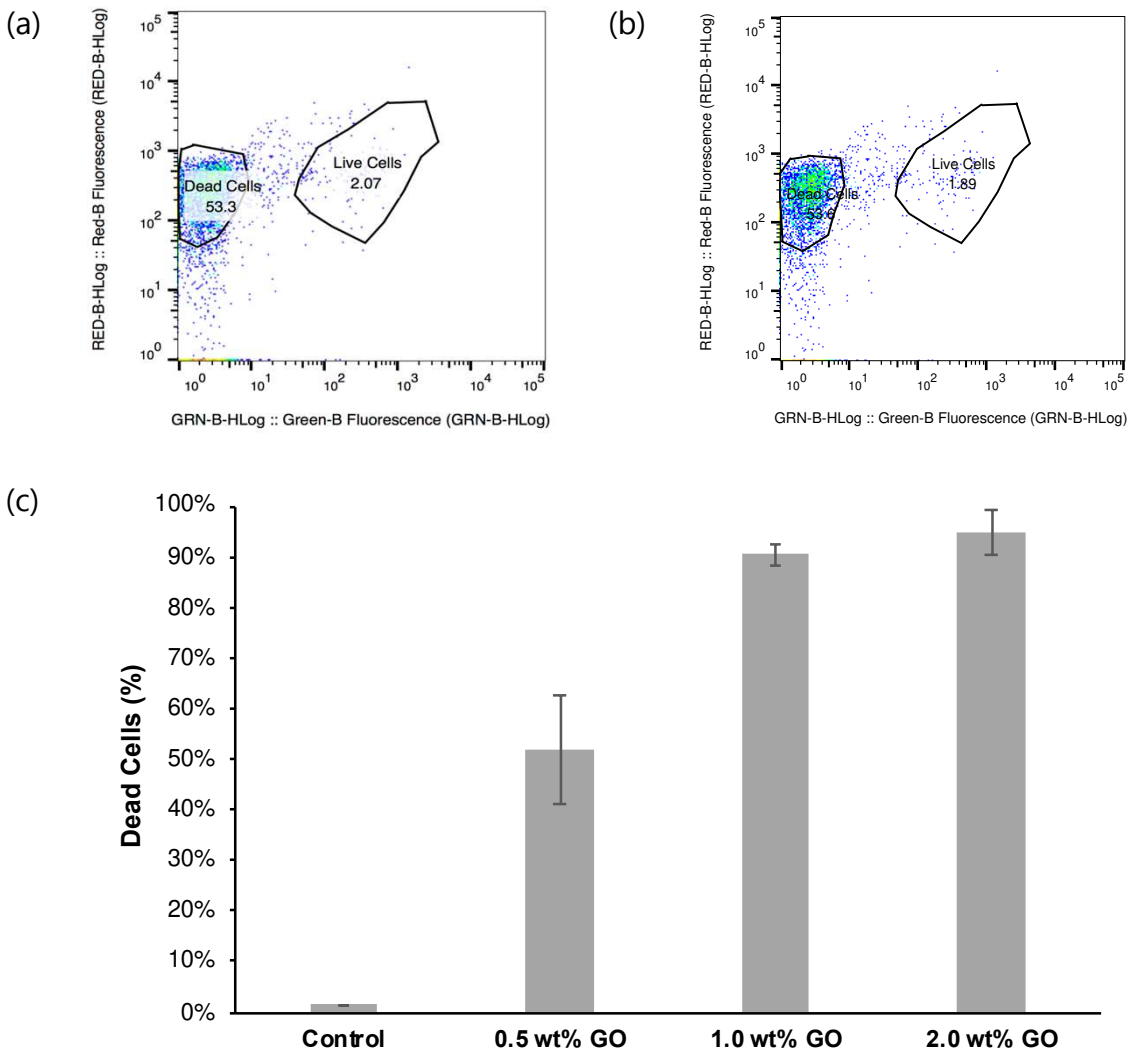

Figure 2: Flow cytometry results obtained by exposing *E. coli* to GO at various concentrations for 24 hours at 37°C and 150 rpm. (a) gating strategy example of *E. coli* bacterial cells after exposure to 1 wt% of GO, (b) gating strategy example of *E. coli* bacterial cells after exposure to 2 wt% of GO, (c) percentage of dead cells after exposure of *E. coli* to various concentrations of GO. Error bars represent standard deviation, (*n = 3*).

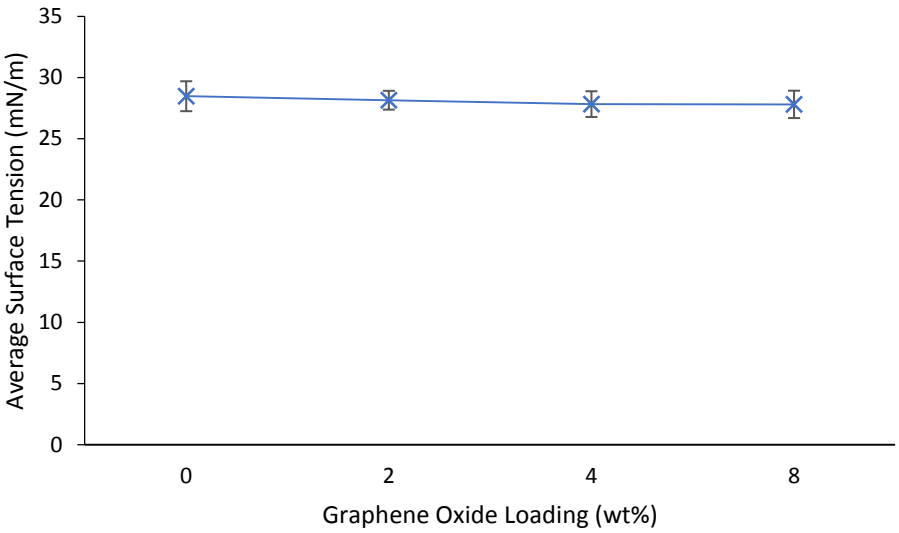

(a)

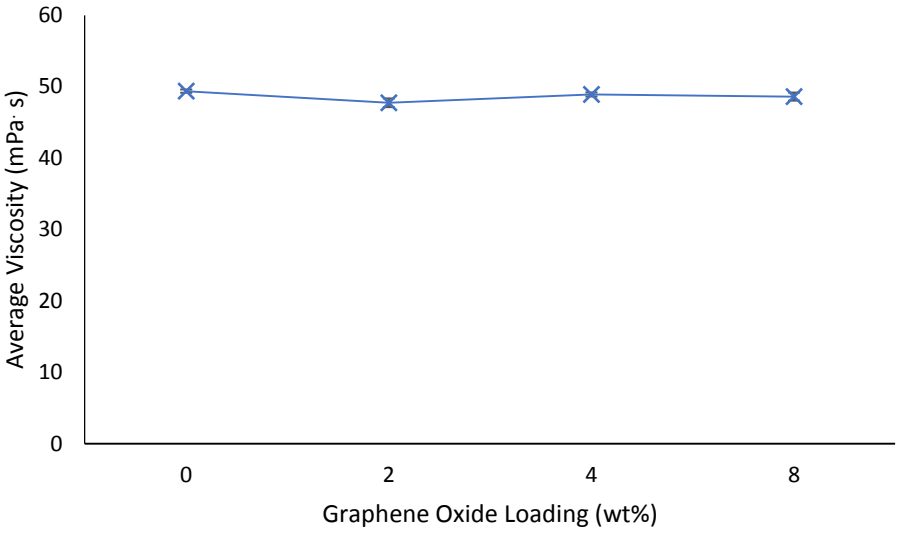

(b)

1011 Figure 3: plot of the (a) average surface tension against GO concentration (n=4);

1012 (b) average viscosity against GO concentration (n=3). Error bars represent

1013 standard deviation.

1014

1015

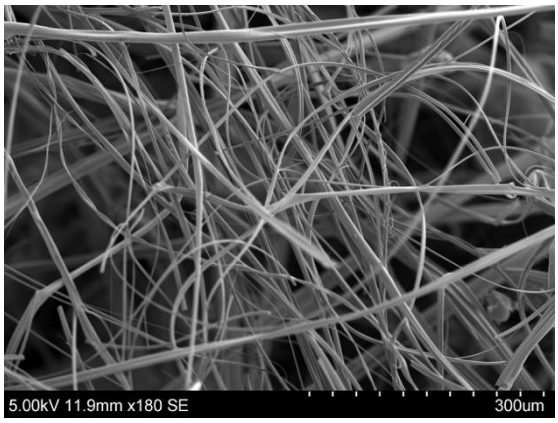
5.00kV 11.9mm x180 SE
300um

(a)

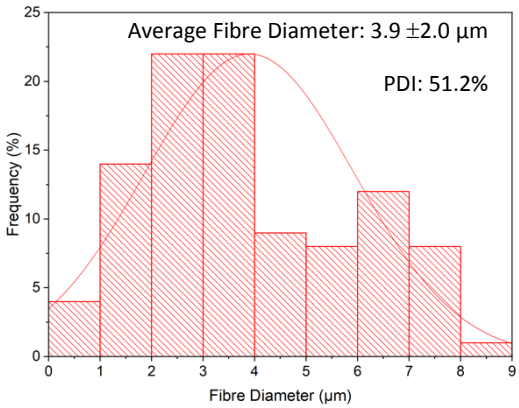
Average Fibre Diameter: 3.9 ±2.0 µm
PDI: 51.2%
Frequency (%)
Fibre Diameter (µm)

(b)

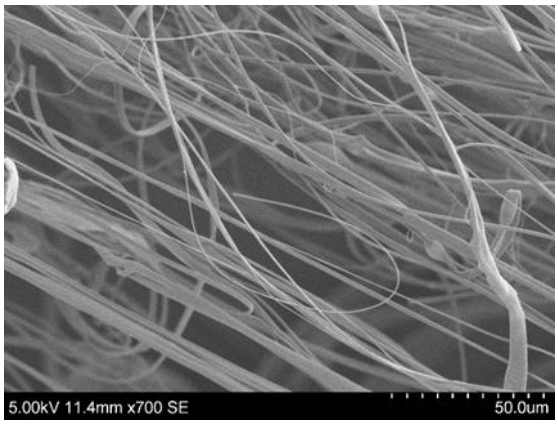
5.00kV 11.4mm x700 SE
50.0um

(c)

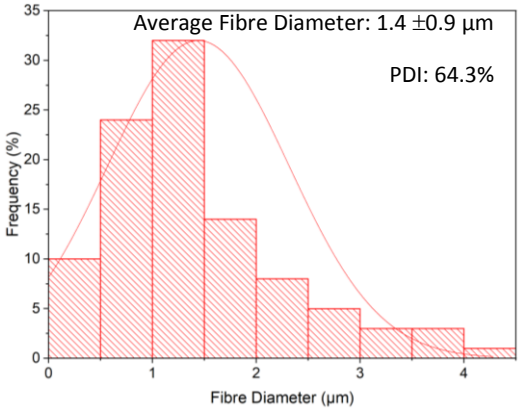
Average Fibre Diameter: 1.4 ±0.9 µm
PDI: 64.3%
Frequency (%)
Fibre Diameter (µm)

(d)

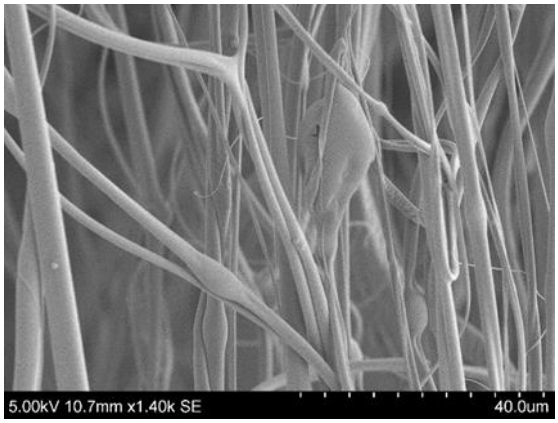
5.00kV 10.7mm x1.40k SE
40.0um

(e)

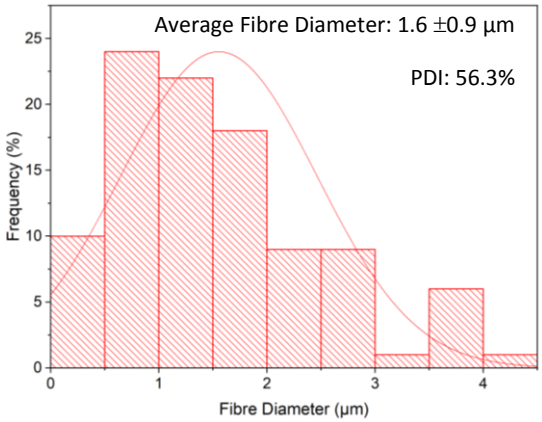
Average Fibre Diameter: 1.6 ±0.9 µm
PDI: 56.3%
Frequency (%)
Fibre Diameter (µm)

(f)

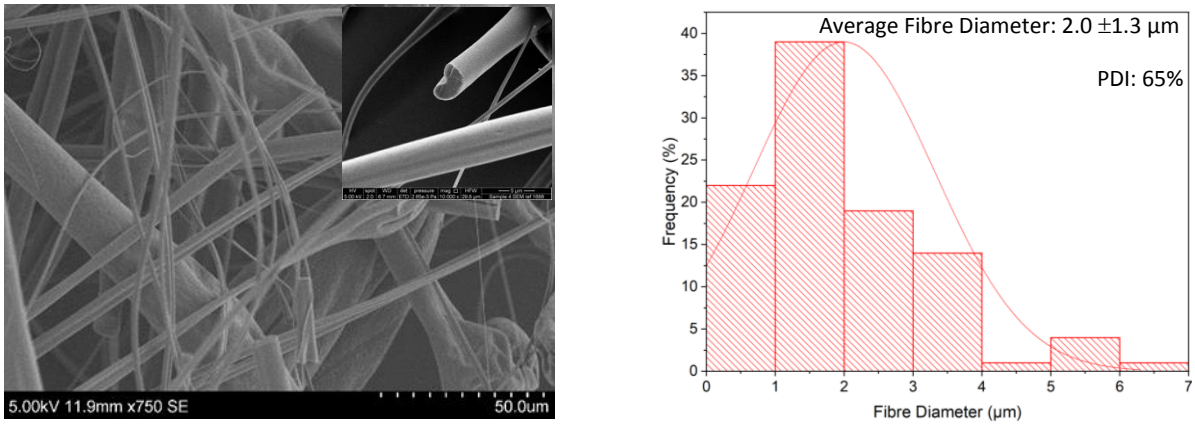

(g) (h)

Figure 4: SEM images and fibre diameter distribution of graphene oxide loaded PMMA fibres. (a) and (b) pure PMMA fibres, (c) and (d) 2wt% GO fibres, (e) and (f) 4wt% GO fibres, (g) and (h) 8wt% GO fibres. In (g) the inset micrograph shows the fibres to have smooth surfaces. Polydispersity index (PDI) values are also displayed on the graphs.

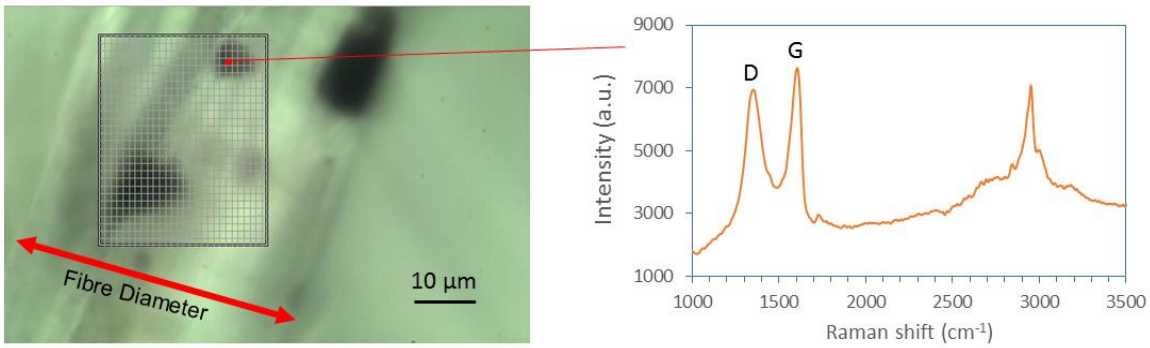

(a)

(b)

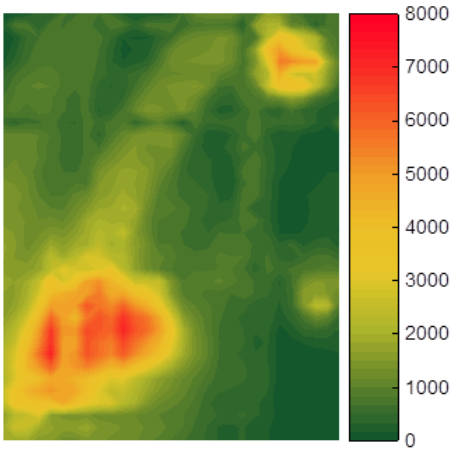

I_D (X,Y)

(c)

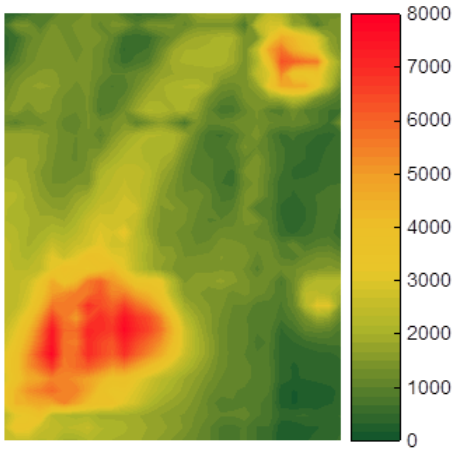

I_G (X,Y)

(d)

Figure 5: Raman microscopic image of 4wt% GO loaded PMMA fibres: microscopic image (a), Raman spectrum (b), and Raman mapping of D (c) and G (d) peaks.

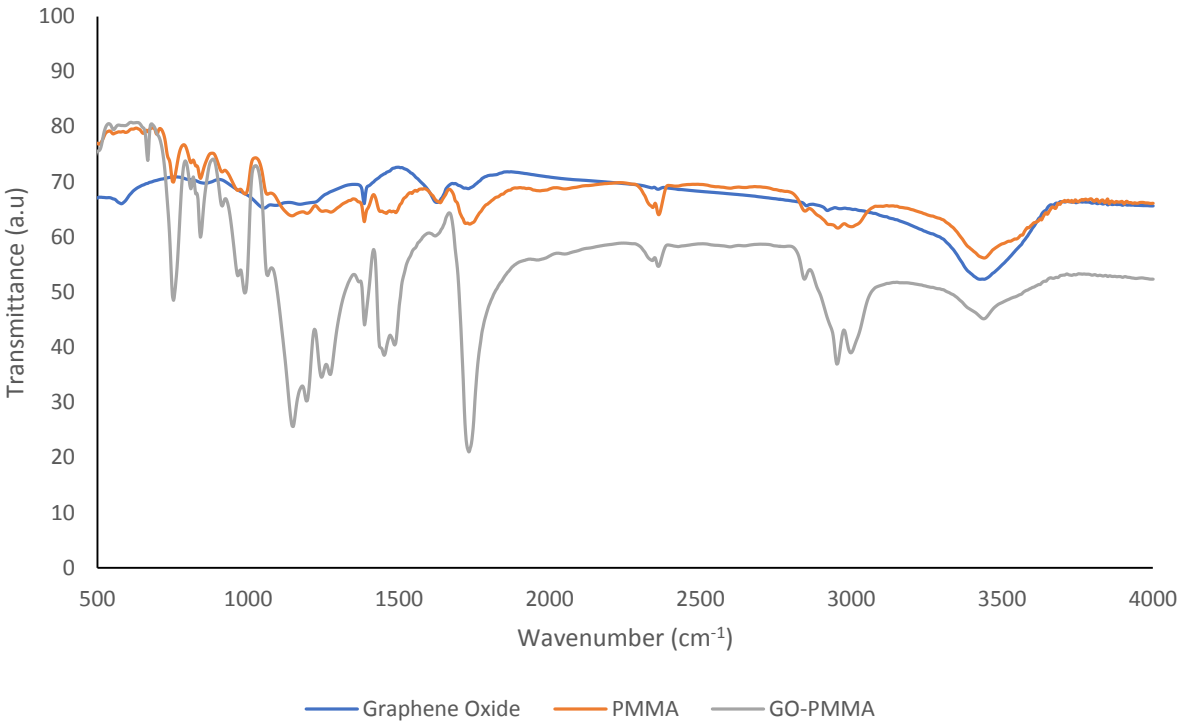

Figure 6: FT-IR spectra of GO, PMMA and 8 wt% GO/PMMA nanocomposite fibres.

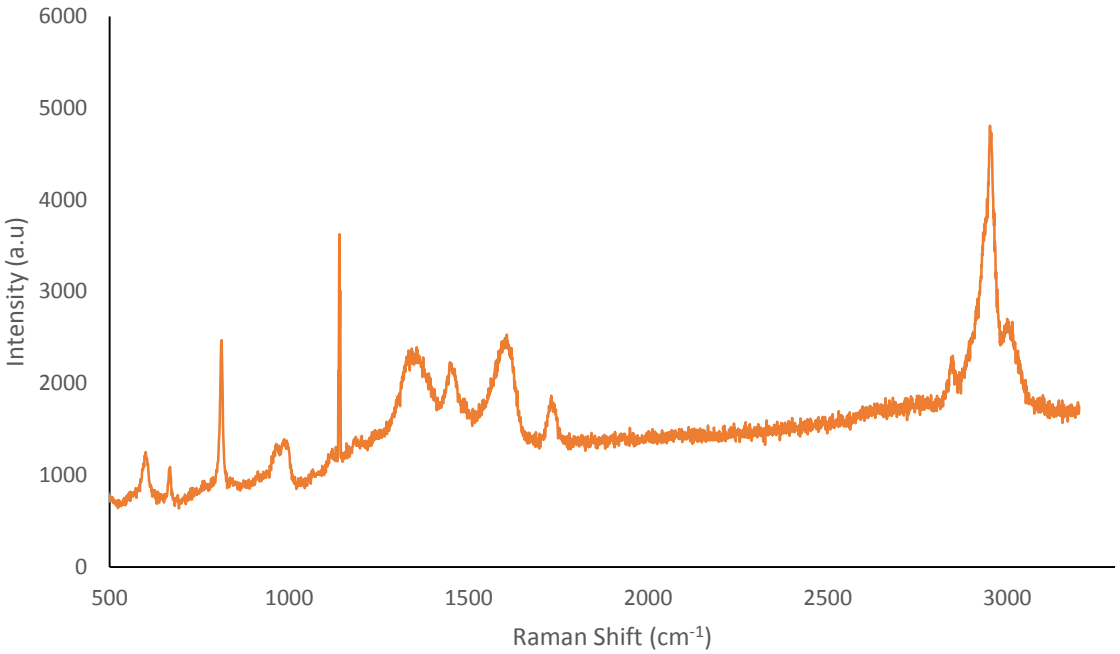

Figure 7: Raman spectrum of 8 wt% GO/PMMA fibres.

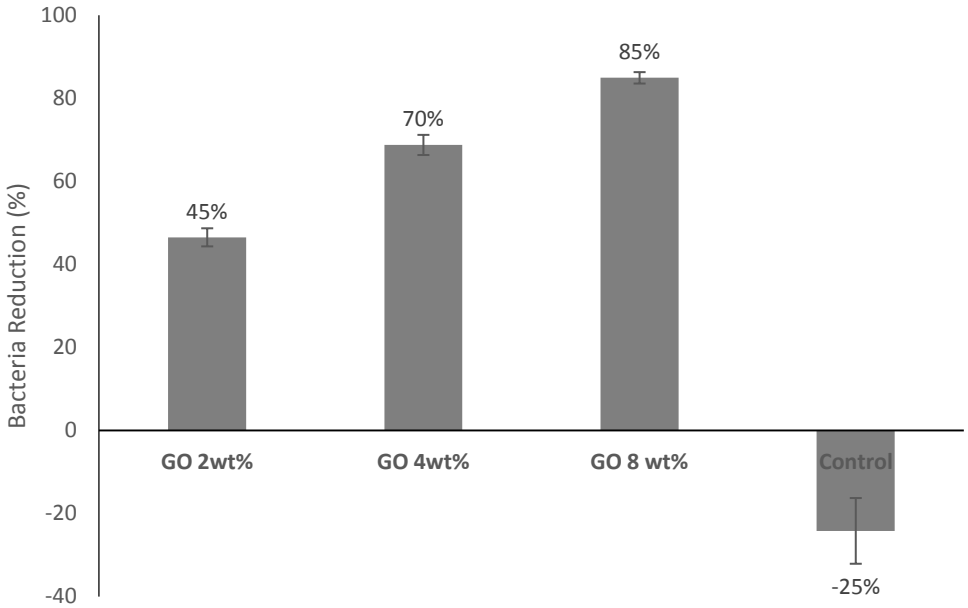

Figure 8: Bacterial reductions observed after incubation of 0, 2, 4 and 8 wt% GO/PMMA fibres with *E. coli* K12 for 24 hours at 150 rpm and 37°C. Pure PMMA fibres with no GO were used as a control group. Error bars represent standard deviation (*n = 3*).

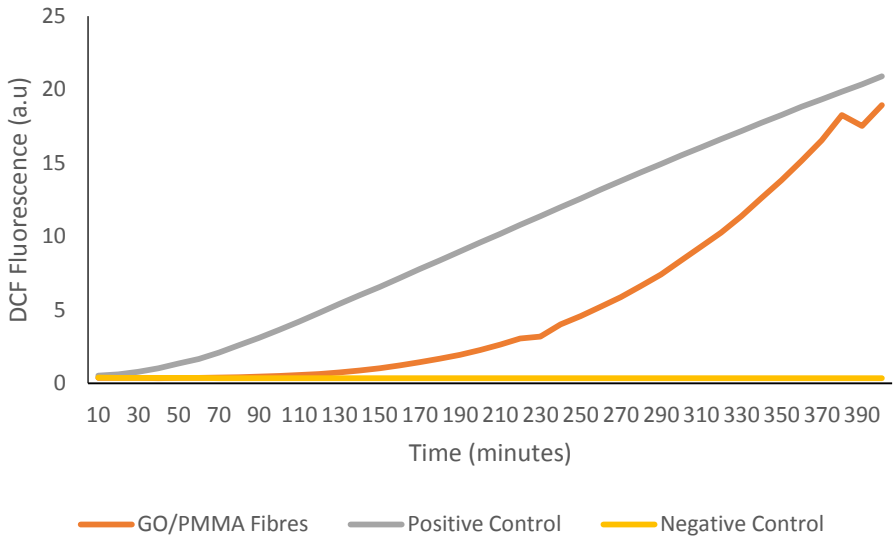

Figure 9: Generation of ROS from 8 wt% GO/PMMA fibres. The fluoresce of DCF was measured using a fluorimeter with excitation at 485 nm and emission at 530 nm. Positive control represents a 1:1 dilution of 30% hydrogen peroxide in PBS, whilst the negative control represents PBS only.

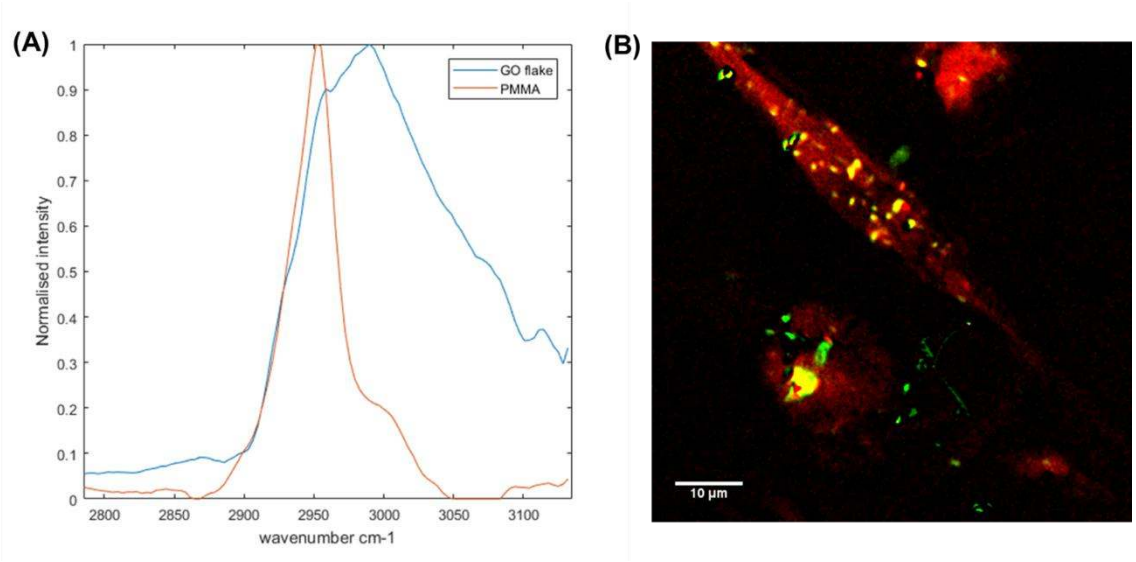

Figure 10: a) Stimulated Raman scattering (SRS) spectra from PMMA and GO in the 8 wt% GO-PMMA *E coli* treated samples. b) The results of Multi-Curve Regression (MCR) analysis performed on a hyperspectral stack of SRS images from bacteria and GO-PMMA. Here the PMMA (red) and GO (green) signals can be separated by the different spectral profiles as shown in (a). Gold colour indicates a mixture of GO and PMMA.

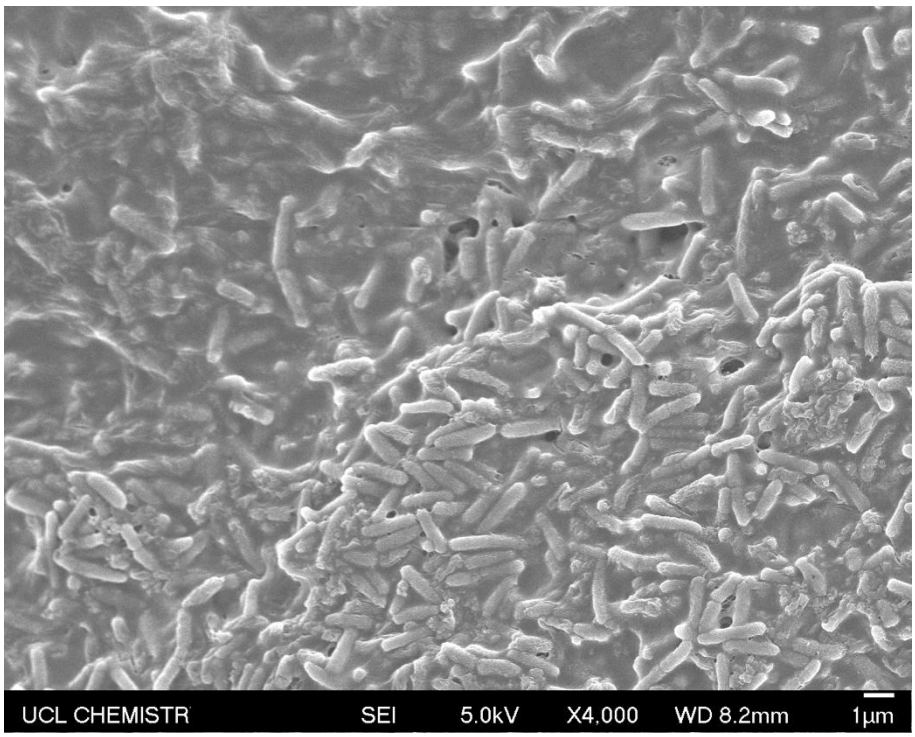

Figure 11: SEM micrograph of the 8 wt% GO/PMMA post incubation with *E. coli*.

Table 1: GO/PMMA solution composition.

	GO Suspension		Polymer Solution		Final Concentration of GO in the Resulting Fibre (wt%)
	GO Particles (g)	Chloroform (mL)	PMMA (g)	Chloroform (mL)	
GO/PMMA0	0.00	10	4	10	0
GO/PMMA2	0.08	10	4	10	2
GO/PMMA4	0.16	10	4	10	4
GO/PMMA8	0.32	10	4	10	8

Microstructure and Antibacterial Efficacy of Graphene Oxide Nanocomposite Fibres

Rupy Kaur Matharu[a,b], Tanveer A. Tabish[c], Thithawat Trakoolwilaiwan[a], Jessica Mansfield[c], Julian Moger[c], Tongfei Wu[d], Cláudio Lourenço[e], Biqiong Chen[f], Lena Ciric[b], Ivan P. Parkin[e], Mohan Edirisinghe[a*]

[a] Department of Mechanical Engineering, University College London, Torrington Place, London, WC1E 7JE, UK.

[b] Department of Civil, Environmental and Geomatic Engineering, University College London, London, WC1E 7JE, UK.

[c] School of Physics and Astronomy, University of Exeter, North Park Road, Exeter, EX4 4QL, UK.

[d] Department of Materials Science and Engineering, University of Sheffield, Mappin Street, Sheffield, S1 3JD, UK.

[e] Department of Chemistry, University College London, Gordon Street, London, WC1H 0AJ, UK.

[f] School of Mechanical and Aerospace Engineering, Queen's University Belfast, Stranmillis Road, Belfast, BT9 5AH, UK.

* Corresponding author email: m.edirisinghe@ucl.ac.uk

Abstract

Antibacterial polymer nanocomposite fibre meshes containing graphene oxide (GO) nanosheets were successfully prepared by pressurised gyration. The morphological and chemical composition of the resulting fibre meshes were determined using Scanning Electron Microscopy (SEM), Raman spectroscopy, Raman mapping and Fourier-Transform Infrared Spectroscopy (FT-IR). SEM showed the fibres to have an average diameter increasing from ~ 1 – 4 μm as the GO loading increased. FT-IR and Raman spectroscopy confirmed the inclusion of GO nanosheets on the fibre surface. The antibacterial potential of GO nanocomposite fibres were investigated using *Escherichia coli* K12. Average bacterial reduction ranged from 46 – 85 % with results favouring the strongest bioactivities of the nanocomposite containing 8 wt% of GO. Finally, bacterial toxicity of the nanocomposites was evaluated by reactive oxygen species (ROS) formation. A mechanism for the antibacterial behaviour of the nanocomposite fibres is presented. Stimulated Raman scattering imaging and spectra of the fibres post antibacterial studies showed flakes of GO distributed across the surface of the poly(methyl 2-methylpropenoate) (PMMA) fibres, which contribute to the high killing efficacy of the composites towards *E. coli*. GO nanosheets embedded in a polymer matrix have demonstrated the ability to retain their antibacterial properties, thus offering themselves as a promising antibacterial agent.

Graphical Abstract

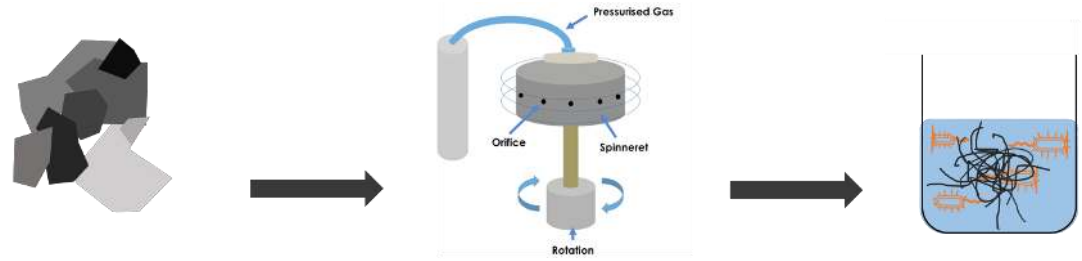

Keywords:

Antibacterial; Graphene Oxide; Nanocomposite; Fibers; Reactive Oxygen Species; Raman Scattering; Nanosheets.

1. Introduction

Airborne and waterborne pathogens are responsible for causing numerous diseases, infections, allergies and toxic reactions[1-5]. These microorganisms are easily spread in a non-uniform manner with air and water currents[1-5]. The concentration of these biological threats in the environment and water supplies greatly fluctuate depending on numerous factors including human activity and environmental exposure [6-10]. Their existence in high concentrations serves as an indication of contamination, thus the implementation of regulators in the industrial, commercial and consumer markets, to reduce, or ideally prevent microbial colonisation and proliferation has become increasingly vital to human health[11]. Sterilisation methods utilising ultraviolet radiation, ions and high pressure and temperature treatments have been used as a means of reducing the number of pathogenic microorganisms[12-16]. However, these techniques have been deemed inefficient and potentially toxic to human health.

Mechanical filtration technologies have emerged as a viable means of controlling aerosols and hydrosols. In particular, micro- and nano- fibres provide chemical-free, cost-effective and environmentally friendly approach for enhancing filtration efficiency and performance[17-22]. Fibrous filtration systems consist of a layer of randomly aligned fibres oriented across the direction of flow[23]. These membranes have an interconnected pores and/or

finer pore structure that allows an effective permeability resulting a higher throughput in comparison to conventional filters[24]. The individual fibres in the mesh typically have a circular or rectangular cross-section, with a small fibre diameter distribution and are ideally porous[23]. The exploitation of fibrous filtration systems has increased over the last 20 years due to their ability to capture particles and microorganisms proficiently via factors including direct interception by fibres, inertial impaction, Brownian movement, convection, gravitational settling and electrostatic effects. One of the challenges in currently used fibre-based filtration systems is that the microorganisms trapped within the fibre meshes are able to survive and proliferate, consequently leading to contamination of air-handling systems, ventilation and air conditioning units and water supply systems [1, 25-32]. This ultimately diminishes filter efficiency and consequently leads to the release of pathogenic microorganisms both dormant and germinating, into the environment and water supplies[1]. Therefore, various antimicrobial treatments, such as antibiotics and antivirals, have been incorporated into filter media to bestow antimicrobial activities[33-37]. However, microorganisms have the ability to resist such treatments from working against it (antimicrobial resistance) and rendering them ineffective. For this reason, the use of alternative antimicrobial agents has been extensively explored.

Graphene-based 2D nanomaterials, such as graphene oxide (GO), porous graphene nanosheets and reduced GO, have demonstrated effective antibacterial properties[38-42]. These carbon-based materials having a higher surface area to volume ratio results in a stronger potency toward bacteria[43-45]. In particular, studies have shown GO to possess the highest antibacterial activity among its counterparts[38]. GO is one of the most extensively explored materials for a wide range of applications. GO is the product formed from the chemical exfoliation of graphite oxide into mono-sheets and is composed of a single atomic plane of carbon molecules arranged in a honeycomb structure with carboxylic groups at its edges and hydroxyl groups in its basal plane[46, 47]. As a result, GO is hydrophilic making it ideal for filtration applications. Recent studies have revealed that a multitude of microorganisms can be inactivated by GO, such as *Escherichia coli*, *Staphylococcus aureus*, Xanthomonas oryzae pv. Oryzae, *Pseudomonas aeruginosa*, *Streptococcus faecalis* and *Candida albicans*[38, 48-54].

The purpose of this study is to fabricate novel antibacterial fibre meshes loaded with GO nanosheets were fabricated using pressurised gyration. In this work, GO nanosheets were synthesised, characterised and the minimum concentration required to inhibit bacterial growth was investigated. The as-prepared nanosheets were incorporated into polymeric fibres using pressurised gyration.

The physical and chemical structure of the nanocomposite fibres were analysed in detail. The antibacterial performance of the fibrous meshes were measured against *E. coli*. The resulting meshes demonstrate a promising scope to inhibit microbial colonisation and proliferation.

2. Experimental Procedures

2.1 Materials

Graphite powder (<20 μm), poly(methyl 2-methylpropenoate) (PMMA) (M_w ~ 120,000 g/mol), chloroform, concentrated sulfuric acid (98%), sodium nitrate, potassium permanganate, hydrogen peroxide (30 wt% in water), ethanol, hydrochloric acid (37%), Luria Bertani (LB) broth, phosphate buffered saline (PBS), glutaraldehyde, 1% osmium tetroxide and hexamethyldisilazane were purchased from Sigma-Aldrich (Gillingham, UK). LB agar was purchased from Invitrogen (Paisley, UK). LIVE/DEAD BacLight Bacterial Viability and Counting Kit was purchased from ThermoFisher Scientific (Paisley, UK). 2-(3,6-diacetyloxy-2,7-dichloro-9H-xanthen-9-yl)benzoic acid (DCFH) was purchased from Cayman Chemicals (Michigan, US). All solvents and chemicals were of analytical grade and used as received or as instructed by the supplier.

2.2 Synthesis of Graphene Oxide Nanosheets

GO nanosheets were prepared by following a modified Hummers' method[55]. Concentrated sulfuric acid (69 mL) was added to graphite flakes (3.0 g) and sodium nitrate (1.5 g), followed by slowly adding potassium permanganate (9.0 g). The reaction temperature was maintained below 20 °C. The initial reactants were heated to 35 °C and stirred for 12 hours. Potassium permanganate (9.0 g) was again added, and was stirred for 8 hours which was maintained at a temperature of 35 °C. The reaction was then cooled to room temperature (25^{o}C) and put into an ice bath (~400 mL) with 30% hydrogen peroxide (3 mL).

The mixture was filtered through filter paper with a particle retention of 12-15 µm. The extracts were washed in succession with distilled water (200 mL), 30% hydrochloric acid (200 mL), and distilled water (200 mL). The remaining solid material was then washed twice with ethanol (200 mL) by centrifugation (9000 rpm for 4 hours, Eppendorf Centrifuge 5804). The purified product was dispersed in distilled water and sifted through a metal U.S. Standard testing sieve (161 µm) after sonication for 1 hour. The GO aqueous suspension was freeze-dried to obtain GO powder.

2.3 Fabrication of Graphene Oxide/ Poly(methyl 2-methylpropenoate) Fibres

Polymer solutions containing varying concentrations of GO nanosheets (0, 2, 4 and 8 wt%) were prepared in a three-step process for fibre forming using

pressurised gyration. (i) GO was added to chloroform as described in Table 1 and sonicated (Branson Ultrasonics Sonifier S-250A) for 24 hours in an ice bath to homogenously disperse GO nanosheets. Then, PMMA was dissolved in chloroform and mixed with the GO dispersion under magnetic stirring for 1 hour. 8 wt% was easily processed by pressurised gyration[56].

The as-prepared GO/PMMA suspensions were processed using pressurized gyration. The experimental setup was made up of a rotating aluminium cylindrical pot (6 cm diameter, 3.5 cm height) with 24 circular orifices (0.5 mm in diameter) along its central horizontal axis. The bottom of the pot was attached to a high-speed rotary motor, whilst the top was connected to a nitrogen gas supply. 5 mL aliquots of the GO/PMMA suspension were loaded into the pot. The system was immediately switched on and allowed to reach the apparent maximum speed of 36000 rpm before applying 0.1 MPa of pressure (nitrogen gas) to the rotating pot. The system was spun until all the suspension had been ejected from the pot. Pressurised gyration experiments were performed at controlled temperature (21±2 °C) and relative humidity (55 ± 3.5%). All fibre samples were prepared in triplicate.

2.4 Characterisation

GO was flushed onto fresh-cleaved mica discs and analysed using Atomic Force Microscopy (AFM) (Veeco) imaging in a tapping mode with a scan rate of 0.5 Hz. Image analysis was carried out using XEI software. Surface tension of the GO/PMMA suspensions were measured using the Du Nouy (Ring) Tensiometry Method and a KRUSS K9 Tensiometer. The surface tension of water was also calculated against a reference value of 73 mN/m. Four measurements were repeated for each suspension to calculate an average. Solvent evaporation during the spinning process induces changes in the viscosity of the plyometric suspensions. Viscosity was calculated using a Brookfield digital rheometer (model DV – III). Morphology of the resulting GO/PMMA hybrid fibres were analysed using a Scanning Electron Microscope (SEM) (JEOLJSM-6301F). The accelerating voltage was kept at 5 kV. Nanocomposites were gold-coated for 90 seconds using a Quoram Q150R ES sputter coater. The average size of fibres was calculated the diameter of 100 fibres using SEM micrographs at low magnifications and ImageJ software (National Institutes of Health, Bethesda, MD, USA). SEM imaging was also performed on fixed fibres post incubation with bacterial cells. Fibres were fixed using glutaraldehyde and 1% osmium tetroxide. The samples were then dried using a series of ethanol and hexamethyldisilazane solutions.

Raman mapping was performed using an inVia Raman microscope. The spectra of samples excited at the wavelength of 514.5 nm with the power of less than 1 mW, spot size of ~1 μm (with a ×50 objective lens (numerical aperture = 0.55)), pixel size of 1 μm (for both x and y directions) and spectral resolution of 2.5 cm^{-1}. The low power was used to avoid heating. The final spectrum of each sample was the average result of three acquisitions. The intensity of the peak was determined from the value of D and G peaks. FT-IR spectra of GO, PMMA and the 8 wt% GO/PMMA fibre samples were determined using a Bruker Optics Tensor-27 FT-IR spectrometer. The spectra were recorded in the wavenumber range of 4,000–500 cm^{-1}. The samples were pressed into pellets by mixing with KBr. Detailed Raman spectra of the 8 wt% GO/PMMA fibres were measured using laser excited 532 nm and at the power of 6 mW.

2.5 Antibacterial Activity of Graphene Oxide Nanosheets and Graphene Oxide in Polymeric Fibres

Escherichia coli K12 was chosen as the model microorganism to assess the antibacterial properties of the synthesised GO and the GO loaded polymeric fibres.

For GO, a single colony of *E. coli* was suspended in 30 mL of sterile LB broth and incubated at 37°C and 150 rpm for approximately 4 hours. 3 mL of this

suspension was then added to GO suspensions, containing 0.5, 1.0 and 2.0 w/v% of GO in 27 mL of sterile LB broth. The suspensions were incubated for 24 hours at 37^{o}C and 150 rpm (Orbital Shaker S150, Stuart).

Flow cytometry (Guava easyCyte®, Merck, UK) was used to determine the viable cell counts with a LIVE/DEAD BacLight bacterial viability kit and InCyte software (Merck, UK). A stock solution containing both dyes (propidium iodide and SYTO®9) was prepared according to manufacturers' recommended protocol. The staining solution was added to the suspensions and incubated in the absence of light at room temperature (22^{o}C) for 15 minutes[57]. Cells were then acquired using a calibrated Guava easyCyte® flow cytometer (Merck, UK) and InCyte software (Merck, UK)[57]. Acquisition gates/regions were outlined using positive (*E. coli* only), negative (media and GO only), fluorescence minus one and compensation controls. *E. coli* populations were identified and gated using forward and side scatter channels. The gated *E. coli* population was then analysed using green and red fluorescent channels (live populations - SYTO®9, and dead populations - propidium iodide). 50,000 events were collected overall. FlowJo (V10, TreeStar, USA) was used to enumerate the number of cells in both live and dead populations.

For GO/PMMA fibres, 0.02 g of each GO/PMMA sample and LB agar plates were sterilised using UV light for 1 hour. A single colony of *E. coli* was harvested using a sterile plastic inoculating loop and suspended in sterile LB broth. The suspension was incubated at 37^{o}C and 150 rpm until the culture reached its mid-exponential phase (at approximately 4 hours, and OD_{600} of 0.035). The culture was then centrifuged at 4600 rpm for 15 minutes (accuSpin 3R, Fisher Scientific). The supernatant was removed. The cells were then pelleted by centrifuging (4600 rpm for 15 minutes) the suspensions. The cells were collected and washed with PBS, before being re-suspended in PBS. The number of live cells present in each suspension was counted using the colony counting method.

The GO/PMMA fibres were incubated with the *E. coli* suspensions for 24 hours at 37^{o}C and 150 rpm. Pure PMMA fibres with no GO nanosheets were used as the control group. The number of live cells remaining in the suspension was estimated using the colony counting method. The number of cells before and after incubation were compared and the bacteria cell reduction was calculated. Experiments were repeated on three separate occasions.

2.6 Reactive Oxygen Species Generation

Reactive oxygen species (ROS) production was measured using the peroxide dependent oxidation of DCFH to form the fluorescent compound 2',7'-dichloro-3',6'-dihydroxy-3H-spiro[2-benzofuran-1,9'-xanthen]-3-one (DCF)[58]. 0.01g of 8 wt% GO/PMMA fibres were incubated in 1.5 mL of PBS, alongside 1.5 mL of a 1:1 dilution of 30% hydrogen peroxide in PBS (positive control) and PBS only (negative control). Then 10 μM of DCFH were added to each well (in the 24 well plate) incubated at 37^{o}C and 150 rpm using a fluorimeter with incubation capacity, the Fluoroskan Ascent - Labsystems. The fluorescent intensity of DCF was measured every 10 minutes for 12 hours using the aforementioned instrument with excitation at 485 nm and emission at 535 nm. The experiment was completed in triplicate and each sample was measured 37 times.

2.7 Imaging Using Stimulated Raman Scattering

Stimulated Raman scattering (SRS) imaging was performed using an InsightX3 fs laser (Newport SpectraPhysics), 1045 nm (as the Stokes beam) and 800 nm (as the pump and probe beam) output. The powers at the sample were 2 mW for the 1045 nm beam and 4 mW for the 800 nm beam. The beams were chipped to generate pulses (ps) and spatially covered in the spectral converging unit (Newport SpectraPhysics)[59]. The temporal overlay was scanned via the Spectral Focusing Timing and Recombination Unit (SF-TRU) to produce Coherent Raman Scattering (CRS) spectra of the samples. Imaging was achieved

on a modified confocal microscope (Olympus FV3000), using a 1.2 NA water immersion objective (Olumpus UPlanSApo 60x). SRS was recorded in the forward direction, with a 1.4NA oil immersion condenser (Nikon D CUO DIC). SRS signals were detected using a photodiode and LockIn amplifier (APE SRS detection set) and the 1045 nm stokes beam was blocked from the photodiode using the following filters (Chroma CARS 890-210 and 950 nm 4OD short pass filter Edmund Optics). The samples were mounted between 2 coverslips.

3.Results and Discussion

3.1 Morphologies of Graphene Oxide

The morphology of as-prepared GO aqueous suspension deposited on mica was examined using AFM (Figure 1). The thickness of single GO sheets was ~0.72 nm according to the literature [60]. The AFM height profile of GO prepared in this study illustrates a thickness of 0.85 ± 0.12 nm for most of the GO single sheets, confirming their monolayer nature. The AFM image shows irregular shapes of GO nanosheets with a typical lateral dimension in the range of 1 – 4 μm.

3.2 Antibacterial Effect of Graphene Oxide Suspensions

E. coli K12 was chosen as a model bacterium to assess the antibacterial properties of GO. The proportion of live and dead cells after seeding with GO was determined using flow cytometry. LB broth without GO particles was used

as a control. The fundamental principle of the use of flow cytometry to determine antibacterial activity relies on the use of fluorescent dyes, Propidium Iodide (PI) and SYTO®9, to allow a clear discrimination between dead and viable cells to be made. SYTO®9 is a green nucleic acid stain that stains both live and dead bacteria in a population, whilst PI is a red nuclear and chromosome counterstain that only penetrates bacteria with damaged membranes.

As shown in Figure 2, the 2 wt% GO dispersion suppressed the growth of *E. coli* the strongest, leading to a bacterial reduction of 96%. Exposure to 1 wt% GO resulted in the death of 91% of the bacterial population, whilst exposure to 0.5 wt% GO caused the death of 53% of the bacterial population (2% cell death detected in the control population).

A number of physical and chemical mechanisms have been proposed which may contribute to the antibacterial activity of GO. Akhavan *et al.* have suggested that antimicrobial actions of GO are typically induced by the physical interaction of the sharp edges of GO with the microbial membrane[61, 62]. During this interaction the GO particles pierce the cell membrane, thus disrupting plasma membrane integrity which outcomes in the release of intra- and sub-cellular contents. This phenomenon was further confirmed by other studies[63-66]. In

addition to membrane disruption, GO particles can wrap around and trap microbial cells in agglomerates, thus isolating them from their neighbouring environment[64, 67, 68]. This also indicate that the essential nutrients in starving cells is important for cell survival.

Researchers have also argued that GOs toxicity is indeed not attributed to its physical interaction with bacterial cells but instead a chemical reaction. Several studies have demonstrated that GO may inactivate bacterial cells without having any direct contact with the particles, therefore suggesting the physical interaction is not a major part of the toxicity mechanism[69, 70]. Few other research work has shown that the antibacterial activity of GO is mainly induced by oxidative stress. During this cascade GO triggers either the ROS-dependent or ROS-independent pathway. Activation of these pathways inhibits bacterial metabolism, disturbs important functions at cellular or sub-cellular, causes intra- and sub-cellular protein inactivation and induces lipid peroxidation, consequently leading to cellular inactivation, programmed cell death (necrosis or apoptosis)[38, 51].

It has evidently been explored that the antibacterial actions of GO are the result of physical-chemical interactions between microbiota and GO, and thus, all

three mechanisms suggested could be responsible for the results observed in this experiment.

3.3 Characterisation of Graphene Oxide/Polymer Suspensions

3.3.1 Surface Tension

GO/PMMA nanocomposite fibres were prepared by pressurised gyration of PMMA and GO chloroform suspensions. The surface tension of PMMA solutions containing various concentrations of GO are shown in Figure 3(a). As can be seen, the surface tension of the nanofluids decrease with increasing GO concentration. However, the range of decrease is not large, as only a 2.4% reduction was observed. The pure PMMA solution had an average surface tension of 28.5 ±1.2 mN/m, this dropped to 28.1 ±0.8 mN/m upon the addition of 2 wt% GO. In this instance GO behaves as a surfactant and increases the electrostatic forces between particles and consequently reduces surface energy and surface tension[71]. Both 4 and 8 wt% GO reduced the average surface tension to 27.8 ±1.1 mN/m.

3.3.2 Viscosity

Figure 3(b) demonstrates the effect GO concentration has on the viscosity of PMMA chloroform solution. It can be seen that the introduction of a small quantity of GO initially reduces the average viscosity from 49.3 ±0.2 mPa·s to

47.7 ±0.6 mPa·s. After which, the increase in GO concentration results in an increase in average viscosity, with 4 wt% GO leading to an average viscosity of 48.9 ±0.3 mPa·s and 8 wt% GO resulting in 48.6 ±0.6 mPa·s. The introduction of a small quantity of GO nanosheets was found to initially decrease viscosity as GO behaved as a surfactant[72, 73]. Thereafter, the viscosity of the solution was found to increase with the volumetric loading of GO nanosheets. When in chloroform suspension, GO nanosheets can easily form clusters and aggregates due to its poor compatibility with chloroform. Clustering and aggregation increase the hydrodynamic diameter of nanosheets leading to the increase in viscosity[74].

3.4 Graphene Oxide/Polymer Fibres

3.4.1 Characterisation of Nanocomposite Fibres

A PMMA-chloroform system was selected for this work as previous work has considered this combination highly suitable for composite fibre fabrication and filtration applications[75-77].

SEM micrographs of the GO/PMMA fibres prepared from the suspension systems showed the fibres formed were generally continuous, porous and had a circular cross section. The successful formation of fibres suggests that for all four GO/PMMA suspensions the intermolecular entanglement and chain overlap

was appropriate to stabilise the polymer jet emitting from the orifices on the pressurised gyration vessel, despite the increasing GO load. The formation of non-beaded fibres also indicates the homogenous dispersion of GO nanosheets in the polymer solution.

From Figure 4 it can be said that the concentration of GO greatly dictates fibre morphology. The introduction of a small quantity of GO drastically decreased the average fibre diameter from 3.9 ±2.0 μm to 1.4 ±0.9 μm. A positive correlation can then be observed between the concentration of GO and the average fibre diameter; as the GO concentration increases within the polymer matrix, the fibres become larger in diameter with a wider fibre diameter distribution. This observation can be related to the viscosity measurements recorded for the corresponding polymer solutions. Previous literature has proven that the solution parameters and processing conditions are responsible for changes in fibre morphology during pressurised gyration[78]. However, as the processing parameters were consistent in this work it can be theorised that the GO incorporation is the sole factor influencing fibre morphology.

The trend seen in the fibre diameters can be attributed to the rheological properties of the GO/PMMA suspension. In this instance GO acted as a surfactant at low concentrations (2 wt%), thus prevented the formation of a

strong polymer network and consequently lowered viscosity and surface tension. This gave rise to thin fibres. At higher GO concentrations (4 and 8 wt%), the solution viscosity of the suspensions slightly increased, and though the applied centrifugal force and pressure difference was sufficiently high to modify the surface tension in supporting the fibre preparation, it was not strong enough to give rise to thin fibres. In addition, the dispersion of GO in the PMMA had a significant impact on fibre morphology. At low GO content, the nanosheets were dispersed relatively well in the polymer, hence the fibre diameter and distribution rates are reduced when compared to the others. High concentration of GO content resulted in improved Van der Waals forces between the GO nanosheets and the PMMA, therefore resulting in the agglomeration of GO and non-uniform dispersion of GO thus leading to a broad fibre diameter distribution [79-82].

Fibre topography included spherical surface pore structures, and its formation has been illustrated using the breath figures model (Figure 4(g)[77, 83]. Such surface features are ideal for filtration applications, as not only do they increase the surface area for bacteria to interact with, but they also work to physically trap the bacteria within their pits.

Raman mapping was used to identify GO in GO-loaded PMMA fibres, as shown in Figure 5. The dark areas in Figure 5(a) is GO, confirmed by Raman spectroscopy in Figure 5(b). The D peak (at 1350 cm^{-1}) arises from the breathing mode of the sp^2 hybridized carbon and induces the disorders including edges, functional groups, and structural defects[84]. The intensity ratio of D and G peaks (I_D/I_G) for GO was 0.88. The sharp peak seen at ~2800 cm^{-1} is due to the single layer of GO in the fibre. It also indicates that the GO may have some defects as a result of fibre formation during pressurised gyration. This peak can also be attributed to the overtone of the D′ peak and is called a 2D′ peak. Figure 5(c, d) show individual Raman mapping images of D peak and G peak within the surface of the PMMA fibre.

The FT-IR spectra of GO, PMMA and GO/PMMA fibres (Figure 6) showed the specific functional groups of C−O−C (~1000 cm^{-1}), C−O (1230 cm^{-1}), C=C (~1620 cm^{-1}) and C=O (1740–1720 cm^{-1}) bonds. The band in the region of 3600–3300 cm^{-1} corresponds to O−H stretching vibrations of hydroxyl and carboxyl functional groups of GO[85, 86]. The spectrum of PMMA showed a peak around 3500 cm^{-1} and a very sharp signal at 1732 cm^{-1}, corresponding to the stretching of hydroxyl and ester groups present in PMMA, respectively[87]. Typical bands at 987 and 1453 cm^{-1} correspond to O–CH_3 bending and stretching deformation of PMMA, respectively, while bands at 1730 and 1250

cm^{-1} belong to stretching of C=O groups[87]. Bands at 1065 and 1197 cm^{-1} represent C–O stretching vibration and chain vibration, respectively. The other bands in the 3000–2800 cm^{-1}, 1490–1275 cm^{-1} and 900–750 cm^{-1} spectral regions belong to CH_3 and CH_2 vibrational modes[88, 89]. The typical characteristics of GO in the FT-IR spectrum (Figure 6) are peaks conforming to the C=O stretching vibrations from carbonyl and carboxylic groups at 1735 cm^{-1}, C-C in aromatic ring at 1639 cm^{-1} and C–O–C stretching from epoxy groups at 1072 cm^{-1}, which confirms the existence of oxygen-related functional groups. Furthermore, a peak at 1382 cm^{-1} and a wide-ranging band at 3400 cm^{-1} are attributed to the stretching vibration of O–H groups[86, 90].

After pressurised gyration, the FT-IR spectra of GO-covered PMMA reveal typical peaks corresponding to PMMA (3001 and 2954 cm^{-1} for C–H stretching, 1735 cm^{-1} for C=O stretching, 1200 and 1148 cm^{-1} for C–O stretching) as well as O–H stretching peak at 3500 cm^{-1}, which is due to oxygen functional groups of GO[91]. These spectra clearly represent the chemical interaction between GO and PMMA. Previously reported work on CNT-PMMA nanocomposites showed the unpaired electrons associated with CNT activates the p-bond of CNT, which binds CNT with polymer chain[92]. GO has comparable physio-chemical characteristics and high specific surface area (in comparison to CNTs). Both

compounds show similar bands in their FT-IR spectra, suggesting that the GO nanosheets are successfully grafted onto the surface of PMMA.

Detailed Raman spectroscopy of the GO/PMMA fibres was performed. The Raman spectrum was compared with those of 'free' GO to investigate the effect of GO on the surface of PMMA. The Raman spectrum of GO/PMMA fibres is presented in Figure 7. The typical Raman peak of GO was characterized by a G band (at ca. 1604 cm-1) and D (1354 cm^{-1}) bands which represent the sp^2 hybridisation of carbon atoms and the breathing mode of k-point phonons of A1g symmetry respectively[86, 90]. The six characteristic bands of GO-covered PMMA observed at 2953, 2848, 1739, 1605, 1453, 1348 cm^{-1}. Raman band 2953 represents the C-H stretching vibration[93]. The band at 1739 cm^{-1} is ascribed to the combination band arising out of ν(C=C) and ν(C–COO) modes[93].

PMMA triggers slight hardening and wide-ranging of the G and 2D peaks. Both G and D peaks are slightly shifted from 1604 and 1354 to 1605 and 1348 cm^{-1} respectively owing to the residual compression strain persuaded by the temperature involved in fibre preparation. The D band indicates defects including vacancies, grain boundaries, and amorphous carbon species[90, 94]. In the GO-covered PMMA fibres, a small change in the D peak is observed, resulting in a slight increase in the ID/IG, undoubtedly demonstrating that sp^3

grafting sites are being introduced onto the carbon lattice. The ID/IG ration can be used to calculate the interdefect distance and number density of grafted sites per unit area[95, 96]. The spectra for graphene related materials show D, G and 2D peaks, allowing the classification of these materials in different hybridisation profiles[97], where the defect density does not exceed the Tunstra-Koenig limit[95]. It has been evidently proved that this peak arises from double resonance in addition to phonon confinement[98]. The decrease in intensities of both peaks (D and G) also indicates improved graphitization. For monolayer graphene, there is a sharp peak at ca. 2848 cm^{-1} which typically represent of the number of layers of graphene. In the current work, the band is observed to be sharp, indicating that as-prepared GO comprises single layer with defects. These defects are also an indication of processing of fibre preparation[99].

Both FT-IR and Raman spectroscopy of the GO/PMMA nanocomposite fibres confirmed the presence of GO on the fibre surface. This fibre characteristic plays a vital role in the antimicrobial mechanism of action of the fibres.

3.4.2 Antibacterial Activity of Graphene Oxide in Polymeric Fibres

The antibacterial activity of GO in PMMA fibres was investigated using *E. coli* K12. As discussed above, antibacterial activity of pure GO nanosheets was

observed at a concentration of 2 wt%, therefore the fibres investigated had GO concentrations of 0, 2, 4 and 8 wt%. In comparison to pure PMMA fibres, the results confirmed that GO-covered PMMA fibres proficiently reduced the number of *E. coli* K-12 cells. The percentage bacterial reductions are shown in Figure 8. The PMMA fibres (negative control) exhibited no antimicrobial activity, as a bacterial increase of 25 ±7.9% was observed. In contrast, all the GO/PMMA fibre meshes displayed antibacterial behaviour. At the lowest GO-covered PMMA concentration, 45 ±2.2% of the total *E. coli* K-12 viability was significantly reduced, while 70 ±2.4% of the total bacteria was reduced after incubation with PMMA with 4 wt% GO. The maximum antibacterial activity was noticed in the case of 8 wt% GO loaded-PMMA, with an 85 ±1.4% reduction in cell numbers being observed. The results showed that the antibacterial activity of the GO/PMMA fibre meshes are a function of GO concentration. The bacterial reduction observed with 8 wt% GO loaded-PMMA is comparable to 8 wt% graphene nanoplatelet loaded-PMMA fibres, where a reduction of 85 ±5% was noted[100]. GO loaded-PMMA fibres present themselves as a favourable alternative, as GO is more easily accessible when compared to pure graphene. The antimicrobial properties of GO loaded-PMMA fibres were less potent than free GO, however incorporating GO into fibres broadens the number of applications GO can be used in. Also, increasing the quantity of GO in PMMA provide evidences for bacteria to interact with GO, therefore causing the

decreased levels of *E. coli*. Our results are consistent with other previously reported work revealing the concentration-dependent GO toxicity[38, 100, 101].

Pure PMMA fibres proved to have little interference with normal bacterial growth and proliferation as a percentage increase in bacterial numbers was observed, despite previous studies showing the contrary[100]. This suggests that the PMMA had no antibacterial properties, and the antibacterial activities seen with the GO/PMMA fibre meshes are solely due to the presence of GO.

The antibacterial activity of PMMA fibres containing 2 wt% of GO were initially tested. These fibres exhibited antibacterial properties with an average bacterial reduction of 45 ±2.2%. This percentage reduction is significantly lower than the observed reduction of pure GO nanosheets. This is due to the GO nanosheets being embedded within the PMMA fibres and not just on the surface. Increasing the GO concentration to 4 wt% increased the antibacterial action of the fibres, showing bacterial reduction at 70%. This indicates a higher concentration of GO nanosheets on the fibre surface, therefore there is more GO for the bacteria to interact with. Increasing the GO concentration further to 8 wt% significantly enhanced the antibacterial action of the fibre, as these fibres showed the strongest antibacterial activity with a cell inactivation percentage of 85 ±1.4% being achieved. Previous literature has reported different minimum inhibition

concentrations (MICs) for GO. Nanda *et al.*, have reported the MIC to be 1 µg/mL[102]. Liu *et al.*, reported the MIC to be 80 µg/mL, with a 91.6% inhibition[38]. Whilst Shubha et al., have reported a MIC of 50000 µg/mL[103]. In this research, when 8 wt% fibres were used, the GO concentration was 530 µg/mL.

A multitude of GO-based antibacterial mechanisms has been explained in literature. However, as the GO nanosheets are not floating free in the bacterial suspension, but instead they are trapped within PMMA fibres and not protruding from the fibre surface, it can be presumed that in this instance the antibacterial mechanism of action involves a chemical reaction, such as oxidative stress.

3.4.3 Reactive Oxygen Species Generation

The oxidative stress caused by GO has been reported as a main toxicity mechanism[104]. In this work, the prepared GO/PMMA nanocomposite fibres were studied to see if they produce ROS. From Figure 9 it is evident that ROS production began at approximately 70 minutes and steadily increased over the 400-minute incubation period. DCFH can react with different ROS such as hydrogen peroxide, HO and other free radicals therefore the delay in the signal may be explained by the participation of other ROS than the hydrogen peroxide

used in the control. Also while the hydrogen peroxide present in the control is readily available to reduce the probe while the GO fibres ROS generation may depend on the generation of an intermediary[105]. Overproduction of ROS is a principal representative of oxidative stress, hence the measurement of ROS indicates ROS-mediated oxidative stress is the likely antibacterial mode of action[104, 106]. It is thought that the GO present on the surface of the fibre produces ROS via the singlet oxygen-superoxide anion radical pathway, which plays a significant role in release of cytochrome c and other pro-apoptotic proteins, which in turn mediate caspase activation and apoptosis through the generation of protein radicals, activation of lipid peroxidation, DNA-strand breakage, modification to nucleic acids, gene expression through activation of redox-sensitive transcription factors and modulation of inflammatory responses through signal transduction[107-114].

3.4.4 Post Treatment Characterisation

3.4.4.1 Imaging Using Stimulated Raman Spectroscopy

GO revealed a strong signal within the SRS channel, this signal has a broad spectral profile which can be attributed to pump-probe interactions within the GO, rather than more chemically specific Raman vibrations[115]. PMMA is also visualised in the SRS channel, the signal from the PMMA shows a strong peak at 2940cm^{-1} which can be attributed to the CH_3 Raman vibrations. Figure 10 a)

compares the spectra of the PMMA and GO-PMMA-bacteria. The intensity of the SRS signal in GO-PMMA is much higher than PMMA alone. Figure 10 b shows the results of Multi Curve Regression (MCR) analysis[116] performed on a hyperspectral data stack of the sample containing PMMA, GO and bacteria. The analysis enabled the signal from the PMMA shown in red from the GO shown in green to be separated based on their spectral properties. The images show flakes of GO distributed across the surface of the PMMA fibres, which contribute to the high killing efficacy of composites towards *E. coli* (which is also demonstrated from antibacterial activities of composites towards programmed cell death of bacteria).

3.4.4.2 Scanning Electron Microscopy

SEM analysis was used to examine the interaction between the microbes and the 8 wt% GO/PMMA fibres and to assess any changes in cell morphology. **Figure 11** shows the bacterial cells, *E. coli*, on the 8 wt% GO/PMMA fibres.

In the presence of 8 wt% GO/PMMA fibres the bacteria showed changes in cell morphology. Healthy prokaryotic cells form a capsule, a protective layer rich in sugars, proteins and alcohol, and/or lipids that help stick bacteria to each other as well as onto the substrate [117, 118]. In addition to this layer, Gram-negative bacteria (*E. coli*) also contain an asymmetric outer membrane whose inner

leaflet is composed largely of glycerophospholipids and an outer leaflet composed of lipopolysaccharides. These capsules cover the entire bacteria as well as the whole space between bacteria. As shown in **Figure 11**, exposure of the bacterial cells to 8 wt% GO/PMMA fibres caused capsule degradation, as the capsule is removed from the exposed parts of bacteria. In addition, visible damage on the *E. coli* cell surface can be seen as the cells have a distorted structure. This characteristic is symptomatic of ROS degradation[119, 120].

The toxic effect of the 8 wt% GO/PMMA on bacterial cells is evident from this research, however their effect on human cells needs to be further investigated. Existing literature gives conflicting opinions, some articles state that GO is cytotoxic, whilst others state that composited GO is not cytotoxic to mammalian cells and can be used in various biomedical constructs [121-124].

4.0 Conclusions

This research showcases the antibacterial activity of prepared GO nanosheets and GO/PMMA nanocomposite fibres for filtration applications. The results collected in this study support the hypothesis that as-prepared GO nanosheets are able to retain their antibacterial properties when processed into composite fibres, therefore demonstrating their effectiveness in the real world.

GO/PMMA nanocomposite fibre meshes were successfully prepared using pressurised gyration and characterised by SEM, FT-IR, Raman mapping, Raman spectroscopy and stimulated Raman mapping. Average fibre diameters ranged between 1.4 μm and 3.9 μm. FT-IR and Raman analysis confirmed the presence of GO nanosheets on the surface of the polymeric fibres. The interaction between bacterial cells and GO/PMMA fibres, demonstrated the fibres antibacterial properties. Colony counting method results showed 8 wt% GO/PMMA fibre meshes to have the strongest antibacterial activity, as a bacterial reduction of 85 ±1.4% was observed, which is stronger to what was observed with GO/poly (vinyl alcohol) fibres when considering poly (vinyl alcohol) is water soluble[125]. These studies showed the biocidal activities of GO to be retained when processed using pressurised gyration. The antibacterial properties of the nanocomposite fibres were dose-dependent, as average bacterial reductions steadily rose from 45 ±2.2% to 85 ±1.4%. The cytotoxicity properties of the nanocomposite fibres are attributed to the production of oxidative stress. Increasing the concentration of GO in the fibres, the bacteria have a higher chance to interact with the toxic GO nanoparticles on the surface of the fibres (as confirmed by post-treatment SEM and stimulated Raman spectroscopy). Compared with previous reports of antimicrobial GO, this work demonstrates the translation of lab-based science to real life application. With the knowledge obtained in this study it can be concluded that GO nanosheets

retain their antibacterial properties when composited in non-water-soluble polymeric fibres, thus providing insight of their potential in a number of applications including filtration.

Acknowledgements

This work was supported by EPSRC grant EP/N034228/1. The authors would like to thank Dr Melisa Canales for her assistance in the Healthy Infrastructure Research Group Laboratory, Department of Civil, Environmental and Geomatic Engineering, University College London, London, WC1E 7JE, UK. Sincerest gratitude to Dr Elaine Allan for use of her equipment in the ROS studies is also acknowledged. The SRS imaging was carried out using the CONTRAST facility which is funded by the EPSRC grant number EP/5009957/1.

CRediT Authorship Contribution:

Rupy Kaur Matharu: conceptualisation, methodology, validation, formal analysis, investigation, writing – original draft, writing – review and editing, visualisation, project administration. **Tanveer A Tabish**: validation, formal analysis, investigation, resources, writing – review and editing, visualisation. **Thithawat Trakoolwilaiwan**: methodology, validation, formal analysis, investigation, writing – review and editing, visualisation. **Jessica Mansfield**: methodology, formal analysis, investigation, resources, writing – review and editing, funding

acquisition. **Julian Moger**: methodology, formal analysis, investigation, resources, writing – review and editing, funding acquisition. **Tongfei Wu**: methodology, formal analysis, investigation, resources, writing – review and editing. **Cláudio Lourenço**: methodology, formal analysis, investigation, resources, writing – review and editing. **Biqiong Chen**: formal analysis, resources, writing – review and editing, supervision, project administration. **Lena Ciric**: writing – review and editing, funding acquisition. **Ivan P Parkin**: project resources, writing – review and editing. **Mohan Edirisinghe**: conceptualisation, methodology, resources, writing – review and editing, supervision, project administration, funding acquisition.

References:

[1] M.C. Verdenelli, C. Cecchini, C. Orpianesi, G.M. Dadea, A. Cresci, Efficacy of antimicrobial filter treatments on microbial colonization of air panel filters, J Appl Microbiol 94(1) (2003) 9-15.

[2] E.S. Chong, G.B. Hwang, C.W. Nho, B.M. Kwon, J.E. Lee, S. Seo, G.N. Bae, J.H. Jung, Antimicrobial durability of air filters coated with airborne Sophora flavescens nanoparticles, Sci Total Environ 444 (2013) 110-114.

[3] H. Burge, Bioaerosols - Prevalence and Health-Effects in the Indoor Environment, J Allergy Clin Immun 86(5) (1990) 687-701.

[4] S. Clark, R. Rylander, L. Larsson, Airborne Bacteria, Endotoxin and Fungi in Dust in Poultry and Swine Confinement Buildings, Am Ind Hyg Assoc J 44(7) (1983) 537-541.

[5] R.E. Dales, S. Cakmak, R.T. Burnett, S. Judek, F. Coates, J.R. Brook, Influence of ambient fungal spores on emergency visits for asthma to a regional children's hospital, Am J Resp Crit Care 162(6) (2000) 2087-2090.

[6] J.M. Daisey, W.J. Angell, M.G. Apte, Indoor air quality, ventilation and healthy symptoms in schools: an analysis of existing information., Indoor Air 13 (2003).

[7] L. Bonadonna, A. Marconi, Aerosol biologici e microclima abitativo. Effetti sanitari e problemi di determinazione., Ambiente. Risorse. Salute 104 (1990) 6.

[8] M. Pitzurra, A. Savino, C. Pasquarella, Microbiological environment monitoring., Annali di Igiene 9 (1997) 6.
[9] A.P. Jones, Indoor air quality and health, Atmos Environ 33(28) (1999) 4535-4564.
[10] J.D. Spengler, K. Sexton, Indoor Air-Pollution - a Public-Health Perspective, Science 221(4605) (1983) 9-17.
[11] P. Jain, T. Pradeep, Potential of silver nanoparticle-coated polyurethane foam as an antibacterial water filter, Biotechnol Bioeng 90(1) (2005) 59-63.
[12] G.B. Hwang, J.H. Jung, T.G. Jeong, B.U. Lee, Effect of hybrid UV-thermal energy stimuli on inactivation of S. epidermidis and B. subtilis bacterial bioaerosols, Sci Total Environ 408(23) (2010) 5903-5909.
[13] J.H. Jung, J.E. Lee, S.S. Kim, Thermal effects on bacterial bioaerosols in continuous air flow, Sci Total Environ 407(16) (2009) 4723-4730.
[14] B.U. Lee, S.H. Yun, J.H. Ji, G.N. Bae, Inactivation of S. epidermidis, B. subtilis, and E. coli bacteria bioaerosols deposited on a filter utilizing airborne silver nanoparticles, J Microbiol Biotechnol 18(1) (2008) 176-82.
[15] C.Y. Lin, C.S. Li, Control effectiveness of ultraviolet germicidal irradiation on bioaerosols, Aerosol Sci Tech 36(4) (2002) 474-478.
[16] J. Peccia, M. Hernandez, UV-induced inactivation rates for airborne Mycobacterium bovis BCG, J Occup Environ Hyg 1(7) (2004) 430-435.
[17] A. Podgórski, A. Bałazy, L. Gradoń, Application of nanofibers to improve the filtration efficiency of the most penetrating aerosol particles in fibrous filters, Chemical Engineering Science 61(20) (2006).
[18] R.S. Barhate, S. Ramakrishna, Nanofibrous filtering media: Filtration problems and solutions from tiny materials, J Membrane Sci 296(1-2) (2007) 1-8.
[19] R. Przekop, L. Gradon, Deposition and filtration of nanoparticles in the composites of nano- and microsized fibers, Aerosol Sci Tech 42(6) (2008) 483-493.
[20] J. Li, H.A. Chase, Applications of membrane techniques for purification of natural products, Biotechnol Lett 32(5) (2010) 601-608.
[21] N. Porcelli, S. Judd, Chemical cleaning of potable water membranes: A review, Sep Purif Technol 71(2) (2010) 137-143.
[22] A. Sato, R. Wang, H.Y. Ma, B.S. Hsiao, B. Chu, Novel nanofibrous scaffolds for water filtration with bacteria and virus removal capability, J Electron Microsc 60(3) (2011) 201-209.
[23] C.S. Wang, Electrostatic forces in fibrous filters - a review, Powder Technol 118(1-2) (2001) 166-170.
[24] A. Cooper, R. Oldinski, H.Y. Ma, J.D. Bryers, M.Q. Zhang, Chitosan-based nanofibrous membranes for antibacterial filter applications, Carbohyd Polym 92(1) (2013) 254-259.
[25] G.A. Mcfeters, D.G. Stuart, Survival of Coliform Bacteria in Natural Waters - Field and Laboratory Studies with Membrane-Filter Chambers, Appl Microbiol 24(5) (1972) 805-811.
[26] R.B. Simmons, S.A. Crow, Fungal Colonization of Air Filters for Use in Heating, Ventilating, and Air-Conditioning (Hvac) Systems, J Ind Microbiol 14(1) (1995) 41-45.
[27] D.G. Ahearn, S.A. Crow, R.B. Simmons, D.L. Price, S.K. Mishra, D.L. Pierson, Fungal colonization of air filters and insulation in a multi-story office building: Production of volatile organics, Curr Microbiol 35(5) (1997) 305-308.
[28] R.B. Simmons, D.L. Price, J.A. Noble, S.A. Crow, D.G. Ahearn, Fungal colonization of air filters from hospitals, Am Ind Hyg Assoc J 58(12) (1997) 900-904.
[29] D.L. Price, R.B. Simmons, I.M. Ezeonu, S.A. Crow, D.G. Ahearn, Colonization of Fiberglass Insulation Used in Heating, Ventilation and Air-Conditioning Systems, J Ind Microbiol 13(3) (1994) 154-158.

[30] T.H. Keuhn, D.Y.H. Pui, D. Vesley, C.D. Berg, M. Peloquin, Matching filtration with health requirements, ASHRAE Trans 97 (1991) 164-169.
[31] S.J. Kemp, T.H. Kuehn, D.Y.H. Pui, D. Vesley, A.J. Streifel, Growth of microorganisms on HVAC filters under controlled temperature and humidity conditions, Ashrae Tran 101 (1995) 305-316.
[32] T.H. Keuhn, D.Y.H. Pui, D. Vesley, C.D. Berg, M. Peloquin, Matching filtration with health requirements, ASHRAE Transactions 97 (1991) 164-169.
[33] G.H. Wagman, J.V. Bailey, M.J. Weinstein, Binding of Aminoglycoside Antibiotics to Filtration Materials, Antimicrob Agents Ch 7(3) (1975) 316-319.
[34] T. Ren, T.V. Dormitorio, M.Y. Qiao, T.S. Huang, J. Weese, N-halamine incorporated antimicrobial nonwoven fabrics for use against avian influenza virus, Vet Microbiol 218 (2018) 78-83.
[35] J.V. Cento, S. Barbaliscia, C.F. Perno, Biotech innovations in the prevention of respiratory infectious diseases, New Microbiol 40(3) (2017) 155-160.
[36] G. Borkow, J. Gabbay, Putting copper into action: copper-impregnated products with potent biocidal activities, Faseb J 18(12) (2004) 1728-+.
[37] B. De Gusseme, L. Sintubin, L. Baert, E. Thibo, T. Hennebel, G. Vermeulen, M. Uyttendaele, W. Verstraete, N. Boon, Biogenic silver for disinfection of water contaminated with viruses, Appl Environ Microbiol 76(4) (2010) 1082-7.
[38] S.B. Liu, T.H. Zeng, M. Hofmann, E. Burcombe, J. Wei, R.R. Jiang, J. Kong, Y. Chen, Antibacterial Activity of Graphite, Graphite Oxide, Graphene Oxide, and Reduced Graphene Oxide: Membrane and Oxidative Stress, Acs Nano 5(9) (2011) 6971-6980.
[39] C. Bora, P. Bharali, S. Baglari, S.K. Dolui, B.K. Konwar, Strong and conductive reduced graphene oxide/polyester resin composite films with improved mechanical strength, thermal stability and its antibacterial activity, Composites Science and Technology 87 (2013) 1-7.
[40] R.K. Matharu, L. Ciric, M. Edirisinghe, Nanocomposites: suitable alternatives as antimicrobial agents, Nanotechnology 29(28) (2018) 282001.
[41] Z.M. Marković, D.M. Matijašević, V.B. Pavlović, S.P. Jovanović, I.D. Holclajtner-Antunović, Z. Špitalský, M. Mičušik, M.D. Dramićanin, D.D. Milivojević, M.P. Nikšić, B.M. Todorović Marković, Antibacterial potential of electrochemically exfoliated graphene sheets, Journal of Colloid and Interface Science 500 (2017) 30-43.
[42] L.Q. Xu, Y.B. Liao, N.N. Li, Y.J. Li, J.Y. Zhang, Y.B. Wang, X.F. Hu, C.M. Li, Vancomycin-assisted green synthesis of reduced graphene oxide for antimicrobial applications, Journal of Colloid and Interface Science 514 (2018) 733-739.
[43] S.M. Dizaj, A. Mennati, S. Jafari, K. Khezri, K. Adibkia, Antimicrobial Activity of Carbon-Based Nanoparticles, Adv Pharm Bull 5(1) (2015) 19-23.
[44] S. Kang, M. Herzberg, D.F. Rodrigues, M. Elimelech, Antibacterial effects of carbon nanotubes: Size does matter, Langmuir 24(13) (2008) 6409-6413.
[45] C. Buzea, I.I. Pacheco, K. Robbie, Nanomaterials and nanoparticles: Sources and toxicity, Biointerphases 2(4) (2007) Mr17-Mr71.
[46] S. Park, R.S. Ruoff, Chemical methods for the production of graphenes, Nat Nanotechnol 4(4) (2009) 217-224.
[47] O.C. Compton, S.T. Nguyen, Graphene Oxide, Highly Reduced Graphene Oxide, and Graphene: Versatile Building Blocks for Carbon-Based Materials, Small 6(6) (2010) 711-723.
[48] S.R.V. Castrillon, F. Perreault, A.F. de Faria, M. Elimelech, Interaction of Graphene Oxide with Bacterial Cell Membranes: Insights from Force Spectroscopy, Environ Sci Tech Let 2(4) (2015) 112-117.
[49] J.H. Li, G. Wang, H.Q. Zhu, M. Zhang, X.H. Zheng, Z.F. Di, X.Y. Liu, X. Wang, Antibacterial activity of large-area monolayer graphene film manipulated by charge transfer, Sci Rep-Uk 4 (2014).

[50] J.N. Chen, X.P. Wang, H.Y. Han, A new function of graphene oxide emerges: inactivating phytopathogenic bacterium Xanthomonas oryzae pv. Oryzae, J Nanopart Res 15(5) (2013).
[51] S. Gurunathan, J.W. Han, A.A. Dayem, V. Eppakayala, J.H. Kim, Oxidative stress-mediated antibacterial activity of graphene oxide and reduced graphene oxide in Pseudomonas aeruginosa, Int J Nanomed 7 (2012) 5901-5914.
[52] S.S. Nanda, D.K. Yi, K. Kim, Study of antibacterial mechanism of graphene oxide using Raman spectroscopy, Sci Rep-Uk 6 (2016).
[53] R.F. Al-Thani, N.K. Patan, M.A. Al-Maadeed, Graphene oxide as antimicrobial against two gram-positive and two gram-negative bacteria in addition to one fungus., OnLine Journal of Biological Sciences 14 (2014) 230-239.
[54] M. Hu, Z. Cui, J. Li, L. Zhang, Y. Mo, D.S. Dlamini, H. Wang, B. He, J. Li, H. Matsuyama, Ultra-low graphene oxide loading for water permeability, antifouling and antibacterial improvement of polyethersulfone/sulfonated polysulfone ultrafiltration membranes, Journal of Colloid and Interface Science 552 (2019) 319-331.
[55] D.C. Marcano, D.V. Kosynkin, J.M. Berlin, A. Sinitskii, Z.Z. Sun, A. Slesarev, L.B. Alemany, W. Lu, J.M. Tour, Improved Synthesis of Graphene Oxide, Acs Nano 4(8) (2010) 4806-4814.
[56] A. Amir, S. Mahalingam, X. Wu, H. Porwal, P. Colombo, M.J. Reece, M. Edirisinghe, Graphene nanoplatelets loaded polyurethane and phenolic resin fibres by combination of pressure and gyration, Composites Science and Technology 129 (2016) 173-182.
[57] C. Bankier, R.K. Matharu, Y.K. Cheong, G.G. Ren, E. Cloutman-Green, L. Ciric, Synergistic Antibacterial Effects of Metallic Nanoparticle Combinations, Sci Rep-Uk 9(1) (2019) 16074.
[58] B. Kalyanaraman, V. Darley-Usmar, K.J. Davies, P.A. Dennery, H.J. Forman, M.B. Grisham, G.E. Mann, K. Moore, L.J. Roberts, 2nd, H. Ischiropoulos, Measuring reactive oxygen and nitrogen species with fluorescent probes: challenges and limitations, Free Radic Biol Med 52(1) (2012) 1-6.
[59] A. Zeytunyan, T. Baldacchini, R. Zadoyan, Module for multiphoton high-resolution hyperspectral imaging and spectroscopy, SPIE2018.
[60] J.W. Suk, R.D. Piner, J. An, R.S. Ruoff, Mechanical properties of monolayer graphene oxide, Acs Nano 4(11) (2010) 6557-64.
[61] O. Akhavan, E. Ghaderi, Escherichia coli bacteria reduce graphene oxide to bactericidal graphene in a self-limiting manner, Carbon 50(5) (2012) 1853-1860.
[62] O. Akhavan, E. Ghaderi, Toxicity of Graphene and Graphene Oxide Nanowalls Against Bacteria, Acs Nano 4(10) (2010) 5731-5736.
[63] I.Y. Kim, S. Park, H. Kim, S. Park, R.S. Ruoff, S.J. Hwang, Strongly-Coupled Freestanding Hybrid Films of Graphene and Layered Titanate Nanosheets: An Effective Way to Tailor the Physicochemical and Antibacterial Properties of Graphene Film, Adv Funct Mater 24(16) (2014) 2288-2294.
[64] J.N. Chen, H. Peng, X.P. Wang, F. Shao, Z.D. Yuan, H.Y. Han, Graphene oxide exhibits broad-spectrum antimicrobial activity against bacterial phytopathogens and fungal conidia by intertwining and membrane perturbation, Nanoscale 6(3) (2014) 1879-1889.
[65] J.L. He, X.D. Zhu, Z.N. Qi, C. Wang, X.J. Mao, C.L. Zhu, Z.Y. He, M.Y. Lo, Z.S. Tang, Killing Dental Pathogens Using Antibacterial Graphene Oxide, Acs Appl Mater Inter 7(9) (2015) 5605-5611.
[66] X.P. Wang, X.Q. Liu, H.Y. Han, Evaluation of antibacterial effects of carbon nanomaterials against copper-resistant Ralstonia solanacearum, Colloid Surface B 103 (2013) 136-142.
[67] A.R. Murray, E.R. Kisin, A.V. Tkach, N. Yanamala, R. Mercer, S.H. Young, B. Fadeel, V.E. Kagan, A.A. Shvedova, Factoring-in agglomeration of carbon nanotubes and nanofibers for better prediction of their toxicity versus asbestos, Part Fibre Toxicol 9 (2012).

[68] I.E.M. Carpio, C.M. Santos, X. Wei, D.F. Rodrigues, Toxicity of a polymer-graphene oxide composite against bacterial planktonic cells, biofilms, and mammalian cells, Nanoscale 4(15) (2012) 4746-4756.
[69] L. Hui, J.G. Piao, J. Auletta, K. Hu, Y. Zhu, T. Meyer, H. Liu, L. Yang, Availability of the basal planes of graphene oxide determines whether it is antibacterial, ACS Appl Mater Interfaces 6(15) (2014) 13183-90.
[70] J.D. Mangadlao, C.M. Santos, M.J.L. Felipe, A.C.C. de Leon, D.F. Rodrigues, R.C. Advincula, On the antibacterial mechanism of graphene oxide (GO) Langmuir-Blodgett films, Chem Commun 51(14) (2015) 2886-2889.
[71] S. Tanvir, L. Qiao, Surface tension of Nanofluid-type fuels containing suspended nanomaterials, Nanoscale Res Lett 7(1) (2012) 226.
[72] J. Cote Laura, J. Kim, C. Tung Vincent, J. Luo, F. Kim, J. Huang, Graphene oxide as surfactant sheets, Pure and Applied Chemistry, 2010, p. 95.
[73] T.M. McCoy, G. Turpin, B.M. Teo, R.F. Tabor, Graphene oxide: a surfactant or particle?, Current Opinion in Colloid & Interface Science 39 (2019) 98-109.
[74] S.M.S. Murshed, K.C. Leong, C. Yang, Investigations of thermal conductivity and viscosity of nanofluids, Int J Therm Sci 47(5) (2008) 560-568.
[75] U.E. Illangakoon, S. Mahalingam, P. Colombo, M. Edirisinghe, Tailoring the surface of polymeric nanofibres generated by pressurised gyration, Surf Innov 4(3) (2016) 167-178.
[76] U.E. Illangakoon, S. Mahalingam, K. Wang, Y.K. Cheong, E. Canales, G.G. Ren, E. Cloutman-Green, M. Edirisinghe, L. Ciric, Gyrospun antimicrobial nanoparticle loaded fibrous polymeric filters, Mat Sci Eng C-Mater 74 (2017) 315-324.
[77] U.E. Illangakoon, S. Mahalingam, R.K. Matharu, M. Edirisinghe, Evolution of Surface Nanopores in Pressurised Gyrospun Polymeric Microfibers, Polymers-Basel 9(10) (2017).
[78] S. Mahalingam, M. Edirisinghe, Forming of polymer nanofibers by a pressurised gyration process, Macromol Rapid Commun 34(14) (2013) 1134-9.
[79] M.P. Weir, D.W. Johnson, S.C. Boothroyd, R.C. Savage, R.L. Thompson, S.M. King, S.E. Rogers, K.S. Coleman, N. Clarke, Distortion of Chain Conformation and Reduced Entanglement in Polymer-Graphene Oxide Nanocomposites, Acs Macro Lett 5(4) (2016) 430-434.
[80] X.W. Wu, S. Mahalingam, A. Amir, H. Porwal, M.J. Reece, V. Naglieri, P. Colombo, M. Edirisinghe, Novel Preparation, Microstructure, and Properties of Polyacrylonitrile-Based Carbon Nanofiber-Graphene Nanoplatelet Materials, Acs Omega 1(2) (2016) 202-211.
[81] Y. Xu, B.K. Zhu, Y.Y. Xu, A study on formation of regular honeycomb pattern in polysulfone film, Polymer 46(3) (2005) 713-717.
[82] M. Weir, D. Johnson, S. Boothroyd, R. Savage, R. Thompson, S. King, S. Rogers, K. Coleman, N. Clarke, Distortion of chain conformation and reduced entanglement in polymer–graphene oxide nanocomposites, Acs Macro Lett 5(4) (2016) 430-434.
[83] A.J. Zhang, H. Bai, L. Li, Breath Figure: A Nature-Inspired Preparation Method for Ordered Porous Films, Chem Rev 115(18) (2015) 9801-9868.
[84] S. Stankovich, D.A. Dikin, R.D. Piner, K.A. Kohlhaas, A. Kleinhammes, Y. Jia, Y. Wu, S.T. Nguyen, R.S. Ruoff, Synthesis of graphene-based nanosheets via chemical reduction of exfoliated graphite oxide, Carbon 45(7) (2007) 1558-1565.
[85] T.A. Tabish, M.Z.I. Pranjol, D.W. Horsell, A.A.M. Rahat, J.L. Whatmore, P.G. Winyard, S. Zhang, Graphene Oxide-Based Targeting of Extracellular Cathepsin D and Cathepsin L As A Novel Anti-Metastatic Enzyme Cancer Therapy, Cancers 11(3) (2019).
[86] T.A. Tabish, M.Z.I. Pranjol, H. Hayat, A.A.M. Rahat, T.M. Abdullah, J.L. Whatmore, S. Zhang, In vitro toxic effects of reduced graphene oxide nanosheets on lung cancer cells, Nanotechnology 28(50) (2017) 504001.

[87] F.J. Tommasini, L.d.C. Ferreira, L.G.P. Tienne, V.d.O. Aguiar, M.H.P.d. Silva, L.F.d.M. Rocha, M.d.F.V. Marques, Poly (Methyl Methacrylate)-SiC Nanocomposites Prepared Through in Situ Polymerization, Materials Research 21 (2018).
[88] I.S. Elashmawi, N.A. Hakeem, Effect of PMMA addition on characterization and morphology of PVDF, Polymer Engineering & Science 48(5) (2008) 895-901.
[89] S. Ramesh, K.H. Leen, K. Kumutha, A.K. Arof, FTIR studies of PVC/PMMA blend based polymer electrolytes, Spectrochimica Acta Part A: Molecular and Biomolecular Spectroscopy 66(4) (2007) 1237-1242.
[90] T.A. Tabish, F.A. Memon, D.E. Gomez, D.W. Horsell, S. Zhang, A facile synthesis of porous graphene for efficient water and wastewater treatment, Sci Rep 8(1) (2018) 1817.
[91] S.N. Tripathi, P. Saini, D. Gupta, V. Choudhary, Electrical and mechanical properties of PMMA/reduced graphene oxide nanocomposites prepared via in situ polymerization., Journal of Materials Science 48(18) (2013) 6223-6232.
[92] S.H.R. Ali, M.K. Bedewy, M.A. Etman, H.A. Khalil, B.S. Azzam, Morphology and properties of polymer matrix nanocomposites, International Journal of Metrology and Quality Engineering 1(1) (2010) 33-39.
[93] K.J. Thomas, M. Sheeba, V.P.N. Nampoori, C.P.G. Vallabhan, P. Radhakrishnan, Raman spectra of polymethyl methacrylate optical fibres excited by a 532 nm diode pumped solid state laser., Journal of Optics A: Pure and Applied Optics 10(5) (2008) 055303.
[94] L.Z. Guan, Y.J. Wan, L.X. Gong, D. Yan, L.C. Tang, L.B. Wu, J.X. Jiang, G.Q. Lai, Toward effective and tunable interphases in graphene oxide/epoxy composites by grafting different chain lengths of polyetheramine onto graphene oxide. , Journal of Materials Chemistry A 2(36) (2014) 15058-15069.
[95] F. Tuinstra, J.L. Koenig, Raman Spectrum of Graphite, The Journal of Chemical Physics 53(3) (1970) 1126-1130.
[96] L.G. Cançado, A. Jorio, E.H.M. Ferreira, F. Stavale, C.A. Achete, R.B. Capaz, M.V.O. Moutinho, A. Lombardo, T.S. Kulmala, A.C. Ferrari, Quantifying Defects in Graphene via Raman Spectroscopy at Different Excitation Energies, Nano Letters 11(8) (2011) 3190-3196.
[97] A.C. Ferrari, Raman spectroscopy of graphene and graphite: Disorder, electron–phonon coupling, doping and nonadiabatic effects, Solid State Communications 143(1) (2007) 47-57.
[98] A.C. Ferrari, D.M. Basko, Raman spectroscopy as a versatile tool for studying the properties of graphene, Nat Nanotechnol 8 (2013) 235.
[99] M. Xia, Z. Su, S. Zhang, Raman spectra of bilayer graphene covered with Poly (methyl methacrylate) thin film., AIP Advances 2(3) (2012) 032122.
[100] R.K. Matharu, H. Porwal, L. Ciric, M. Edirisinghe, The effect of graphene-poly(methyl methacrylate) fibres on microbial growth, Interface Focus 8(3) (2018).
[101] J.N. Chen, L. Sun, Y. Cheng, Z.C. Lu, K. Shao, T.T. Li, C. Hu, H.Y. Han, Graphene Oxide-Silver Nanocomposite: Novel Agricultural Antifungal Agent against Fusarium graminearum for Crop Disease Prevention, Acs Appl Mater Inter 8(36) (2016) 24057-24070.
[102] S.S. Nanda, D.K. Yi, K. Kim, Study of antibacterial mechanism of graphene oxide using Raman spectroscopy, Sci Rep-Uk 6(1) (2016) 28443.
[103] P. Shubha, K. Namratha, K. Byrappa, Graphene oxide – a promising material for antimicrobial surface against nosocomial pathogens, Materials Research Innovations 22(2) (2018) 85-90.
[104] Y. Zhang, S.F. Ali, E. Dervishi, Y. Xu, Z. Li, D. Casciano, A.S. Biris, Cytotoxicity effects of graphene and single-wall carbon nanotubes in neural phaeochromocytoma-derived PC12 cells, Acs Nano 4(6) (2010) 3181-6.
[105] A. Gomes, E. Fernandes, J.L.F.C. Lima, Fluorescence probes used for detection of reactive oxygen species, J Biochem Bioph Meth 65(2-3) (2005) 45-80.

[106] S. Gurunathan, J.W. Han, V. Eppakayala, J.H. Kim, Green synthesis of graphene and its cytotoxic effects in human breast cancer cells, Int J Nanomedicine 8 (2013) 1015-27.
[107] E.R. Stadtman, B.S. Berlett, Reactive oxygen-mediated protein oxidation in aging and disease, Chem Res Toxicol 10(5) (1997) 485-94.
[108] G. Poli, G. Leonarduzzi, F. Biasi, E. Chiarpotto, Oxidative stress and cell signalling, Curr Med Chem 11(9) (2004) 1163-82.
[109] H.F. Poon, V. Calabrese, G. Scapagnini, D.A. Butterfield, Free radicals and brain aging, Clin Geriatr Med 20(2) (2004) 329-59.
[110] M.D. Evans, M. Dizdaroglu, M.S. Cooke, Oxidative DNA damage and disease: induction, repair and significance, Mutat Res 567(1) (2004) 1-61.
[111] P.P. Fu, Q. Xia, X. Sun, H. Yu, Phototoxicity and environmental transformation of polycyclic aromatic hydrocarbons (PAHs)-light-induced reactive oxygen species, lipid peroxidation, and DNA damage, J Environ Sci Health C Environ Carcinog Ecotoxicol Rev 30(1) (2012) 1-41.
[112] P.P. Fu, Q. Xia, H.M. Hwang, P.C. Ray, H. Yu, Mechanisms of nanotoxicity: generation of reactive oxygen species, J Food Drug Anal 22(1) (2014) 64-75.
[113] T.A. Tabish, C.J. Scotton, D.C.J. Ferguson, L. Lin, A.v.d. Veen, S. Lowry, M. Ali, F. Jabeen, M. Ali, P.G. Winyard, S. Zhang, Biocompatibility and toxicity of graphene quantum dots for potential application in photodynamic therapy, Nanomedicine 13(15) (2018) 1923-1937.
[114] T. Dutta, R. Sarkar, B. Pakhira, S. Ghosh, R. Sarkar, A. Barui, S. Sarkar, ROS generation by reduced graphene oxide (rGO) induced by visible light showing antibacterial activity: comparison with graphene oxide (GO), RSC Advances 5(98) (2015) 80192-80195.
[115] E. Hendry, P.J. Hale, J. Moger, A.K. Savchenko, S.A. Mikhailov, Coherent Nonlinear Optical Response of Graphene, Physical Review Letters 105(9) (2010) 097401.
[116] D. Zhang, P. Wang, M.N. Slipchenko, D. Ben-Amotz, A.M. Weiner, J.-X. Cheng, Quantitative Vibrational Imaging by Hyperspectral Stimulated Raman Scattering Microscopy and Multivariate Curve Resolution Analysis, Analytical Chemistry 85(1) (2013) 98-106.
[117] U. Cvelbar, M. Mozetic, N. Hauptman, M. Klanjšek-Gunde, Degradation of Staphylococcus aureus bacteria by neutral oxygen atoms, Journal of Applied Physics 106(10) (2009) 103303.
[118] T.-Y. Wang, M.D.J. Libardo, A.M. Angeles-Boza, J.-P. Pellois, Membrane oxidation in cell delivery and cell killing applications, ACS chemical biology 12(5) (2017) 1170-1182.
[119] S. Khan, M.R. P, A. Rizvi, M.M. Alam, M. Rizvi, I. Naseem, ROS mediated antibacterial activity of photoilluminated riboflavin: A photodynamic mechanism against nosocomial infections, Toxicol Rep 6 (2019) 136-142.
[120] A. Al-Sharqi, K. Apun, M. Vincent, D. Kanakaraju, L.M. Bilung, Enhancement of the antibacterial efficiency of silver nanoparticles against gram-positive and gram-negative bacteria using blue laser light, International Journal of Photoenergy 2019 (2019).
[121] F. Pahlevanzadeh, H. Bakhsheshi-Rad, E. Hamzah, In-vitro biocompatibility, bioactivity, and mechanical strength of PMMA-PCL polymer containing fluorapatite and graphene oxide bone cements, Journal of the mechanical behavior of biomedical materials 82 (2018) 257-267.
[122] G. Gonçalves, S.M. Cruz, A. Ramalho, J. Grácio, P.A. Marques, Graphene oxide versus functionalized carbon nanotubes as a reinforcing agent in a PMMA/HA bone cement, Nanoscale 4(9) (2012) 2937-2945.
[123] K.-H. Liao, Y.-S. Lin, C.W. Macosko, C.L. Haynes, Cytotoxicity of graphene oxide and graphene in human erythrocytes and skin fibroblasts, Acs Appl Mater Inter 3(7) (2011) 2607-2615.
[124] J. Liu, L. Cui, D. Losic, Graphene and graphene oxide as new nanocarriers for drug delivery applications, Acta biomaterialia 9(12) (2013) 9243-9257.

[125] X. Hu, N. Ren, Y. Chao, H. Lan, X. Yan, Y. Sha, X. Sha, Y. Bai, Highly aligned graphene oxide/poly(vinyl alcohol) nanocomposite fibers with high-strength, antiultraviolet and antibacterial properties, Composites Part A: Applied Science and Manufacturing 102 (2017) 297-304.

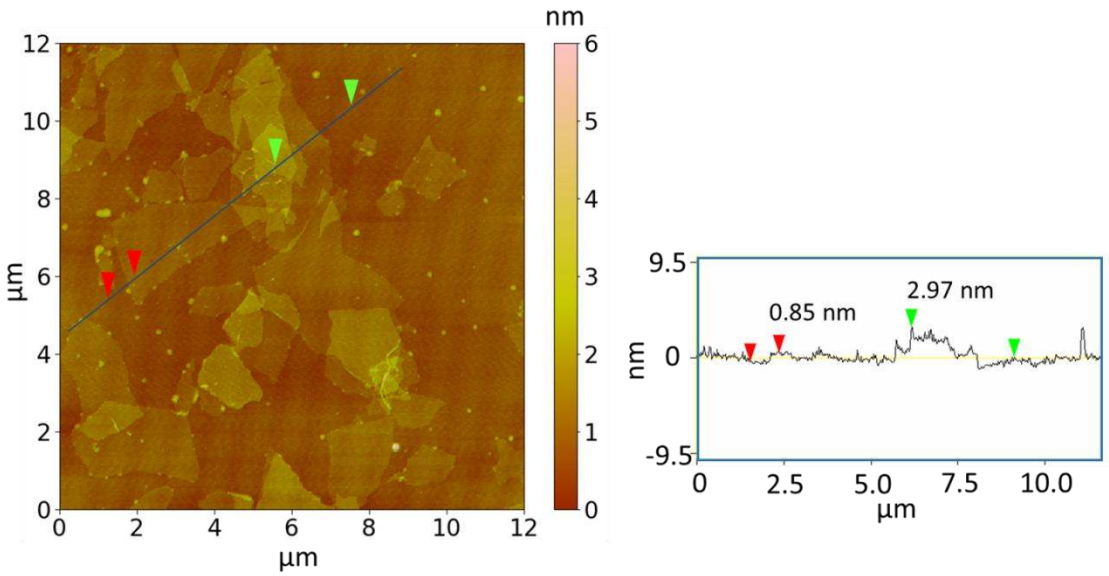

Figure 1: (A) AFM micrograph and (B) height profile of synthesised GO nanosheets showing its thickness.

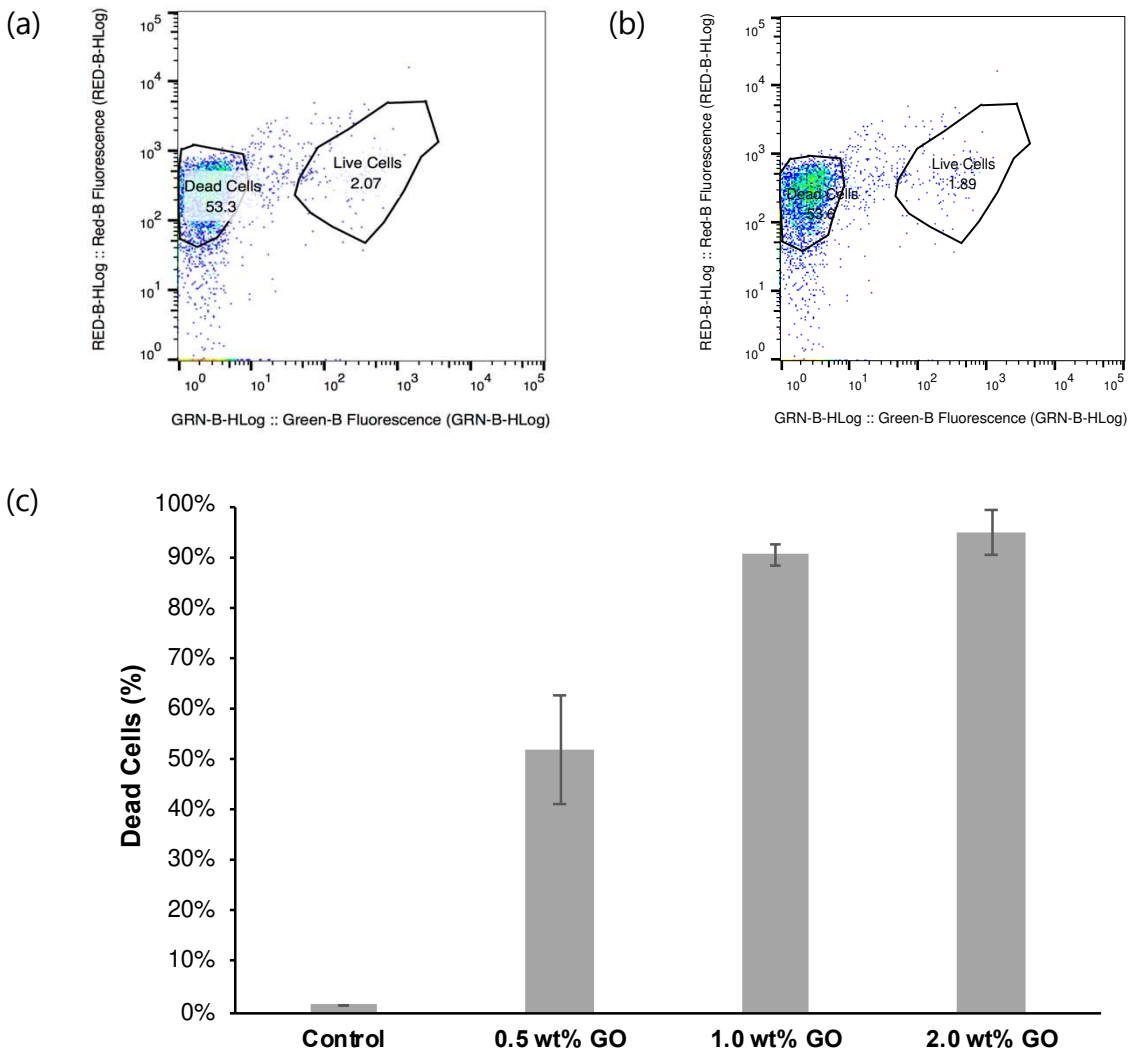

Figure 2: Flow cytometry results obtained by exposing *E. coli* to GO at various concentrations for 24 hours at 37°C and 150 rpm. (a) gating strategy example of *E. coli* bacterial cells after exposure to 1 wt% of GO, (b) gating strategy example of *E. coli* bacterial cells after exposure to 2 wt% of GO, (c) percentage of dead cells after exposure of *E. coli* to various concentrations of GO. Error bars represent standard deviation, (*n = 3*).

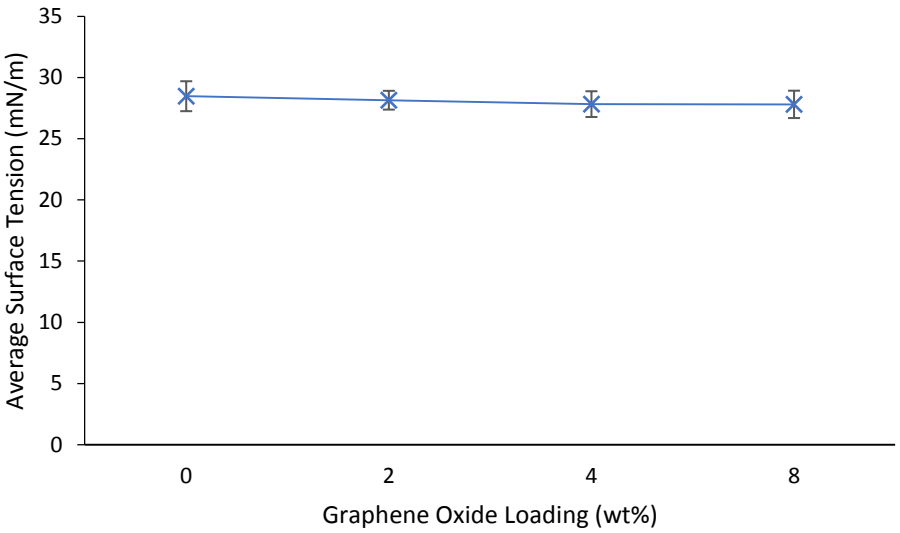

(a)

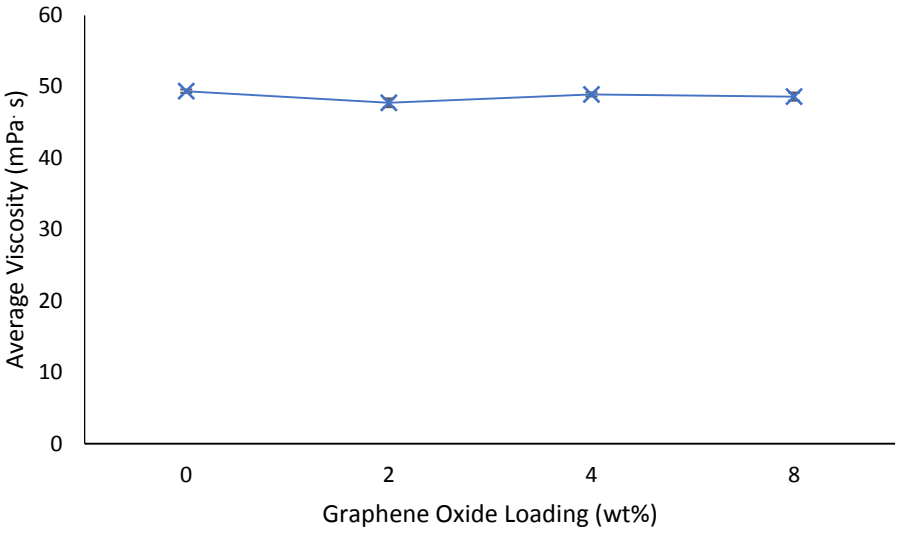

(b)

1011 Figure 3: plot of the (a) average surface tension against GO concentration (n=4);
1012 (b) average viscosity against GO concentration (n=3). Error bars represent
1013 standard deviation.

1014

1015

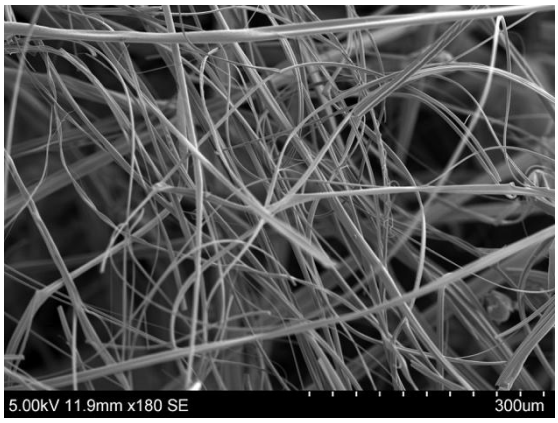
5.00kV 11.9mm x180 SE
300um

(a)

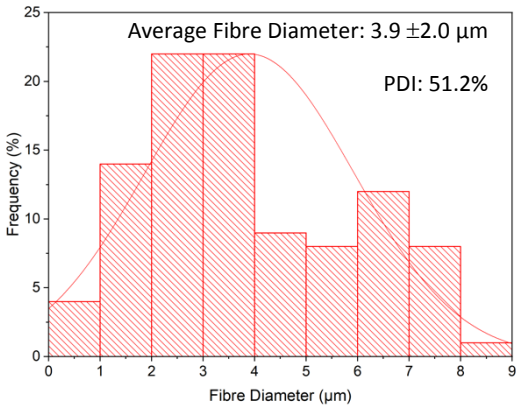
Average Fibre Diameter: 3.9 ±2.0 µm
PDI: 51.2%
Frequency (%)
Fibre Diameter (µm)

(b)

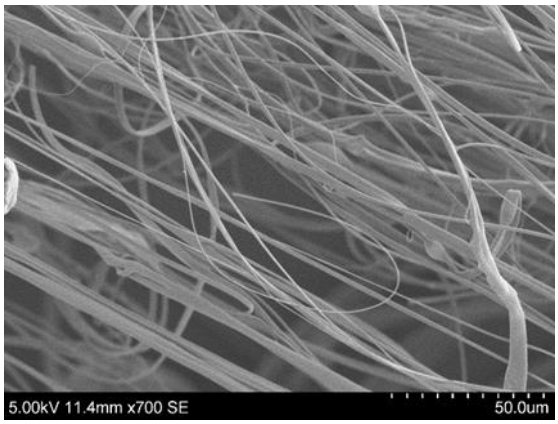
5.00kV 11.4mm x700 SE
50.0um

(c)

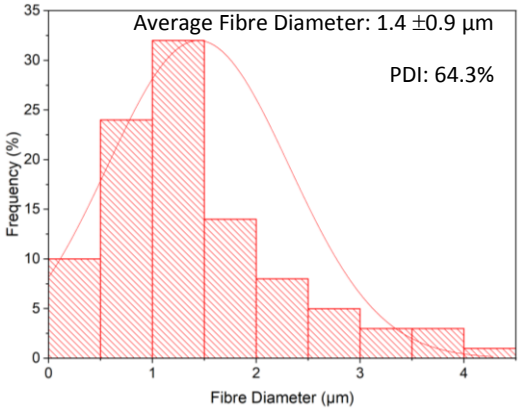
Average Fibre Diameter: 1.4 ±0.9 µm
PDI: 64.3%
Frequency (%)
Fibre Diameter (µm)

(d)

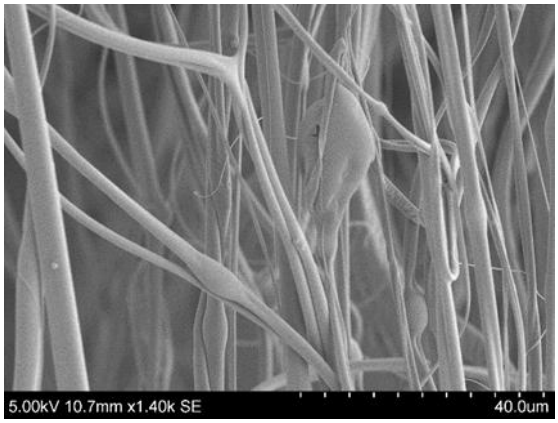
5.00kV 10.7mm x1.40k SE
40.0um

(e)

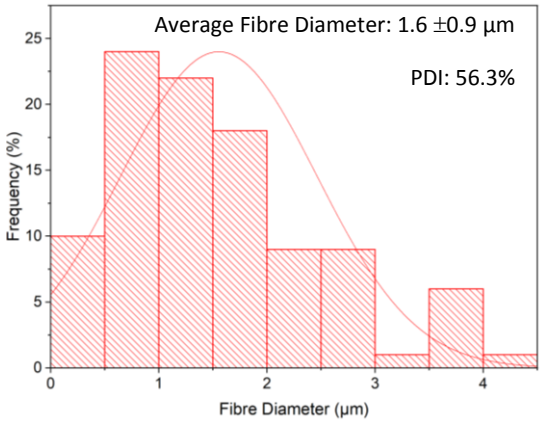
Average Fibre Diameter: 1.6 ±0.9 µm
PDI: 56.3%
Frequency (%)
Fibre Diameter (µm)

(f)

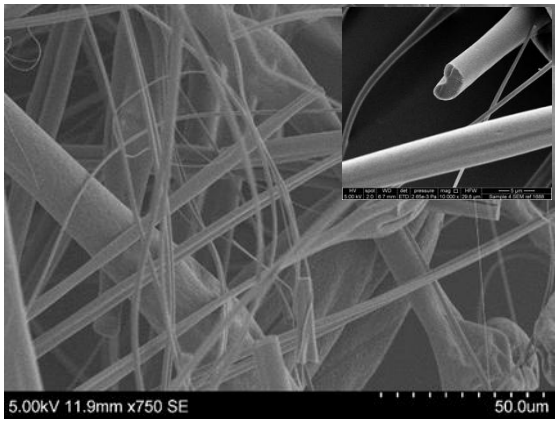

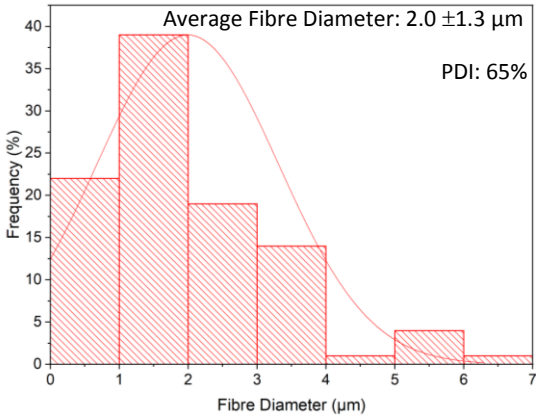

(g) (h)

Figure 4: SEM images and fibre diameter distribution of graphene oxide loaded PMMA fibres. (a) and (b) pure PMMA fibres, (c) and (d) 2wt% GO fibres, (e) and (f) 4wt% GO fibres, (g) and (h) 8wt% GO fibres. In (g) the inset micrograph shows the fibres to have smooth surfaces. Polydispersity index (PDI) values are also displayed on the graphs.

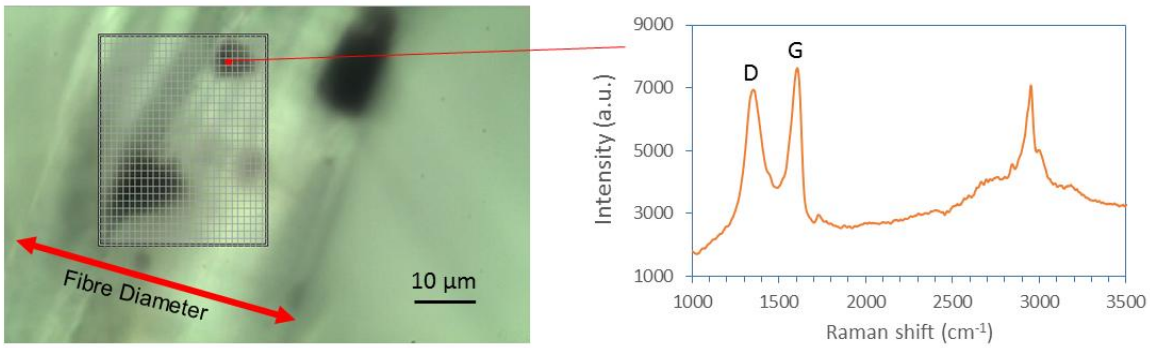

(a)

(b)

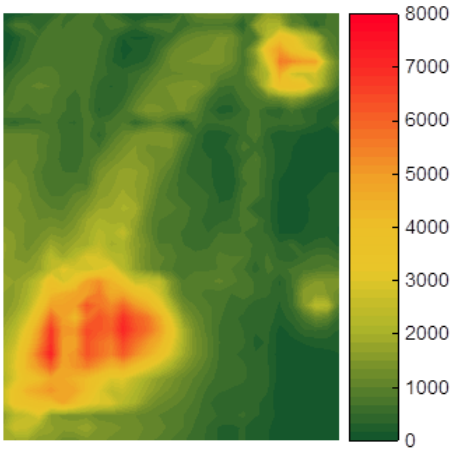

I_D (X,Y)

(c)

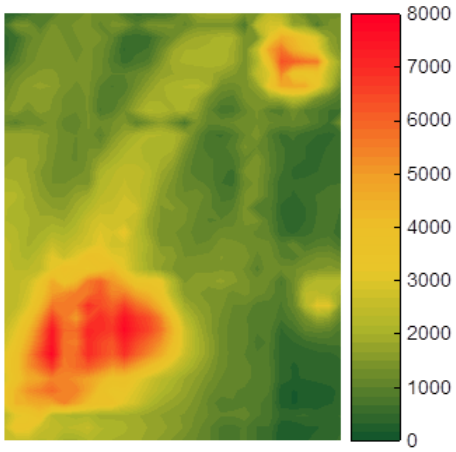

I_G (X,Y)

(d)

Figure 5: Raman microscopic image of 4wt% GO loaded PMMA fibres: microscopic image (a), Raman spectrum (b), and Raman mapping of D (c) and G (d) peaks.

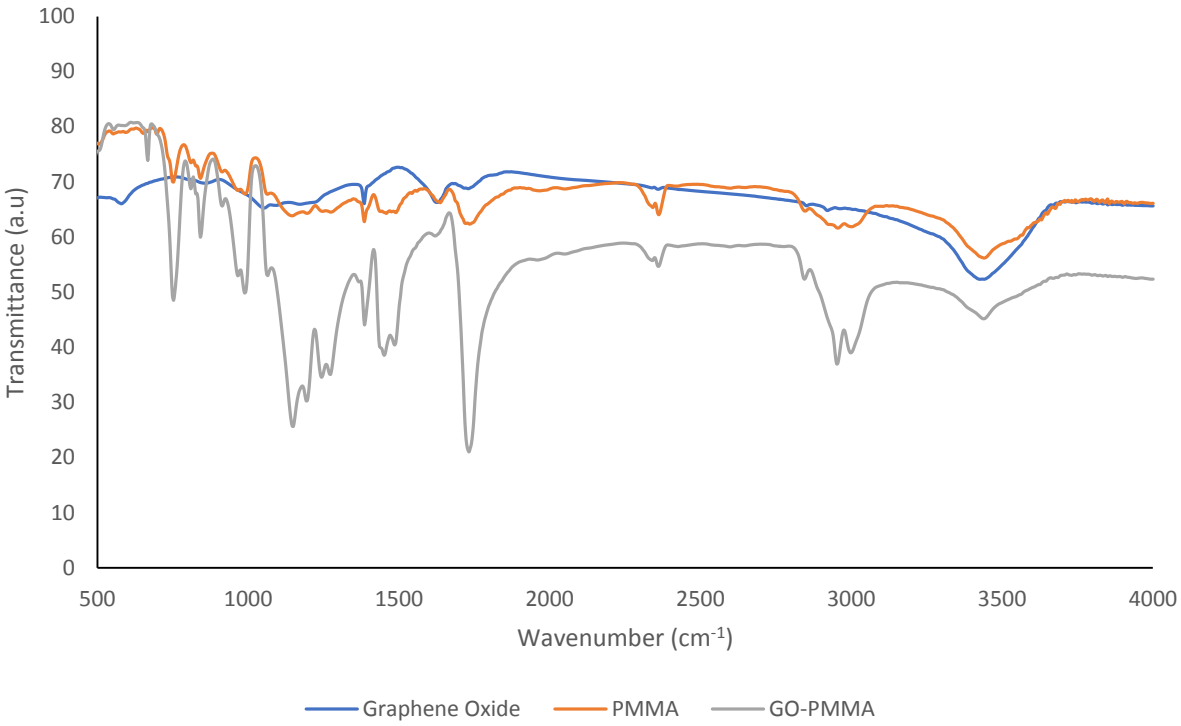

Figure 6: FT-IR spectra of GO, PMMA and 8 wt% GO/PMMA nanocomposite fibres.

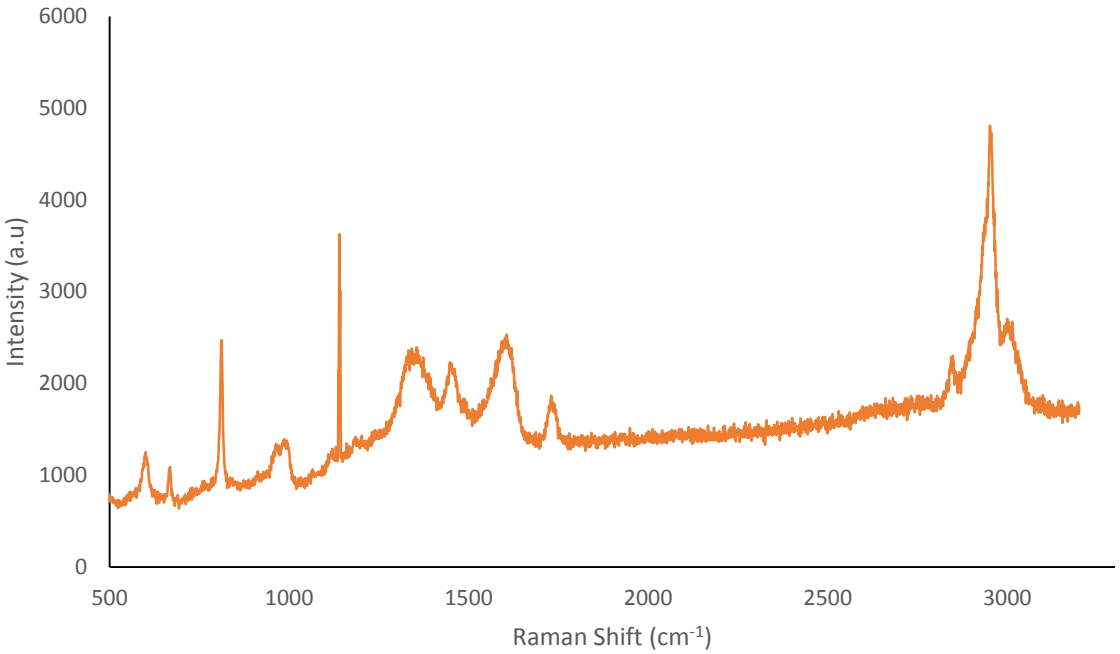

Figure 7: Raman spectrum of 8 wt% GO/PMMA fibres.

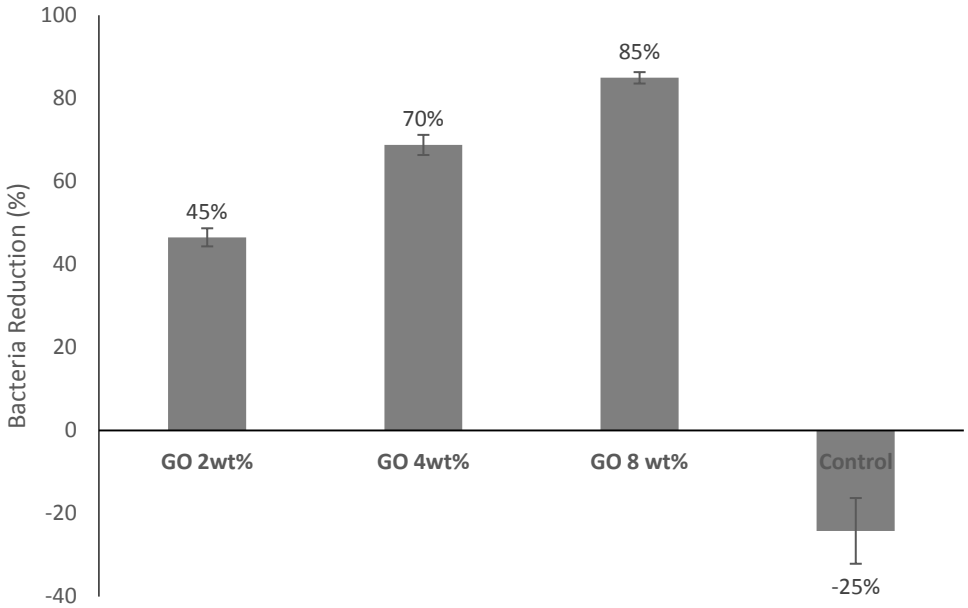

Figure 8: Bacterial reductions observed after incubation of 0, 2, 4 and 8 wt% GO/PMMA fibres with *E. coli* K12 for 24 hours at 150 rpm and 37°C. Pure PMMA fibres with no GO were used as a control group. Error bars represent standard deviation (*n = 3*).

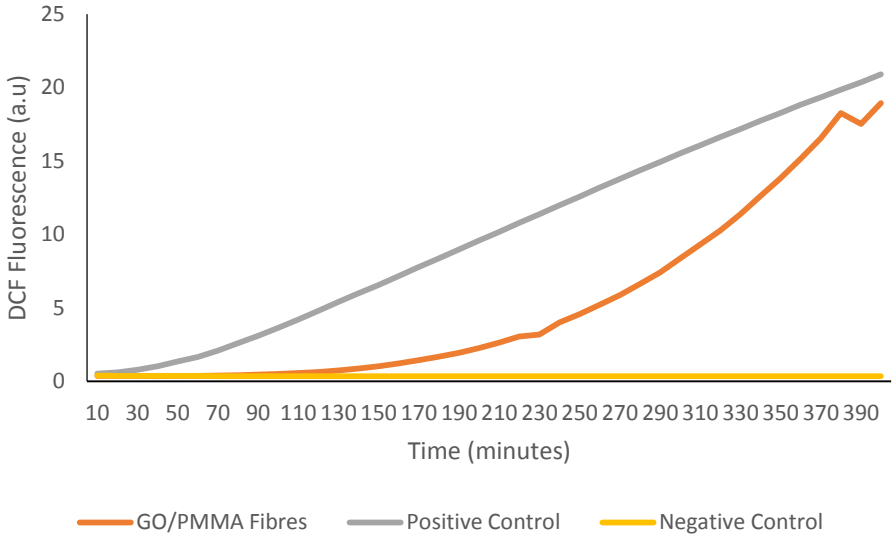

Figure 9: Generation of ROS from 8 wt% GO/PMMA fibres. The fluoresce of DCF was measured using a fluorimeter with excitation at 485 nm and emission at 530 nm. Positive control represents a 1:1 dilution of 30% hydrogen peroxide in PBS, whilst the negative control represents PBS only.

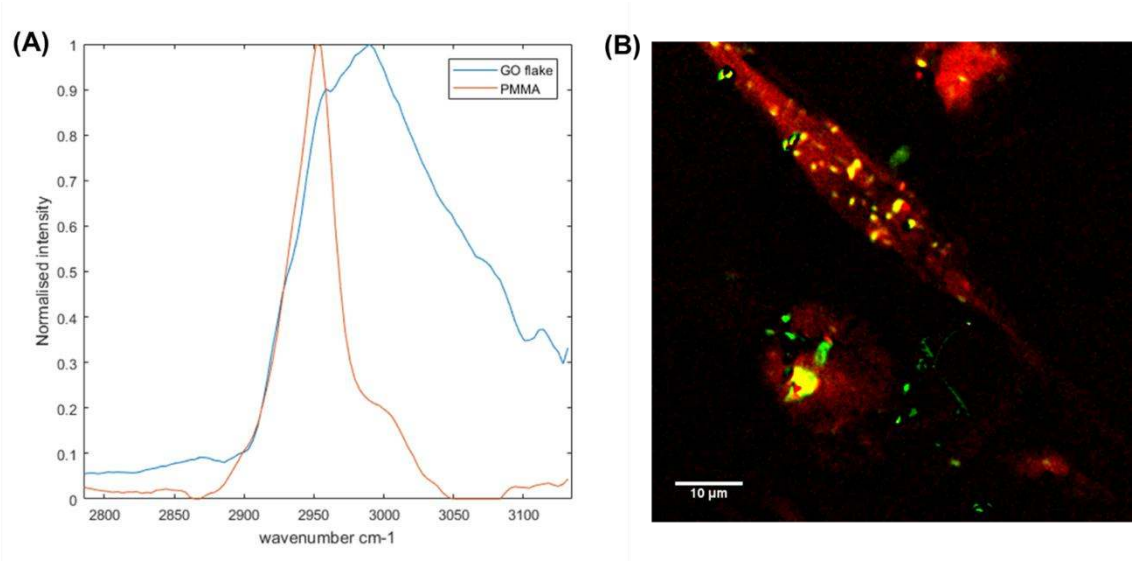

Figure 10: a) Stimulated Raman scattering (SRS) spectra from PMMA and GO in the 8 wt% GO-PMMA *E coli* treated samples. b) The results of Multi-Curve Regression (MCR) analysis performed on a hyperspectral stack of SRS images from bacteria and GO-PMMA. Here the PMMA (red) and GO (green) signals can be separated by the different spectral profiles as shown in (a). Gold colour indicates a mixture of GO and PMMA.

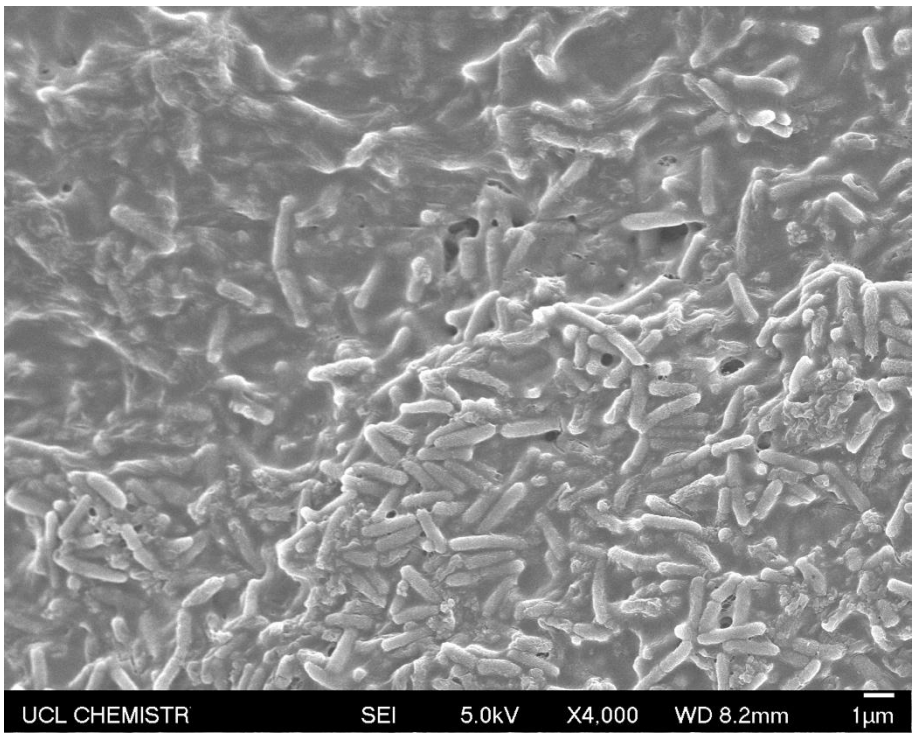

Figure 11: SEM micrograph of the 8 wt% GO/PMMA post incubation with *E. coli*.

Table 1: GO/PMMA solution composition.

	GO Suspension		Polymer Solution		Final Concentration of GO in the Resulting Fibre (wt%)
	GO Particles (g)	Chloroform (mL)	PMMA (g)	Chloroform (mL)	
GO/PMMA0	0.00	10	4	10	0
GO/PMMA2	0.08	10	4	10	2
GO/PMMA4	0.16	10	4	10	4
GO/PMMA8	0.32	10	4	10	8

***Declaration of Interest Statement**

Declaration of interests

☒ The authors declare that they have no known competing financial interests or personal relationships that could have appeared to influence the work reported in this paper.

☐The authors declare the following financial interests/personal relationships which may be considered as potential competing interests:

*Credit Author Statement

Rupy Kaur Matharu: conceptualisation, methodology, validation, formal analysis, investigation, writing – original draft, writing – review and editing, visualisation, project administration. Tanveer A Tabish: validation, formal analysis, investigation, resources, writing – review and editing, visualisation. Thithawat Trakoolwilaiwan: methodology, validation, formal analysis, investigation, writing – review and editing, visualisation. Jessica Mansfield: methodology, formal analysis, investigation, resources, writing – review and editing, funding acquisition. Julian Moger: methodology, formal analysis, investigation, resources, writing – review and editing, funding acquisition. Tongfei Wu: methodology, formal analysis, investigation, resources, writing – review and editing. Cláudio Lourenço: methodology, formal analysis, investigation, resources, writing – review and editing. Biqiong Chen: formal analysis, resources, writing – review and editing, supervision, project administration. Lena Ciric: writing – review and editing, funding acquisition. Ivan P Parkin: project resources, writing – review and editing. Mohan Edirisinghe: conceptualisation, methodology, resources, writing – review and editing, supervision, project administration, funding acquisition.